Spring 5-31-1993

# Constitutive equation for concrete using strain-space plasticity model

Yuxiang Xing
*New Jersey Institute of Technology*

# Copyright Warning & Restrictions

The copyright law of the United States (Title 17, United States Code) governs the making of photocopies or other reproductions of copyrighted material.

Under certain conditions specified in the law, libraries and archives are authorized to furnish a photocopy or other reproduction. One of these specified conditions is that the photocopy or reproduction is not to be "used for any purpose other than private study, scholarship, or research." If a, user makes a request for, or later uses, a photocopy or reproduction for purposes in excess of "fair use" that user may be liable for copyright infringement,

This institution reserves the right to refuse to accept a copying order if, in its judgment, fulfillment of the order would involve violation of copyright law.

Please Note: The author retains the copyright while the New Jersey Institute of Technology reserves the right to distribute this thesis or dissertation

Printing note: If you do not wish to print this page, then select "Pages from: first page # to: last page #" on the print dialog screen

# ABSTRACT

## Constitutive Equation for Concrete Using Strain-Space Plasticity Model

by
Yuxiang Xing

Plasticity theory has been used to model the concrete constitutive relationship for about two decades. With the modifications and refinement based on experimental data, achievement has been made in these plasticity models for concrete. Almost all the existing models are developed in stress space. With a lot of experimental data and more understanding about stress states of concrete, the stress-space model shows many advantages. Because of this and also due to conventional engineering practice, the stress-space plasticity approach has been in the dominant position. However, the conventional stress-space plasticity method has one inherent drawback in which it cannot deal with the softening part of materials. To model effectively the descending part of the strain softening materials such as concrete on the basis of plasticity theory, strain space concept must be adopted. Some researcher used it as a supplemental means to the stress-space model for the post-peak stage. Inspired by this basic idea, attempt was made in this study, to set up a strain surface of concrete at critical stress, then an initial yield surface and subsequent yield surfaces were constructed in strain space according to the existing experimental results. A non-proportional hardening rule and a non-associated flow rule were adopted. Finally, a strain-space plasticity theory was presented in modeling the nonlinear multiaxial strain-hardening-softening behavior of concrete.

It has been found that the model predictions of the ascending branch of stress-strain behavior are in good agreement with the experimental results

involving a wide range of stress states and different types of concrete. The most important inelastic behavior of concrete, such as brittle failure in tension; ductile behavior in compression; hydrostatic sensitivities; and volumetric dilation under compressive loadings are included in these comparisons. It has also been found that the model can predict well the descending branch of strain-softening behavior of concrete.

# CONSTITUTIVE EQUATION FOR CONCRETE USING STRAIN-SPACE PLASTICITY MODEL

by
Yuxiang Xing

A Dissertation
Submitted to the Faculty of
New Jersey Institute of Technology
in Partial Fulfillment of the Requirements for the Degree of
Doctor of Philosophy

Department of Civil and Environmental Engineering

May 1993

## APPROVAL PAGE

**Constitutive Equation for Concrete**
**Using Strain-Space Plasticity Model**

**Yuxiang Xing**

---

Dr. C. T. Thomas Hsu, Thesis Advisor ( Date )
Professor of Civil and Environmental Engineering, NJIT

---

Dr. George Weng, Committee Member ( Date )
Professor of Mechanical and Aerospace Engineering, Rutgers University

---

Dr. M. Ala Saadeghvaziri, Committee Member ( Date )
Assistant Professor of Civil and Environmental Engineering, NJIT

---

Dr. D. Raghu, Committee Member ( Date )
Professor of Civil and Environmental Engineering, NJIT

---

Dr. W. R. Spillers, Committee Member ( Date )
Professor and Chairman of Civil and Environmental Engineering, NJIT

## BIOGRAPHICAL SKETCH

**Author:** Yuxiang Xing

**Degree:** Doctor of Philosophy in Civil Engineering

**Date:** May 1993

**Undergraduate and Graduate Education:**

- Doctor of Philosophy in Civil Engineering,
  New Jersey Institute of Technology, Newark, NJ, 1993
- Master of Science in Civil Engineering,
  Wuhan University of Technology, Wuhan, PR China, 1987
- Bachelor of Science in Civil Engineering,
  Wuhan University of Technology, Wuhan, PR China, 1982

**Major:** Civil Engineering

**Publications:**

Xing, Yuxiang, and Li, Gueiqing. " The Effect of Subjective Uncertainties on Structural Safety." *Journal of Wuhan Institute of Urban Construction*, No. 4, 1987, (in Chinese).

Xing, Yuxiang, and Li, Gueiqing. "An Experimental Study of R/C Frame with Partition Walls." *Journal of Wuhan University of Technology*, No. 2, 1988, (in Chinese).

Xing, Yuxiang, and Li, Gueiqing. " Fuzzy Reliability of Seismic Structures." *Journal of Wuhan University of Technology*, No. 2 , 1990, (in Chinese).

Xing, Yuxiang, and Hsu, C. T. T. "Constitutive Equation for Concrete Using Strain-Space Plasticity Model." *Journal of Engrg. Mech., ASCE*, (Tentatively Accepted).

This thesis is dedicated to
my dear wife Lin Wang

## ACKNOWLEDGMENT

The author wishes to express his sincere gratitude to his supervisor, Professor C. T. Thomas Hsu, for his guidance, friendship and moral support throughout this research.

Special thanks to Dr. G. Weng, Dr. M. A. Saadeghvaziri, Dr. D. Raghu and Dr. W. R. Spillers for serving as members of the committee

Finally, the author expresses his gratitude to the Department of Civil and Environmental Engineering and the Office of Graduate Studies for continuous financial support in the pursuit of this degree.

TABLE OF CONTENTS

Chapter Page

# LIST OF TABLES

## LIST OF FIGURES

Figure Page

Figure Page

# CHAPTER 1

# INTRODUCTION

## 1.1 General

The rapid development of modern numerical analysis technique and high speed digital computers have opened a new research field in concrete technology, that is, the nonlinear numerical analysis of concrete structures. Such a structural analysis is based on the fundamental principle of continuum mechanics, rather than on empirical formulas.

In the past years, the methods of analysis and design for concrete structures were mainly based on elastic analysis combined with various classical procedures as well as on empirical formulas, using the results of a large amount of experimental data. Such approaches are still necessary and continue to be the most convenient for the ordinary design. However, the finite element method now provides engineers with a powerful tool to explore possible new concept in analysis and design. With the tool of finite element method, the tests can be fewer in number and more fundamental, and consequently test results will be more generally useful. The need for large-scale testing of members over the full range of variables is greatly reduced.

The first attempt to apply the finite element method to a reinforced concrete structure was made by Ngo and Scordelis (1967) in 1967. They adopted the linear elastic-fracturing model for concrete in tension and bilinear elastic-plastic model for reinforcement and for concrete in compression. Since then, the importance of formulation of general constitutive equation for concrete in finite element analysis has been well recognized, and a large variety of models have been proposed for the stress-strain relation under short-term load,

based mainly on nonlinear elasticity, plasticity, continuous damage theory, and endochronic theory of inelasticity, respectively.

Among these theories, plasticity theory, when not interpreted too narrowly, is a most flexible model frame. In addition, it is rather simple. Thus it has been a very active field.

In the classical plasticity, stress is treated as a basic quantity, and the strain as a function of the stress. This form of stress-space plasticity is consistent with human habit in stress-strain analysis. With a lot of experimental data available, the stress-space plasticity theory has been in a dominant position. On the basis of Drucker's postulates, it has been successfully used in metals and other materials including concrete. However, it has one inherent drawback that it cannot deal with softening part of materials.

In strain-space plasticity, on the other hand, strain is the basic quantity, the stress is a function of the strain. By using Il'iushin's postulates, the strain softening part as well as strain hardening part can be accounted in the same way. Comparing with the stress-space counterpart, the strain-space plasticity is much less used due to conventional engineering practice. This unbalanced situation in concrete field was pointed out by Hsu (1972), and Bazant (1971). Dougill (1976), Bazant et al (1979), and Han et al (1986) had used the strain-space plasticity concept for concrete constitutive law. They used it only as a kind of supplemental ingredient to account for strain softening with very rough approximations on loading surfaces. The significance of their research is that the descending branch of stress-strain relation can be obtained using strain-space approach. Since the yield and subsequent yield surfaces are not well established for strain states of concrete, much improvement is needed. In addition, to carry out the complete stress-strain behavior of concrete by strain-space plasticity theory is a tremendous challenge. This is the motivation of the

present research. In this study, attempt was made to set up a strain surface of concrete at the critical stress, then an initial yield surface and subsequent yield surfaces were constructed according to the existing experimental results. A non-proportional hardening rule and a non-associated flow rule were adopted. Finally, a strain-space plasticity theory was presented in modeling the nonlinear multiaxial strain-hardening-softening behavior of concrete. It is the belief that with enough experimental data about strain states and more understanding of strain behavior, the strain-space plasticity theory will become more powerful tool to study the nonlinear behavior of concrete.

## 1.2 Scope and Objective of Research

The objective of this research work is to develop a short-term rate-independent constitutive model for concrete, which can be used in finite element analysis of concrete structures. The model is developed in the plasticity framework with strain-space formulations. It is capable of predicting the stress-strain relation with a reasonable accuracy. The stress states could be biaxial or triaxial tension, mixed tension and compression, biaxial or triaxial compression. The most important features of concrete behavior, including brittle cracking in tension, strain-hardening and quasi-ductile behavior in compression, hydrostatic sensitivities, nonlinear volumetric dilatancy and strain-softening, can be represented by the constitutive model. This study will be performed mainly in the following four aspects:

(1) To study the existing multiaxial experimental data, and analyze them to reveal the strain characteristics of concrete under multiaxial loadings.

(2) To define the initial yield surface, critical surface and subsequent yield surfaces in a strain space.

(3) To formulate the strain-space plasticity in concrete, including hardening rules, flow rule, and incremental stress-strain relationship.

(4) To compare the proposed model with the existing experimental stress-strain results of concrete under multiaxial states of loadings.

Some of the important assumptions of the proposed model are stated below:

(1) Concrete is considered macroscopically as isotropic and homogenous material.

(2) Deformations are small enough to disregard the nonlinear terms of the strain displacement relations.

(3) Elastic and plastic deformation are uncoupled in the strain hardening.

(4) The system is considered to be under isothermal conditions.

(5) The rate of loading is slow enough to disregard the inertia effects.

## 1.3 Statement of Originality

The concept of strain-space plasticity is relatively new and the followings may be found original in this field of study:

(1) To select a critical surface in strain space.

In the conventional plasticity model for concrete, the initial yield surface are defined according to the stress-space failure surface which is known and available. By the same token, a reference surface called critical surface is required in strain-space plasticity to define the strain-space initial yield surface.

(2) To derive a closed initial yield surface in strain space.

For metals, the yield condition has a physical meaning and can be determined by tests. However, the yield condition for concrete is a fictitious quantity, and is usually defined according to the reference surface. Many previous research defines the yield surface as reduced size and same shape as the reference surface. Thus, the initial yield surface from an open-ended failure surface has also got an open end. It has been pointed out, however, that the initial yield surface in stress space should be a closed shape. The strain-space initial yield surface should also have an end along the hydrostatic pressure axis.

(3) To propose a non-proportional hardening rule.

The critical surface is one of the loading surface which has an open end. During the change from the closed-ended initial yield surface to the open-ended loading surfaces, the cross sectional shapes of the surfaces on the deviatoric plane do not change, but their meridians are varied. This means that high compression zone and low compression or even tension zone have different strain hardening.

(4) To propose a non-associated flow rule.

The associated flow rule confines the plastic stress increment vector normal to the loading surface, which implies no plastic volume contraction occurs all the way in the plastic flow for certain loading range. In addition, concrete has a large amount of volumetric expansion after the critical stress. Therefore, the non-associated flow rule must be used to define the ratio of the plastic stress components.

## 1.4 Structure of Thesis

Following this introductory chapter, Chapter 2 starts with the general features of concrete behavior, which will help develop the proposed model. A review of the constitutive modeling of concrete is made. Several modeling techniques are briefly discussed. And a general consideration of the proposed model is discussed.

Chapter 3 is devoted to analyzing the strain state of concrete under multiaxial loadings and to setting up the strain-space critical surface.

Chapter 4 contains the proposed constitutive model based on strain-space plasticity theory. This is followed by definitions of an initial yield surface and subsequent yield surfaces, description of the non-proportional hardening rule, explanation of the influence of hydrostatic pressure and lode angle, adoption of the non-associated flow rule and special treatment for the strain softening stage.

Chapter 5 contains model predictions and comparison with test results.

Finally, summary and conclusions are presented in Chapter 6.

# CHAPTER 2

# CONSTITUTIVE MODELING OF CONCRETE

## 2.1 Introduction

Characterization of stress-strain behavior of concrete has been a subject of active research for a long time. A lot of constitutive models have been developed. All these models have intrinsic advantages and disadvantages dependent largely on their particular application. Before reviewing them, a brief discussion on the features of concrete behavior is presented. In light of these features, the merits and limitations of the reviewed models can be found. Based on the literature review, a general consideration of the proposed model is discussed, from which the basic thought of the proposed model can be seen and the original concepts can be traced.

## 2.2 Features of Concrete Behavior

Concrete is a composite material. It consists of coarse aggregates and continuous matrix of mortar which itself comprises a mixture of cement paste and smaller aggregate particles. Its physical behavior is very complex, involving phenomena such as inelasticity, cracking, creep, etc., being largely determined by the structure of the composite material, such as the ratio of water to cement, the ratio of cement to aggregate, the shape and size of aggregate, and the kind of cement used. The following discussion is confined to the stress-strain behavior of an average ordinary concrete. The structure of the material is ignored and the rules of material behavior are developed on the basis of a

homogeneous continuum. Also the material is customarily assumed to be initially isotropic.

Typical uniaxial compressive and tensile stress-strain curves are shown in Figs. 2.1 and 2.2, respectively. The most distinct features are a lower strength and brittle failure in tension as well as a higher strength and relatively ductile failure in compression. Such a shape of stress-strain curve is closely associated with the occurrence and development of the microcracks.

Concrete contains a large number of microcracks, especially at interfaces between coarse aggregates and mortar, even before the application of external load. These initial microcracks are caused by segregation, shrinkage, or thermal expansion in the cement paste. Under applied loading , further microcracking may occur at the interface which is the weakest link in the composite system. The progression of these microcracks with the application of the externally

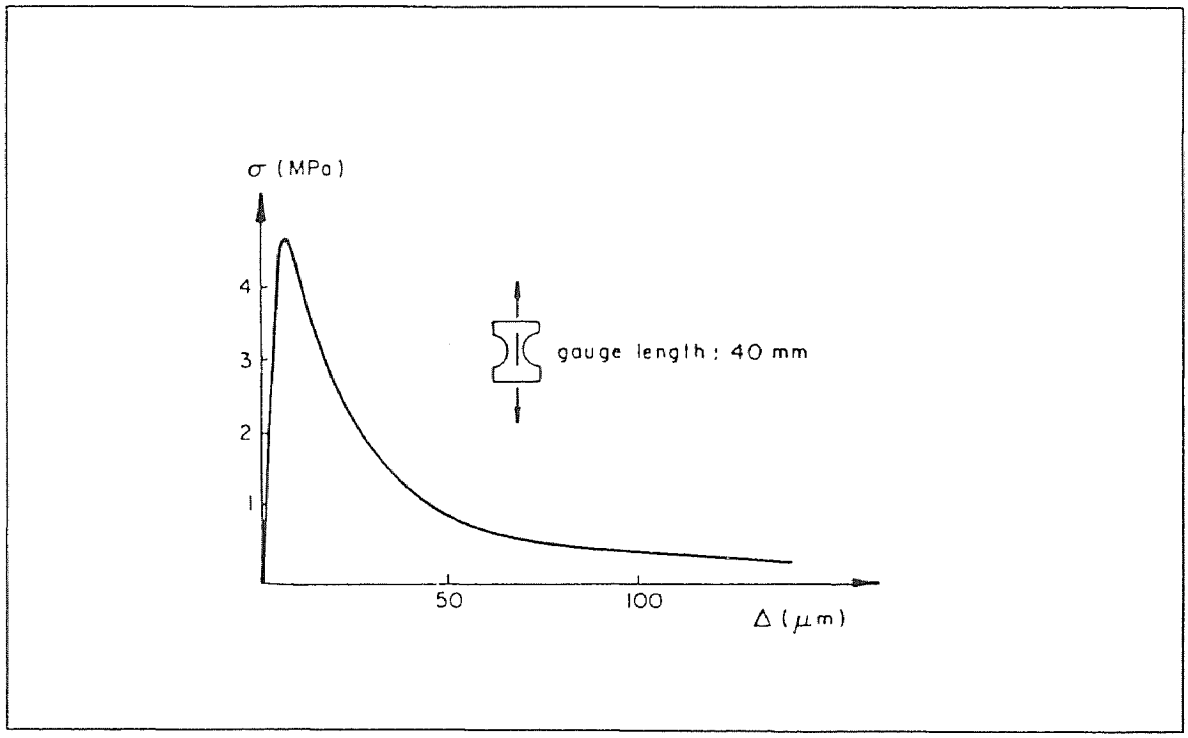


**Fig. 2.1** Uniaxial Tensile Test (Peterson (1981))

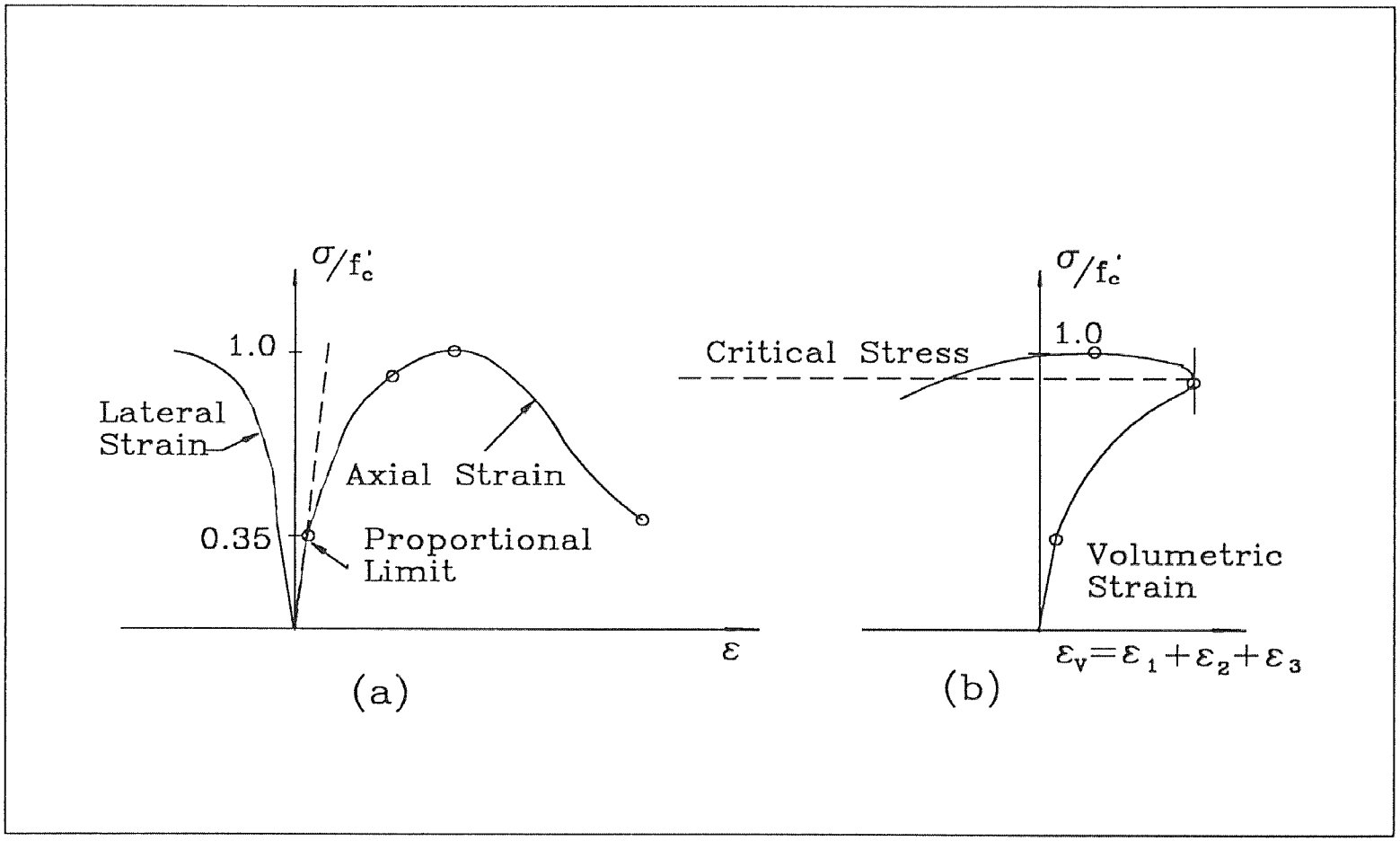


**Fig. 2.2** Unixial Compressive Test

applied loads contributes to the generally obtained nonlinear stress-strain behavior and plastic deformation of concrete.

Such a process of crack propagation can be described in three stages (Chen (1982)). The first stage corresponds to a stress in the region up to 30~40 percent of the maximum compressive stress $f_c'$. At this stage, the cracks existing in concrete before loading remain nearly unchanged. Hence the stress-strain behavior is nearly linear elastic. The stress between 30~40 to about 75~90 percent of $f_c'$ belongs to the second stage, in which bond cracks at nearby aggregate surfaces start to bridge in the form of mortar cracks. With significant cracking, material nonlinearity becomes more evident. But the crack propagation is stable until the stress reaches the level of about 75~90 percent of $f_c'$. Hence this point is termed critical stress (Richard et al (1929)), which corresponds to the minimum volumetric strain. Further increase of the load eventually results in unstable fracture and comes the third stage in which failure of concrete is primarily caused by microcracks zones or internal damage. With increasing compressive strain, damage to concrete material continues to accumulate, and concrete enters the descending portion of its stress-strain curve.

The above observation, relating microcracking to macro phenomena in a uniaxial compression, may be extended to triaxial compressive loading situations. At moderate stress levels, when the fracture process is confined to an isolated microcracking, an almost linear elastic response is measured. According to Newman and Newman (1972), the elastic response is observed up to the stress levels $\sigma_3 = 0.4 \sim 0.5\sigma_{3,peak}$ in uniaxial and triaxial compressions. When this limit is exceeded, the microcracks start propagating in a stable manner, and the limit is referred to as 'lower bound criterion for failure'. In a later investigation by Kotsovos and Newman (1977), this boundary is redefined as 'onset of stable fracture propagation' (OSFP). For an increasing principal stress

$\sigma_3$, eventually the above mentioned minimum volume can be obtained. Newman and Newman (1972) refer to this boundary as 'upper bound criterion for failure', and later Kotsovos and Newman term this boundary as 'onset of unstable fracture propagation' (OUFP). Upon further increasing stress, beyond OUFP, a maximum stress level is reached. When proper measures are taken, the fracture process also remains stable beyond peak stress, and a descending branch is obtained. When the hydrostatic pressure is very large, the concrete may get crushed at the maximum stress level. Thus, no strain softening follows.

In Fig. 2.3(a), the above mentioned stages in the progressive fracture process are shown in the meridian plane in principal stress space. The meridian plane contains all loading combinations that can be investigated with standard triaxial cylinder tests. In Fig. 2.3(b), the strain-space counterparts are plotted. Fig. 2.3 show that the OSFP curve is closed, while the OUFP envelope and ultimate strength envelope are open ended with regard to the hydrostatic axis. According to Kotsovos and Newman (1977), the OSFP-envelope is associated with the fatigue strength of the concrete. Below this level, concrete does not suffer from any significant cracking. The OUFP-level is associated with the long-term strength of the material.

Concrete is a dilatant material. As illustrated in Fig. 2.2(b), the change in volume is almost linear up to the critical stress. At the point of critical stress, however, the direction of volume change is reversed, resulting in a volumetric expansion. For the multiaxial cases (Kupfer and Gerstle (1973)), the volumetric strain against the octahedral stress is shown in Fig. 2.4. Before the point of critical stress, the volumetric strain decreases. After the critical stress, however, the tendency is reversed with increasing stress. The volume expansion near failure is due mainly to the voids within the body which are caused by the crack propagation.

In the tension case, as the tension state of stress tends to arrest the cracks much less frequently than the compressive state of stress, the interval of stable crack propagation is quite short. Then starts the unstable crack propagation. That is why the deformation behavior in tension is quite brittle. In addition, the aggregation-mortar interface has a significantly lower tensile strength than that of the mortar. This is why the concrete material has a very low tensile strength. Under uniaxial tension, the stress-strain diagram is linear or nearly linear up to failure stress (Kupfer et al (1969) , Carino et al (1976)). As for the biaxial tension and triaxial tension, it is reported (Ahmad (1981)) that the behavior is similar to that under uniaxial tension and the tensile strength is almost the same as the one under uniaxial tension.

The occurrence of microcracking and slip also leads to softening degradation of the stiffness. Fig. 2.5 (Sinha et el (1964)) illustrates a typical stress-strain curve of concrete under compressive cyclic loading. The envelope curve has a descending part beyond the ultimate stress, and the unloading-reloading curves are not straight-line segments but loops of changing size with decreasing average slopes. Assuming that the average slope is the slope of a straight line connecting the turning points of one cycle and that the material behavior upon unloading and reloading is linearly elastic (dotted line in the figure). Then the elastic modulus degrades with increasing straining. For the descending part, a significant degradation of stiffness can be observed.

In summary, concrete is a material which has higher strength and larger ductility in compression than those in tension; it has a significant volumetric expansion after the point of critical stress, and also a significant amount of irrecoverable strain during unloading. In general, the stress-strain curve experiences an elastic-plastic-hardening-softening process under monotonically compressive loading.

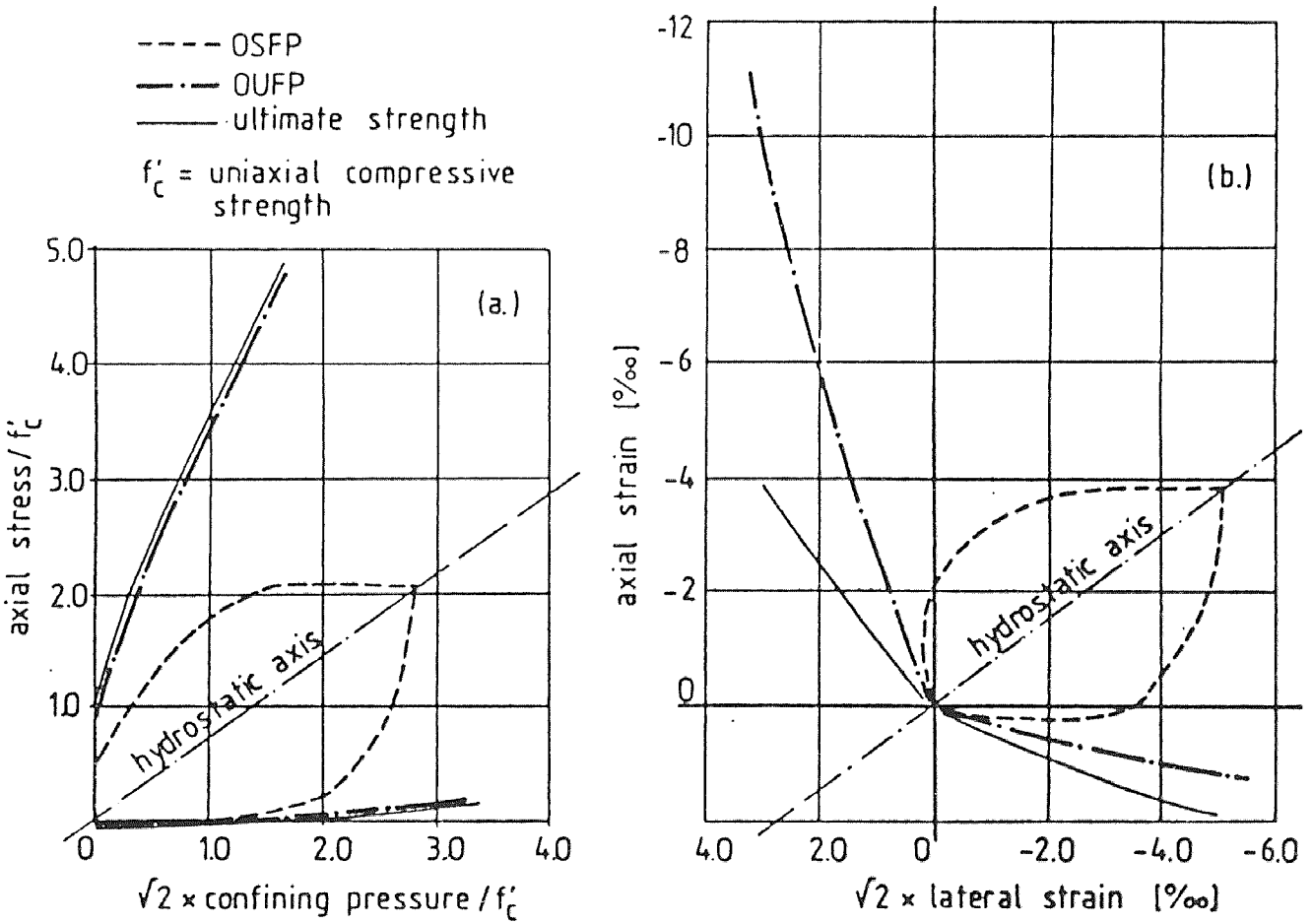


**Fig. 2.3** OSFP, OUFP and Ultimate Strength Envelopes for Concrete

(Kotsovos and Newman (1977))

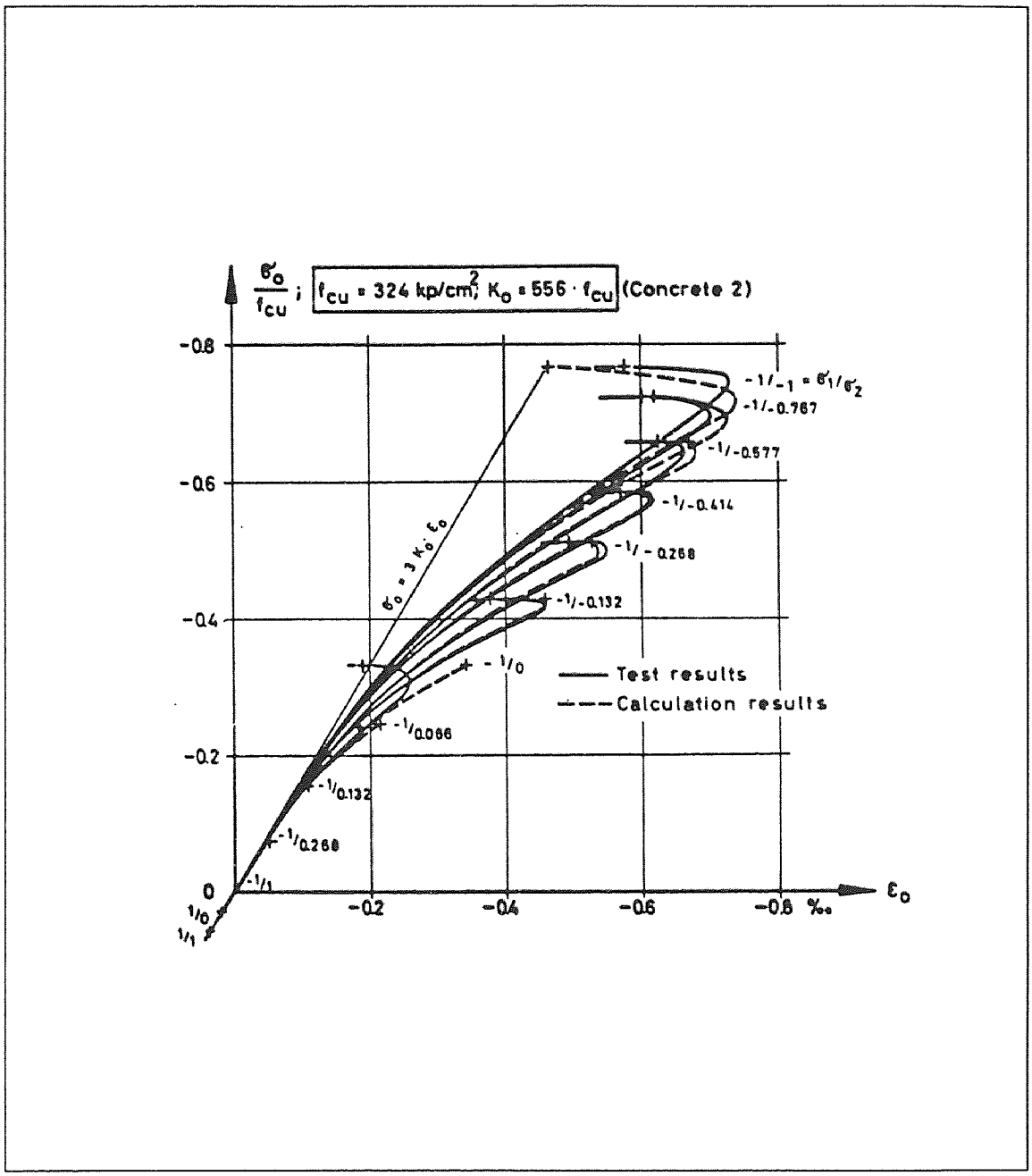


Fig. 2.4 Octahedral Normal Stress-Strain Relationship

(Kupfer and Gerstle (1973))

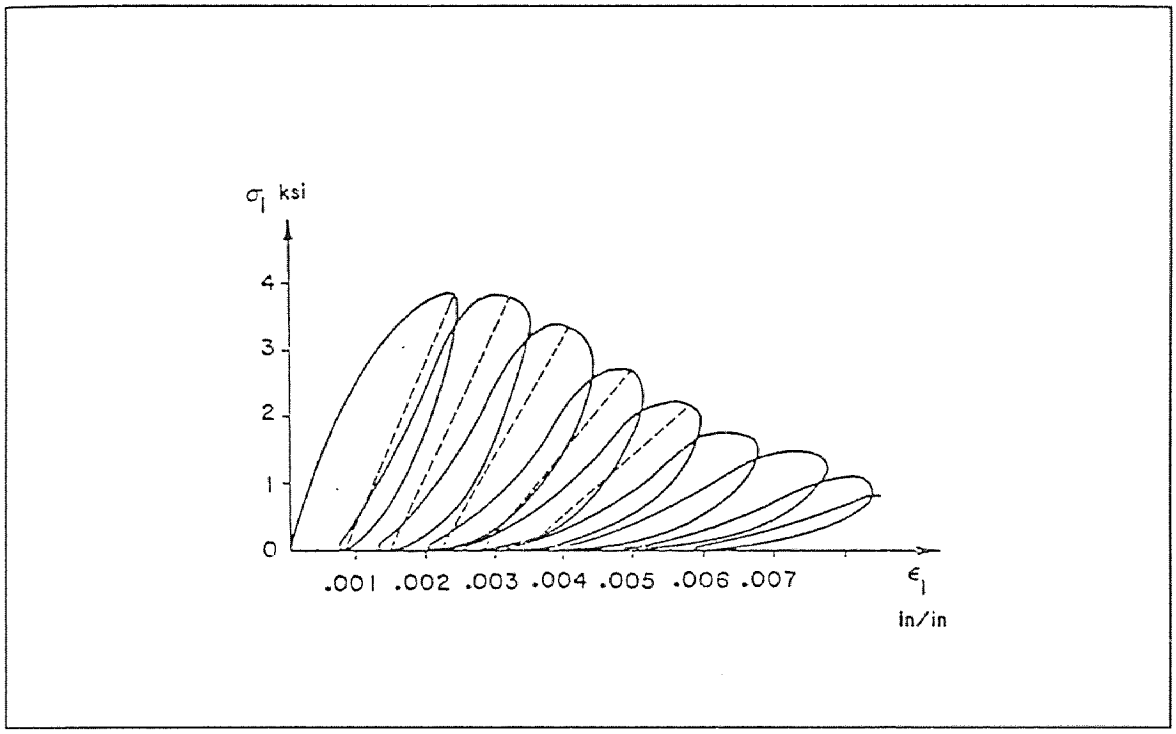


**Fig. 2.5** Cyclic Uniaxial Compressive Stress-Strain Curve (Sinha (1964))

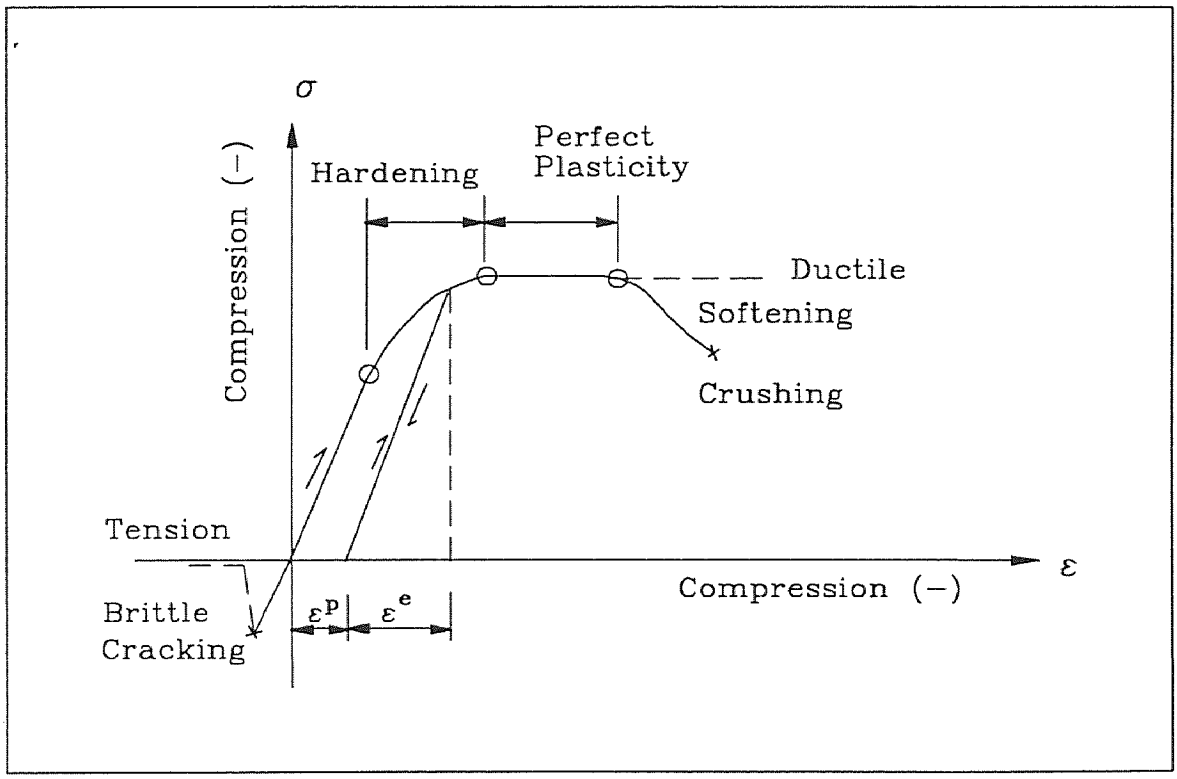


**Fig. 2.6** Schematic Stress-Strain Relation for Concrete

## 2.3 Literature Review

In recent years, a large variety of analytical models have been proposed to characterize the short-term, rate-independent stress-strain behavior of concrete materials. The existing approaches can be categorized as nonlinear elasticity theory, plasticity theory, continuous damage theory, and endochronic theory. Here only the basic ideas are reviewed.

### 2.3.1 Elasticity-Based Model

The nonlinear elasticity models assume that the nonlinear behavior of concrete can be represented by appropriately changing the tangent modulus (for incremental formulation of hypoelastic type) or changing the secant modulus (for total stress-strain formulation of Cauchy type and hyperelastic type). Among many propositions, the nonlinear incrementally orthotropic models (Darwin et al (1974), Liu et al (1972)) are based on the equivalent uniaxial stress-strain relationships. Different forms of material functions have been proposed to make the model more flexible in curve-fitting of the biaxial test data. The limiting state of the nonlinear elastic model is usually defined by a biaxial stress failure envelope. These nonlinear models can be applied to biaxial loading only. They give no information on the value of the third normal strain component. For triaxial analysis, the nonlinear elastic isotropic models have been proposed (Kupfer et al (1973) ,Cedolin et al (1977), Kotsovos et al (1978)). These models use stress(strain) dependent secant or tangent bulk and shear modulus. Based on experimental results, a consistent octahedral stress-strain relationship can be written for all states of stress, and a generalized bulk modulus and a generalized shear modulus can be used as the nonlinear material coefficients. Following the similar concept, Ottosen (1979) proposed a more general form of triaxial stress-

strain relation. In his model, a sophisticated failure surface (Ottosen (1977)) is used as the limiting surface, and a stress point inside this surface is mapped to a nonlinearity index. This index in turn corresponds to a secant elastic modulus. To simulate the volume expansion, the model allows the secant value of Poisson's ratio to increase proportionally if the index is larger than certain value. In a similar way, Ottosen's model even can handle the softening behavior (Ottosen (1982)).

In general, nonlinear elasticity models are simple to use, and usually can generate stress-strain response accurately if a broad data base is available. However, its applicability is restricted to a particular type of stress condition. Usually the material functions are directly determined from a curve-fitting procedure. There can be no guarantee of general usefulness outside the range that is covered by the data on which the rules are based. Moreover, this approach can not include the residual strain, and thus the unloading can not be considered. This greatly restricts the application of the approach from the fundamental point of view. Since even for a monotonic loading condition, local unloading often occurs during the progressive yielding and fracture of the concrete.

### 2.3.2 Plasticity-Based Model

In plasticity-based modeling, the number of unknowns is significantly reduced, which is credited to the postulated rules for inviscid elastic-plastic materials with work-hardening. The classical theory of plasticity is well-founded on a physical and a mathematical basis with a long history of successful applications in metals. Concrete exhibits a quasi-ductile behavior in compressive loading, and has a significant irrecoverable strain during unloading. The schematic stress-strain behavior is illustrated in Fig. 2.6. Thus, it is natural to apply the plasticity

theory to concrete. Suidan and Schonobrich (1973) first used this theory in concrete. In their work, the von Mises yielding criterion was used with augmentation of a tension-cut-off surface to account for the low tensile capacity of concrete. Following the similar idea, Drucker-Prager criterion and Mohr-Coloumb criterion were used with augmentation of tension-cut-off in many computer programs for concrete structural analysis (Argyris et al (1974), (1976)). Later it was recognized that these criteria predicted a much higher strength value than the experimental data. This was due to the fact that the straight meridians were used in the yield surfaces. Chen and Chen (1975) and Buyukozturk (1977) considered separate yield criteria for compression zone and tension zone, respectively, and used the curved meridians, which predicted the biaxial failure envelope with good accuracy. With more experimental investigations reported, the shape of failure surface became more and more clear. And the mathematical representations of failure functions were obtained ( Hsieh, Ting, and Chen (1982), Willam and Warnke (1974), and Ottosen (1977)). They are generally accepted failure surfaces. As soon as the failure function has been chosen, the yield function is usually assumed to have the same form but reduced in size. Thus, the constitutive relation can be formulated by the conventional approach that is used in metal.

The essential elements of any model based on classical plasticity theory are the yield criterion, the flow rule and the hardening rule. Because concrete is not an ideal elastic-plastic material, modifications and refinement must be made. To this end, much work around the above three aspects was done, such as the work by Han and Chen (1985). They used the non-proportional hardening rule and close-ended initial yield surface to solve the problem that previous models overestimated the plastic tensile strain for tensile loading and underestimated the compressive strain for confined compressive loading.

Torrent et al (1987) solved it through a different approach. Buyukozturk (1979) improved the volume expansion after the critical stress by using the non-associated flow rule and a dilantancy factor, which was a function of the hardening parameter.

The use of plasticity models of concrete behavior has many advantages. It accounts for the history-dependent behavior. Residual strain due to unloading can be evaluated. It allows unloading and reloading, thus provides rooms for modeling cyclic loading problems. However, one tremendous disadvantage for this model is that the strain softening behavior can not be evaluated in the traditional stress-space plasticity methods. This is because the softening behavior is a history of strain rather than stress. In the compression test, a complete stress-strain curve including the descending part can only be obtained under strain control condition. In this sense, the strain-space plasticity methods is needed for the studying of strain softening materials.

The possibility of formulating plasticity theory in strain-space was recognized by Drucker (1950). However, the details of a strain-space formulation were not completed. A strain space formulation of plasticity was first presented by Il'iushin (1961). Nevertheless, Il'iushin's work was not aimed at developing a new approach to the theory of plasticity, but rather to introduce a general plasticity postulate, which is less restrictive than Drucker's postulates, and has the advantage to treat simultaneously stable and unstable behavior of the materials. It is by Naghdi and Trapp (1975) and Casey and Naghdi (1981,1983a) that the significance of a strain-space formulation of plasticity is recognized. In their studies, new criteria for plastic loading were presented that were of general validity including the case of softening materials.

Meanwhile, Dougill (1976) adopted the strain-space formulation in developing an ideal material (the so-called progressively fracturing solid model).

He suggested a way in which a continuum theory may be devised to describe the effects of stable progressive fracture in a heterogeneous solid. Dafalias (1977a, b) examined the thermodynamic aspects of the work of Il'iushin, and he presented formulations which, for isothermal conditions, were similar to the ones presented by Naghdi and his coworkers. A different approach in the context of strain-space plasticity was followed by Yoder and Iwan (1981), who introduced a relaxed stress as an equivalent notion of the plastic strain. And they claimed that the stress-space and strain-space formulations of plasticity were equivalent. Although this conclusion does not hold according to Casey and Naghdi (1983b), it has been shown that many of the familiar features of stress-space plasticity can be carried over to the strain-space plasticity.

The attempt of strain-space plasticity in concrete was made by Bazant and Kim (1979). In their work, a Drucker-Prager formulation in strain space was adopted as the fracturing surface. Inspired by Bazant and Kim's work, Han and Chen (1986) discussed in details the strain-space plasticity formulas incorporating the fracture contribution to the loading surface. In their study, the loads before the peak load used the conventional stress-space loading surfaces. After the peak load, the stress-space loading surfaces were replaced by the strain-space loading surfaces for the descending part. The feature of volume dilatancy was used as a loading condition and the loading surfaces actually were the planes parallel to the $\pi$ plane. The shift from stress-space to strain-space at the peak point was good, but the simple loading surfaces for the softening part lost much information of deviatoric component. Further study in this aspect is needed.

Recently, there appeared two papers in the field of the strain-space plasticity-based approach. They introduced the loading surfaces in strain-space in different ways. Mizuno and Shigemitsu (1992) selected three-parameter Lade

type load function in stress space as a basis and derived the strain-space loading function by the method proposed by Naghdi and Trapp (1975). The loading parameter was defined directly as a function of plastic work through the tests of their own. Their model was developed to discuss the confined uniaxial loading case. For a general 3D situation, it inherits two problems: a) The initial loading surface is not closed along the negative hydrostatic axis. b) The relation between the loading parameter and plastic work is too difficult to obtain for general usefulness.

Pekau et al (1992) defined the peak strength state as an initial failure state and the fracture point state as a final failure state. They constructed the initial yield surface and initial failure surface using the test data of Kotsovos (1979). The final failure surface was assumed as an outward isotropic expansion surface with respect to the initial failure surface. They used the concept of closed initial yield surface. The contribution was no doubt by using a closed initial yield surface and the attempt to set up the surfaces in strain space directly through the experimental data. However, there are some problems: a) The strain state is too sensitive to the test environment. Thus, an accurate strain measurement in the multiaxial case is extremely hard to obtain at failure (Gerstle (1980)). It has been found that the existing data of strain state at ultimate strength are very scattered. Therefore, it is unsuitable for or not reliable to setting up a surface based on these test data at failure state. b) The loading surface can not be all closed according to the test results by Kotsovos (1979). c) Only an associated flow rule was used, which implies underestimating the plastic volume contraction. d) The assumed initial yield surface had little relation with the defined failure surface. This may result in an inconsistency in the constitutive equation for tension, and tension-compression regions.

**Table 2.1** Literature Review Chart for Plasticity Based Model

| *Stress-Space Plasticity* | *Strain-Space Plasticity* | |
|---|---|---|
| Classical Theory of Plasticity for Metals<br>Prager (1949): Loading Function, Loading-Unloading Criteria<br><br>Drucker's Postulates (1951): Consistency Condition, A Unified Method | Basic Theory of Strain-Space Plasticity<br>Drucker (1950): Possibility of Strain-space Formulation<br><br>Iliushin's Postulates(1961): Basis of Strain-Space Formulation, Less Restrictions | Dafalias (1977): Further Proof and Development<br><br>Naghdi et al (1975): Strain-space Formulation, Significance, And Comparison with Stress-space Formulation |
| In Concrete<br>Suidan and Schonobrich (1973): Introduce Plasticity to Concrete Von Mises Yield Surface with Tension-cut-off Cap for Tension<br><br>Chen and Chen (1975): Buyukozturk (1977): Separate Yield Criteria for Compression and Tension, Curved Meridian Loading Surfaces<br><br>Buyukozturk (1979): Non-associated Flow Rule, Dilatancy Factor<br><br>Han (1985), Torrental (1987): Closed Yield Surface, Non-proportional Hardening Rule | Bazant and Kim (1979): First Use Strain-space Plasticity to Concrete. Drucker-Prager Form in Strain Space<br><br>Han and Chen (1986): General Formulation, Volume Expansion as Loading Criteron for Strain Softening<br><br>Mizuno et al (1992): Use Naghdi's Method on Lade Type Surface, Confined Uniaxial Case<br><br>Pekau et al (1992): Define Strain Surface at Failure, From Existing Data | Dougill (1976): Special Formulation (Stiffness Degradation Included), Special Loading Surface and Hardening Relation<br><br>Yoder and Iwan (1981): Stress Relaxation Concept, Von Mise Form Loading Surfaces in Strain Space |

In summary, one more inherent disadvantage of these two recent constitutive models just mentioned is that too many parameters are needed to define the constitutive equation, thus the model are too complicated.

Table 2.1 shows a review chart for the plasticity-based model.

### 2.3.3 Continuous-Damage Model

Continuous damage mechanics was introduced by Kachanov (1958). He used the effective stress concept to model the creep rupture of metals. The effective stress concept has been applied to concrete by Krajcinovic (1979), Loland (1980), and Mazars (1981). Continuous damage mechanics is concerned with the description of progressive weakening of solids due to the development of microcracks and microvoids. The microcracking destroys the bond between material grains, affects the elastic properties, and may also result in permanent deformation. Many damage models were proposed (Krajcinovic et al (1981), Krajcinovic et al (1985), Ortiz (1985), Simo and Ju (1985), and Resende (1987)). A general continuous damage model has three essential parts: a set of independent internal variables, a set of equations of the stress to the strain and the internal variables, and a set of flow rules specifying the way in which the internal variables increase when loading proceeds. It has been realized that there are several facets of concrete behavior that cannot be represented by this type of model, most of all is the plastic flow caused by slip process.

### 2.3.4 Plastic-Damage Model

Since both microcracking and plastic flow are present in the nonlinear response of concrete, a constitutive model should address equally the two physically distinct modes of irreversible damages and should satisfy the basic postulates of mechanics and thermodynamics. The plastic-damage theory gives a unified

approach to the modeling of concrete. It was first proposed by Dragon and Mroz (1979), and Bazant and Kim (1979). This type of model generally has the advantages of both plasticity model and continuous damage model.

Within the general formulation of plastic-damage theory, two surfaces are established, a plasticity surface and a damage surface. This is accomplished by using the second law of thermodynamics, expressed in the form of the internal dissipation inequality. The two surfaces are then invoked simultaneously to obtain the increments of plastic strain and an additional strain due to damage. Sometimes, only one surface is used as a loading surface from which the sum of contributions of microcracking and plastic flow can be induced with the introduction of damage parameter into classical plasticity. This is why the plastic-damage theory (or plastic-fracturing theory) is generally considered in the category of plasticity. Recently, a lot of work were done in this field (Han and Chen (1986), Lubliner et al (1989), Frantziskonis et al (1987), and Yazdani et al (1990)). With the improvement of both plasticity method and damage approach, the new version of plasticity-damage model can be developed along the general line.

### 2.3.5 Endochronic Theory

The endochronic theory was originally proposed by Valanis (1971) in viscoelasticity and was first applied to concrete by Bazant et al (1976). It uses a strain-increment-dependent non-decreasing scalar variable, called intrinsic time to represent the evolution of the increase of irreversible damage from which the inelastic strain can be obtained. The intrinsic time measured is comparable to that of the effective plastic strain measured in plasticity theory. The theory does not require specific definitions of yielding or hardening. The inelastic strains are related to the intrinsic time through a series of mappings. The mapping functions

also depend on the current state of stress and strain and are determined from the experimental data. Consequently, the model is incrementally nonlinear. This type of model can cover many phenomena like nonlinear behavior, inelastic volume dilatancy, hydrostatic pressure sensitivity and strain-softening, etc. However, these can be achieved only at the expense of greater complexity and increasing number of material parameters, and the model involves many functions which are computed by a complicated optimal-fitting procedure. Besides , the incremental nonlinearity of the stress-strain relation is inconvenient for numerical structural analysis, which requires iterations within each increment of loading.

In short, each theory has its advantages and disadvantages. In this study, the strain-space plasticity theory will be used in modeling the nonlinear mutiaxial strain-hardening-softening behavior. Compared to the other sophisticated theories, plasticity is easier to use in application. It requires only a few typical experimental data to determine the material constants. It is a most flexible theory and most of the problems can be solved within the framework. Thus, it is currently the best choice for the numerical modeling and analysis of concrete structures. In the proposed model, the plasticity theory including the concept of plastic damage is used to model the nonlinear multiaxial strain hardening and softening behavior of concrete.

## 2.4 General Consideration of Strain-Space Plasticity Model

### 2.4.1 Advantages of Strain-Space Formulation

Stress and strain are two equally important quantities in studying the material properties. Their relationship is the so called constitutive equation for the material. Mathematically, there are two ways to express the relationship. One is

to use stress as basic variable and stress as function. The equation obtained is called stress-space formulation. The other is to use strain as basic input and stress as function. This later form is the strain-space formulation.

For the linear stage of material, Hooke's law is used, hence, one formulation can be derived from the other. They are equivalent. However, when material gets into nonlinear stage, especially when the material enters into strain softening region, these two versions do have some differences.

Consider a typical uniaxial stress-strain curve shown in Fig. 2.7. The material behavior is said to be stable along the ascending (hardening) part OP of the curve, and unstable along the descending (softening) part PQ. The feature of unstable behavior is that as the strain increases, the stress decreases, otherwise the material would accelerate to failure if the stress keeps constant. On the other hand, if the strain is decreased instead of increased at a point C in the descending part, the stress still decreases but now along an elastic unloading line CH. Reloading would trace back the unloading line until the yield stress at point C is reached. Such a complete stress-strain curve including the descending (softening) part can only be obtained from a test under strain control condition. Therefore, softening is a history of strain rather than stress which must be determined from the equilibrium at all times.

This one-dimensional unstable behavior is generalized to a multiaxial state of stress and strain in a similar manner to that of stable material. In stress space, a state of stress is represented by a point, as can be seen in Fig. 2.8(a). If a point A is on the loading surface $f = 0$ and the material is stable, a stress increment $d\sigma$ must be directed outward in order to induce a plastic as well as elastic increment of strain, otherwise an increment directed inward would cause elastic strain only. The outward motion of the stress point, which carries the yield surface along with it, corresponds to a hardening stress-strain curve for

increasing stress in one-dimension. On the other hand, if the material is unstable, plastic deformation causes the yield surface to shrink or move inward at the current stress point. This inward motion corresponds to a descending stress-strain curve for increasing strain in one dimension. For elastic unloading, too, the stress increment $d\sigma$ points inward of the loading surface. Hence, the stress space formulation presents difficulties in distinguishing between a reduction of stress which causes additional plastic deformation and one due to elastic unloading. In addition, Drucker's postulate, the basis of hardening plasticity theory does not work for unstable material, because the softening behavior appears not only in terms of a negative work done by the external agency along some path such as CD (Fig. 2.8(a)) but also as an inability to perform a stress cycle when starting from an unstable point such as C and producing some plastic deformation. Therefore, the alternative way to formulate the softening behavior is to use the concept of strain space and Il'iushin's postulate (1961).

It can be seen that at both points A and C in Fig. 2.7, the strain increment $d\varepsilon$ is always positive for plastic loading and negative for elastic unloading along AG and CH. A generalization to multi-dimensional strain space is shown in Fig. 2.8(b), where the loading surface, $F = 0$ is a function of strains. And for any strain point (A or C for example) on the loading surface, the strain increment $d\varepsilon$ directs outward, which represents the plastic loading, or inward, which represents the elastic unloading. There is no ambiguity. In addition, the strain space expression poses no problem in performing a strain loading cycle and Il'iushin's postulate can be used as a basis to formulate the constitutive relation for both hardening and softening behavior.

Besides the advantage that in the strain space a unified loading criterion can be proposed for both hardening and softening stages, such strain-space

formulation of plasticity also has following positive features: (1) The displacement method in finite element analysis of nonlinear structures is consistent with material expression in strain space. In the iteration process, the stresses do not need to be computed unless they are specifically desired. (2) For the method of variable stiffness iteration, the iterations can be performed in both the hardening and softening stages when strain is used as the variable. (3) When the stiffness matrix is formed at the midpoint value of strain or stress of the preceding load step, the results in strain space are better, particular in the region near the ultimate strength. A good and clear statement of the advantages about the strain-space plasticity can be found in Naghdi et al (1975) and Yoder et al (1981).

Having above attractive merits, in this study, the strain-space plasticity theory is chosen as the basis to set up a relatively comprehensive model to describe the behavior of concrete including both strain hardening and strain softening. For metals and other materials with the same properties in compression and tension, the application of the strain-space plasticity method has been successfully proved. Its use in concrete is relatively new. The pioneer work of Bazant et al (1979) and Han et al (1986) showed the promising and feasibility in comprehensive and further research.

### 2.4.2 Current Status on Strain States of Concrete

Although the strain-space formulation has the above advantages, it has one tremendous disadvantage that very few test data are available for the strain states of concrete. Thus relatively less is known about the strain states behavior under multiaxial loadings, which makes it difficult to set up loading surfaces of the strain-space plasticity theory. In multiaxial space, whether in stress space or in strain space, a surface is used to define the state of a material. For example,

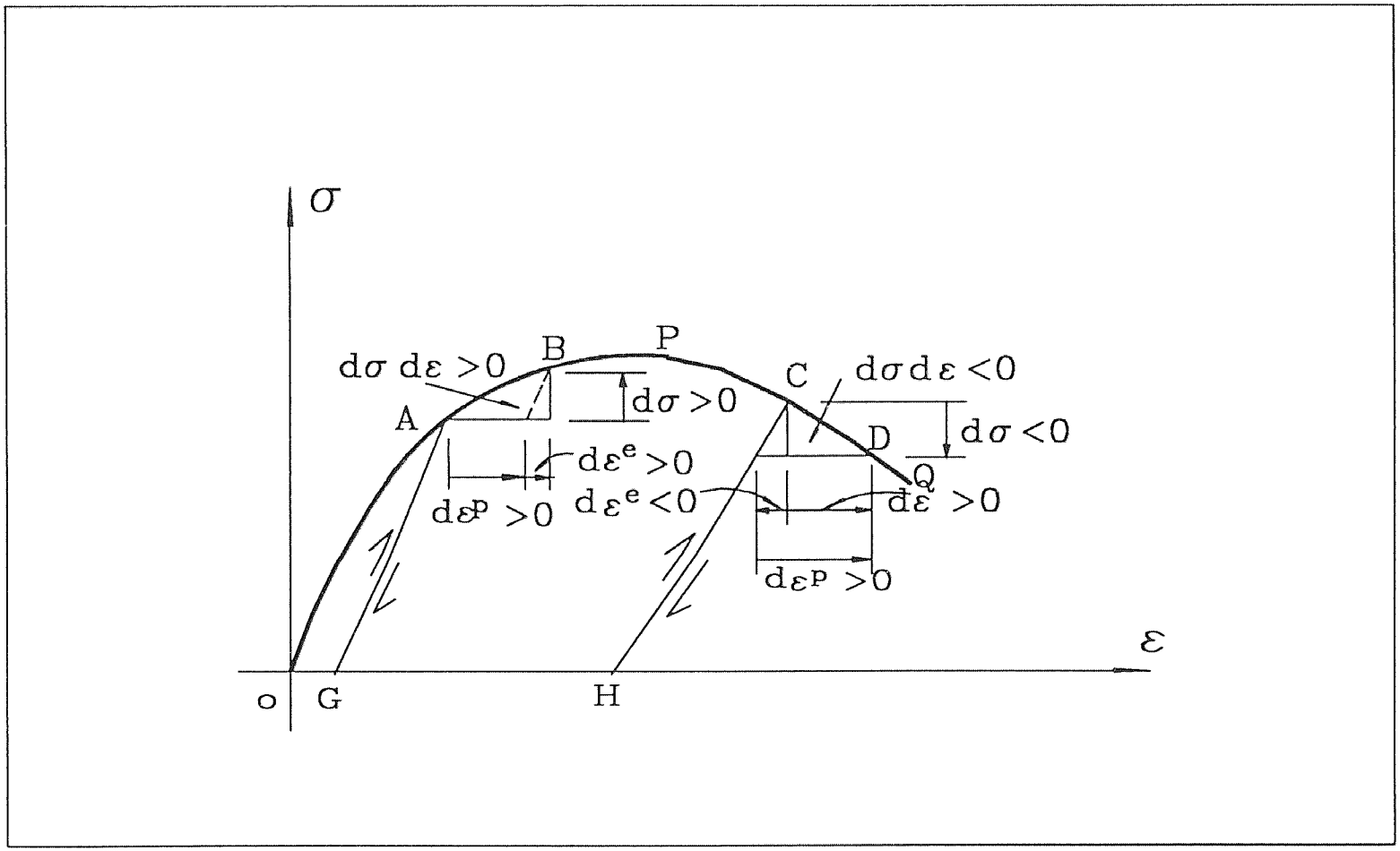


**Fig. 2.7** Features of Softening Behavior

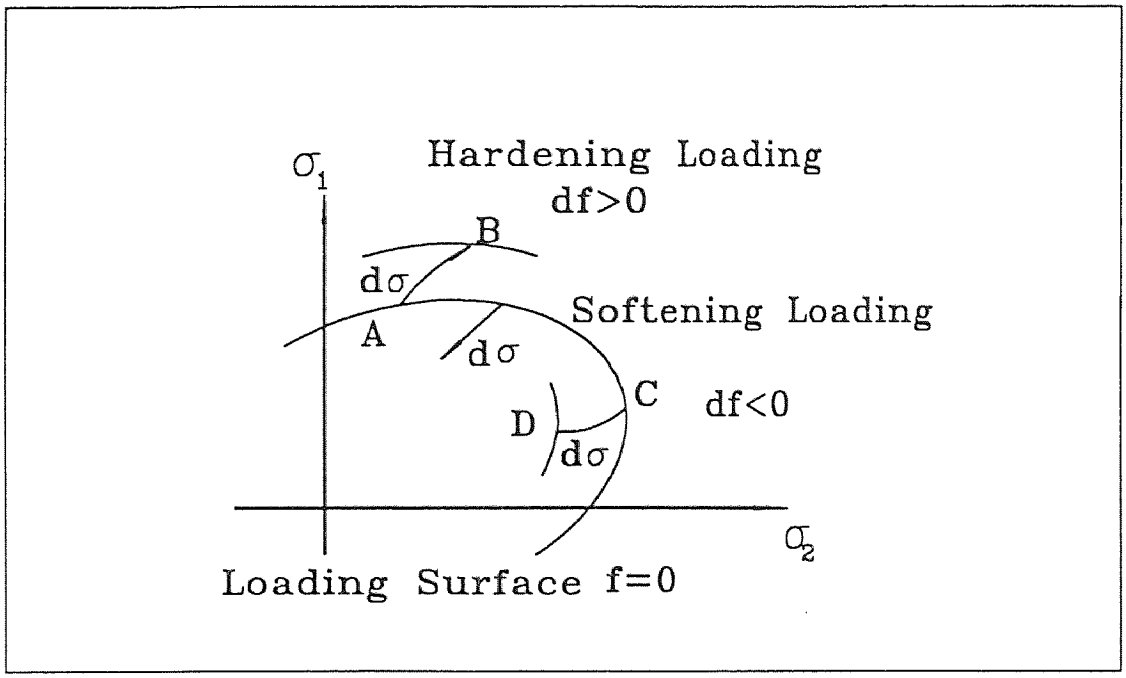


(a) In Stress Space

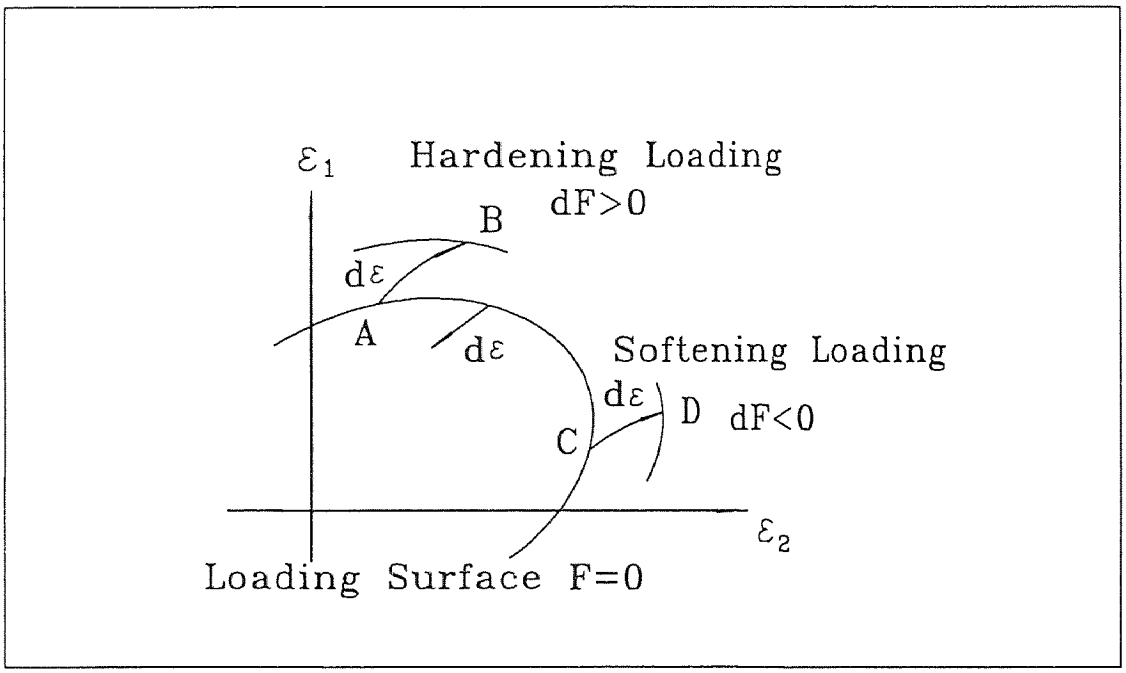


(b) In Strain Space

**Fig. 2.8** Loading Surfaces Defined in Stress and Strain Space

a failure surface in stress space defines the ultimate strength for any ratio of stresses. Table 2.2 gives the information about the important states of concrete in both stress space and strain space. It shows that in stress space, the function of failure surface is considered known and it has actually been used widely, while in strain space, little is known. Although many researches have been done in this aspect, the results are far from satisfactory. To completely and accurately analyze the strain states of concrete, a compressive experimental research is needed with strain-controlled testing methods. Almost all the existing multiaxial test data are obtained from the stress-controlled tests. At present situation, a good attempt may be made to quantitatively analyze the strain states by extracting information from the existing data together with appropriate assumptions. Then check and verify the derived equations with the test data.

### 2.4.3 Initial and Subsequent Yield Surfaces

Yield criterion defines the elastic limit in a multiaxial stress state or the corresponding strain state. For metals, the yield condition can generally be determined by tests. However, for concrete, yield stress or yield strain is a matter of definition and is usually a fictitious quantity that is used only for the convenience of mathematical constitutive model. In a stress-space analysis of concrete, due to the fact that the failure surface is known, many previous plasticity models assume that the yield surface has a similar shape to that of failure surface but with a reduced size, as shown in Fig. 2.9. Then, shape-modification technique was added (Han et al (1985)). It has been generally accepted that a close-ended initial yield surface like that in Fig. 2.10 is much more reasonable.

If a similar concept is carried over to the strain space, the key problem is to have a surface in strain space like the failure surface in stress space. In the

present model, such a surface will be chosen and set up at the critical stress point according to the test data. This surface will be used as a reference surface to define the initial yield surface and subsequent yield surfaces and also a surface corresponding to the peak strength, which is the boundary between the strain hardening and strain softening.

**Table 2.2** Little Is Known About Strain States Under Multiaxial Loadings

| | | Elastic Limit | Critical stress | Ultimate strength | Fracture |
|---|---|---|---|---|---|
| U-C | Stress | *** | *** | *** | *** |
| U-C | Strain | *** | *** | *** | *** |
| M-C | Stress space | ** | ** | *** | |
| M-C | Strain space | * | * | * | |

U-C is for uniaxial case and M-C for multiaxial case.
*** has been completely studied; ** has been partially studied;
* has been little studied; and blank is nothing that has been worked out..

In this study, the initial yield surface with a closed shape is assumed and a non-proportional hardening rule is adopted. Fig. 2.11 shows the meridians of the initial and subsequent yield surfaces, which expand as well as change the shapes. Each of these surfaces corresponds to a certain value of hardenig parameter. It also shows that the curvature of the meridians is reduced from its maximum at an initial yield surface to zero at the peak strength. At the post peak stage, the loading surfaces are assumed to move horizontally along the positive hydrostatic strain axis.

### 2.4.4 Hardening and Softening Control

The loading surfaces intersect the uniaxial compressive loading path. Then each hardening parameter can be mapped to a certain value of effective strain and it corresponds to a plastic modulus given by the experiment uniaxial compressive plastic stress-strain curve (Fig. 2.12). However, it has been found out that the plastic modulus defined by this approach can not predict the plastic stress components adequately. Hence, a modification factor, as a function of the volumetric stress and lode angle has been introduced to account for the hydrostatic pressure sensitivity behavior. Then, the plastic modulus used is equal to the original value multiplied by this factor.

In strain space, strain softening and strain hardening essentially have no much difference. Softening is only a continued hardening after the stress state reaches the ultimate value. In this model, the elastoplastic coupling or the stiffness degradation is considered in the softening stage in a way analogous to that of Han et al (1986).

### 2.4.5 Non-Associated Flow Rule

A non-associated flow rule is used to account for the large volume expansion of the material. Here, a Drucker-Prager type of plastic potential with the dilatancy factor taken as a function of hardening parameter has been assumed.

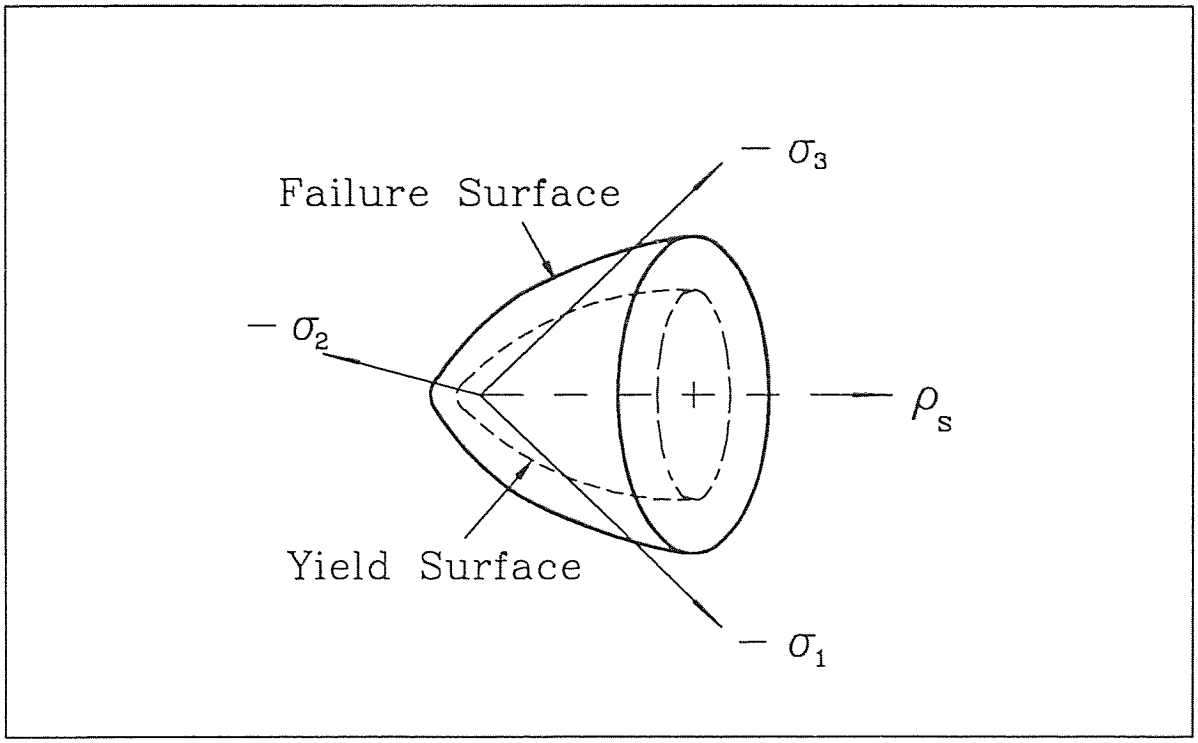


**Fig. 2.9** Yield Surface with Open End

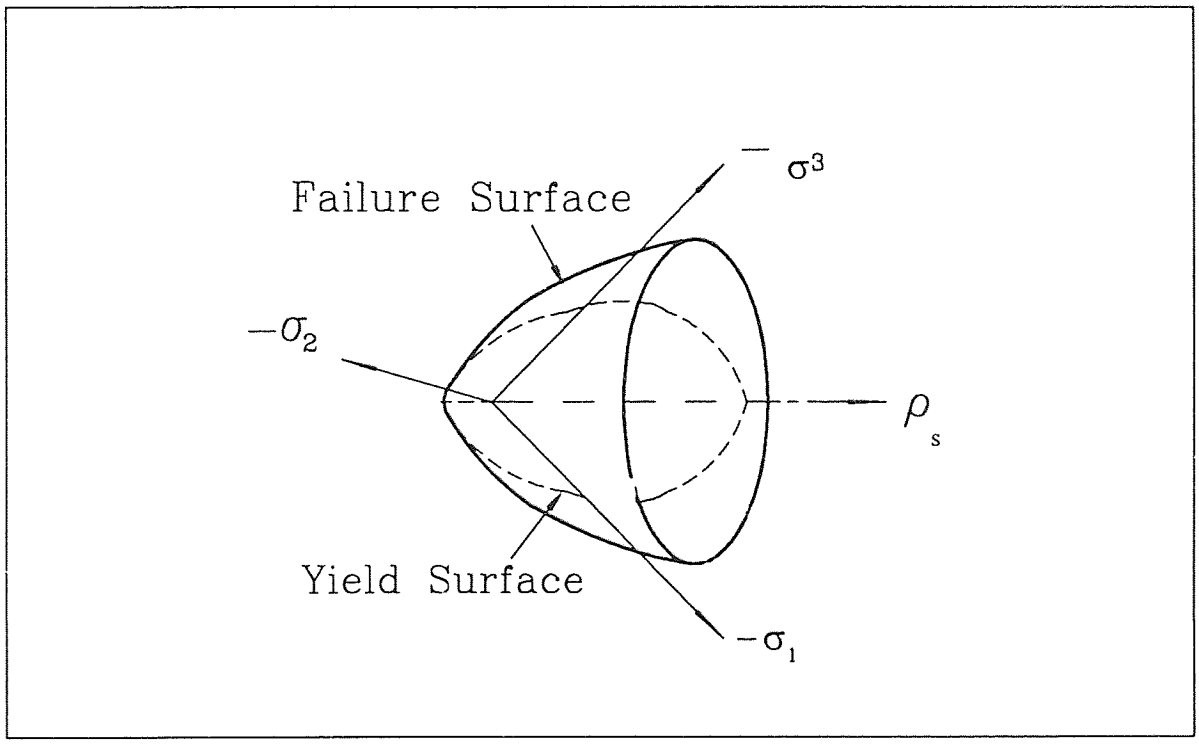


**Fig. 2.10** Yield Surface with Closed End

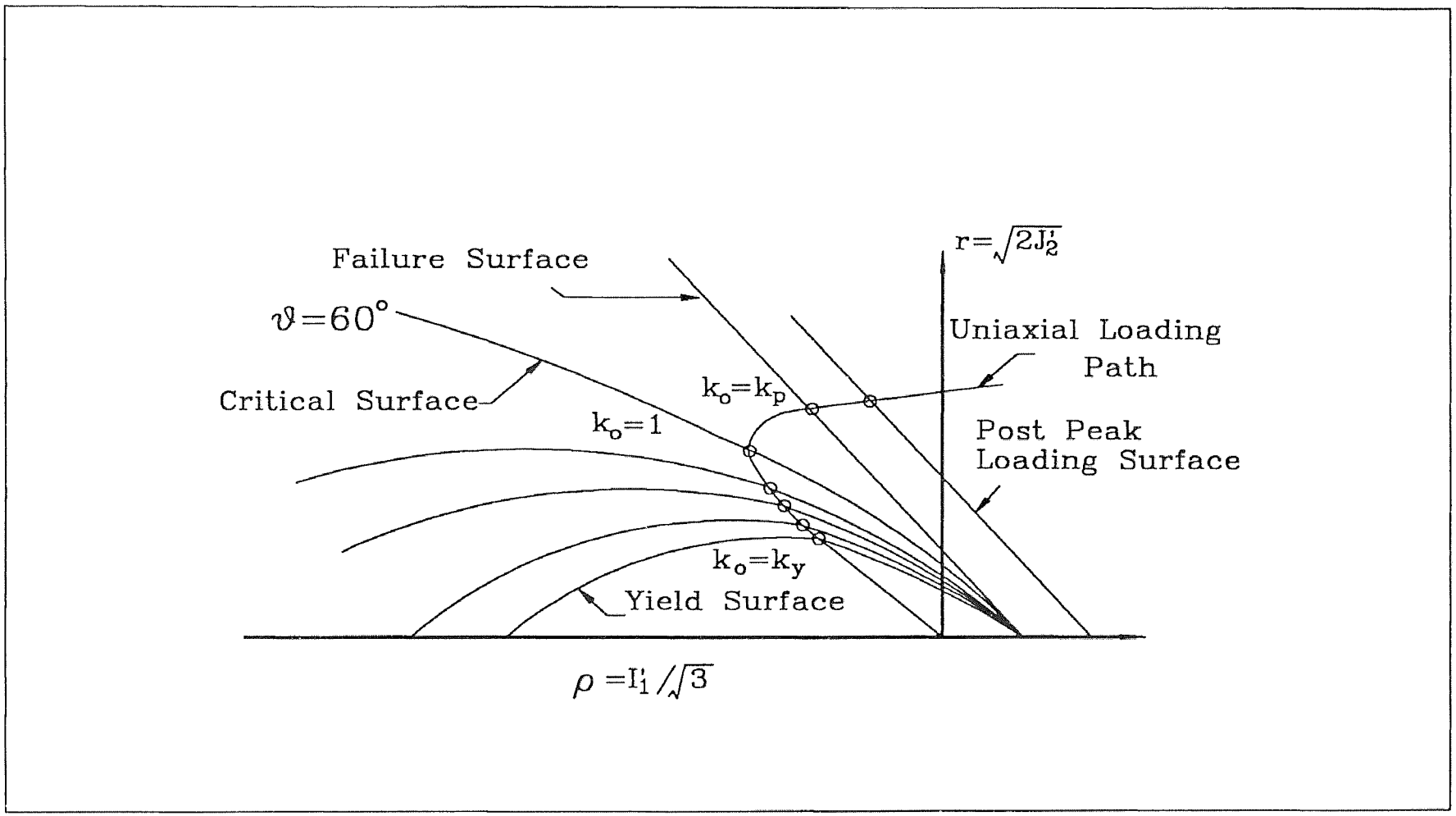


**Fig. 2.11** Loading Surfaces of Modified Isotropic Hardening

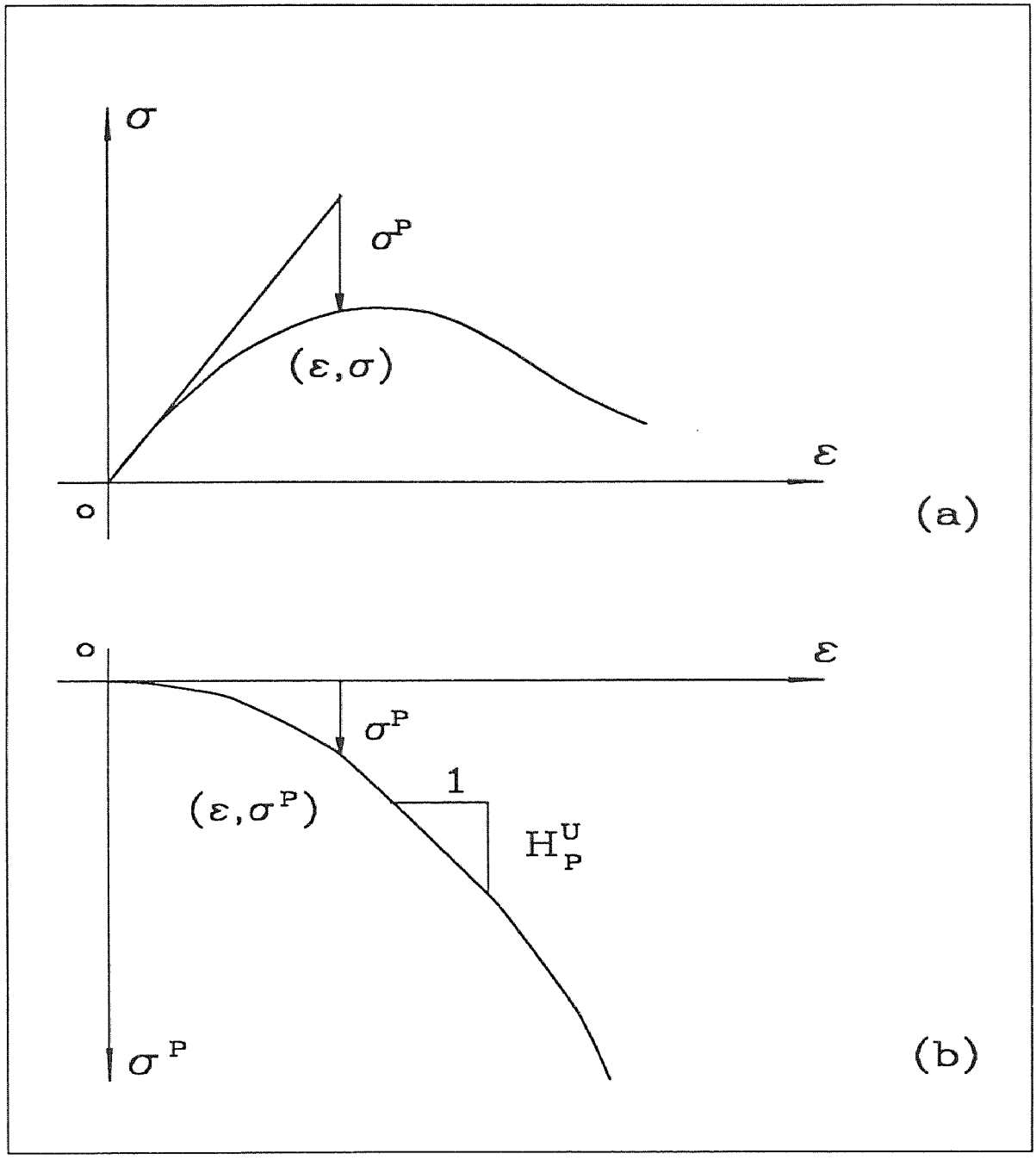


**Fig. 2.12** Plastic Stress-Strain Relationship

# CHAPTER 3

# STRAIN-SPACE CRITICAL SURFACE

## 3.1 Introduction

In plasticity theory, the yield surface is a basic input of the material. For concrete, yield criterion is a matter of definition and is usually a fictitious quantity. It is used only for the convenience of mathematical modeling. The general method in stress-space plasticity is using the failure surface as a reference surface and defining the yield surface according to the failure surface. The precondition for using this approach is that the reference surface is available. If the yield surface in strain space is constructed in a similar way, a strain-space reference surface is a must. Unfortunately, very little quantitative information about strain state is known. Now the problem becomes where and how to set up the strain-space reference surface. To best describe the material, the reference strain state should be the one with an important physical meaning. Also it must be relatively easy to be constructed, and convenient to set up other surfaces.

## 3.2 Strain-Space Critical Surface

### 3.2.1 General

At the strain state during failure, the physical meaning is clear. It is naturally considered as a possible reference surface. Analysis was made of available test data of the strain state at the ultimate strength. But the result were very scattered. The basic reason is that when the load approaches the peak value, the stress state changes very little, while the strain state increases sharply, Thus the stress-strain curve becomes flat and close to the horizontal line. This makes

it very difficult to determine the right strain state at peak strength. Further, the brittle failure of concrete makes the obtained data not reliable (Gerstle (1980)). In view of the loading system, the strain state is too sensitive to the test environment. In short, an accurate strain measurement in the multiaxial loading system is very hard to obtain when approaching the ultimate strength state. Although with special attention, a good result may be obtained like that of Kotsovos et al (1979), in practical use, the strain state at failure of a specific concrete still suffers from the instability of strain state when trying to obtain the basic input data. Because of this, the failure state in strain space is not chosen as a reference surface. This was unexpected before performing the data analysis on strain states of concrete.

Another important strain state is called the critical stress (Richard (1929)), which corresponds to the minimum volumetric strain. The experimental data at the critical stress are much more reliable. According to Shah et al (1968), when the stress is beyond the critical stress, there is a sharp increase in the length of continuous cross-linked microcracks. And this will cause concrete dilatation. They pointed out that macroscopically, the critical stress is related to strengths of concrete under short-term , repetitive and long-time loading, respectively. This critical stress also affects the fracture toughness in a microscopic sense. It indicates the beginning of significant slow crack growth. The states at the critical stress was called 'onset of unstable fracture propagation' (OUFP) in the work of Kotsovos and Newman (1977). And Newman and Newman (1972) used it for an upper bound failure criterion.

Since the critical stress is such an important material parameter, discussions of the corresponding strain states in a multiaxial case, which can be called the critical strain state, is of significance. The corresponding surface in a

strain space herein is called "the critical surface", which is selected as a reference surface for the strain-space yield surface.

At present, the strain state at the critical stress is not fully understood. The test data are very limited and restricted mainly on the two situation: (1) $\varepsilon_1 = \varepsilon_2 > \varepsilon_3$, and (2) $\varepsilon_1 > \varepsilon_2 = \varepsilon_3$. A quantitative expression of the critical surface can only be achieved through appropriate assumption based on the existing test data.

### 3.2.2 Mathematical Preliminaries

The critical strain state for an isotropic and homogeneous material can be expressed in terms of three principal strains as

$$f(\varepsilon_1, \varepsilon_2, \varepsilon_3) = 0 \tag{3.1}$$

where $\varepsilon_1, \varepsilon_2, \varepsilon_3$ are the principal strains. The tensile strains are considered to be positive. It is convenient to use invariants of the strain tensor $\varepsilon_{ij}$ and to use the Haigh-Westergaard coordinate system.

For this purpose, any point $P(\varepsilon_1, \varepsilon_2, \varepsilon_3)$ in the strain space is described by the coordinates $(\rho, r, \theta)$, in which $\rho$ is the projection on the unit vector $\bar{e} = (1, 1, 1) / \sqrt{3}$ on the hydrostatic axis, and $(r, \theta)$ are polar coordinates on the deviatoric plane, which is orthogonal to vector (1, 1, 1) (Fig. 3.1).

It can be proved that

$$\rho = |\overline{ON}| = I_1' / \sqrt{3}$$

$$r = |\overline{NP}| = \sqrt{2J_2'}$$

$$\theta = \cos^{-1} \frac{\sqrt{3} e_1}{2\sqrt{J_2'}} \quad \text{where}$$

$$e_1 = \varepsilon_1 - I_1'/3 \quad \text{for} \quad \varepsilon_1 > \varepsilon_2 > \varepsilon_3$$

$$I_1' = \varepsilon_1 + \varepsilon_2 + \varepsilon_3$$

$$J_2' = \tfrac{1}{6}[(\varepsilon_1 - \varepsilon_2)^2 + (\varepsilon_2 - \varepsilon_3)^2 + (\varepsilon_3 - \varepsilon_1)^2]$$

in which, $\rho$ represents the hydrostatic component, $r$ is a deviatoric component, and $\theta$ is called Lode angle. $I_1'$ is the first strain invariant and $J_2'$ is the second deviatoric strain invariant.

Therefore, Eq.(3.1) can be stated more conveniently as

$$f(\rho, r, \theta) = 0 \tag{3.2}$$

Assume that the concrete is an isotropic material, the labels 1, 2, 3 attached to the coordinate axes are arbitrary. Thus, the cross-sectional shape of the surface must have a threefold symmetry shown in Fig. 3.1(a). Therefore, it is necessary to explore only the sector from $\theta = 0^o$ to $\theta = 60^o$, the other sectors can become known by symmetry.

### 3.2.3 General Properties of Critical Surface

In an experimental determination of critical surface, as it appears in the Haigh-Westergaard coordinate system of Fig. 3.1, $\theta = 60^o$ meridian ($\varepsilon_1 = \varepsilon_2 > \varepsilon_3$) and $\theta = 0^o$ meridian ($\varepsilon_1 > \varepsilon_2 = \varepsilon_3$) are essential to construct such a surface. On the basis of test data by Kupfer et al (1969), Hobbs (1974), Green and Swanson (1973), Jiang et al (1991), Gerstle (1980), Tasuji et al (1978), Schickert and Winkler (1977), Ferrara et al (1976), and by Kotsovos and Newman (1979), the 0 and 60-degree meridians are found by the regression curves as illustrated in Figs. 3.2 and 3.3. In Fig. 3.2, since the data are from different tests, all the reading are nondimensionalized by the uniaxial strain value at the critical

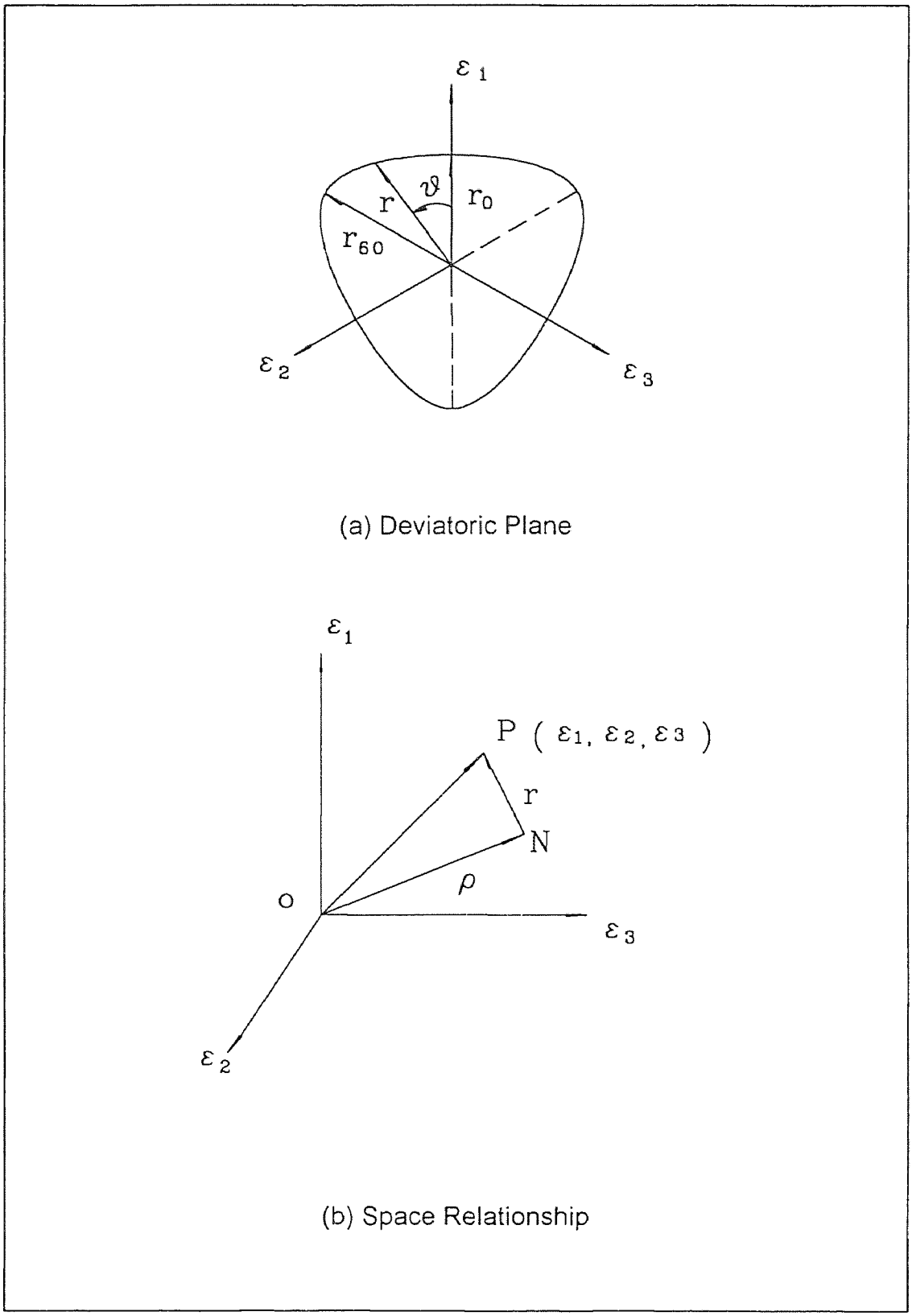


**Fig. 3.1** Haigh-Westergaard Strain Space

stress. Both figures show that the meridians are curved, smooth, convex and $r$'s value increases with increasing hydrostatic strains $\rho$, and that $r_o/r_{60}$, where the indices 0 and 60 represent 0 and 60 degree meridians respectively, lies between 0.5 and unity.

From these features, one may conclude that the critical surface in strain space is a cone shape with smooth curved meridians and convex sections between circular and triangular shapes on the deviatoric strain plane.

### 3.2.4 Formulation of Critical Surface in Strain-Space Domain

With the analogy of the strain-space critical surface to that of the stress-space failure surface of concrete, similar mathematical formulations from the available stress-space failure surface is found useful. A possible critical surface function in Hsieh-Ting-Chen form is given below (Hsieh, Ting, and Chen 1982).

Fig. 3.4 shows a possible critical surface cross-section on the deviatoric plane. For a constant value $k$, $r\cos\theta = k$ represents an equilateral triangle, and $r=k$ is a circle on the deviatoric plane with $|\theta| \le 0$. Hence, for given two positive constants $\alpha, \beta$ with $\alpha+\beta=1$, a combined equation $r(\alpha\cos\theta+\beta) = k$ yields a smooth function between $|\theta| \le 60^o$ on the deviatoric plane and it is bounded by the two extremes of equilateral triangular and circular shapes $(\alpha=0, \beta=0)$. Recall the convex meridians in Figs. 3.2 and 3.3. This indicates that for a constant value of $\theta$ and $r$, there is a nonlinear parabola-like function of $\rho$. Hence, $\rho$ and $r^2$ terms are added and the resulting form is given by,

$$f(\rho, r, \theta) = ar^2 + (\alpha\cos\theta+\beta)r + c\rho - 1 = 0 \qquad (3.3)$$

where the parameter can be nondimensionalized by using the uniaxial compressive strain value at critical stress. The four parameters $a$, $\alpha$, $\beta$ and $c$ are material constants, which need to be evaluated.

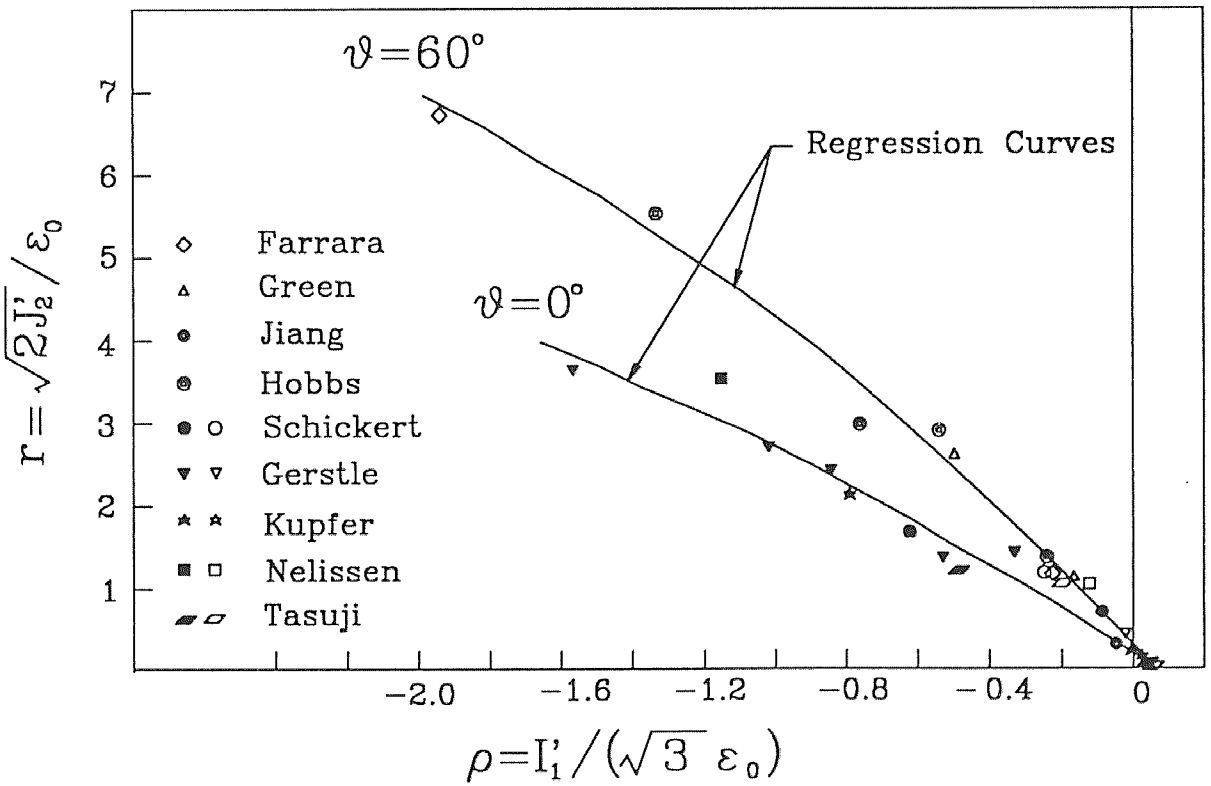


**Fig. 3.2** The 0° and 60° Meridians from Existing Data

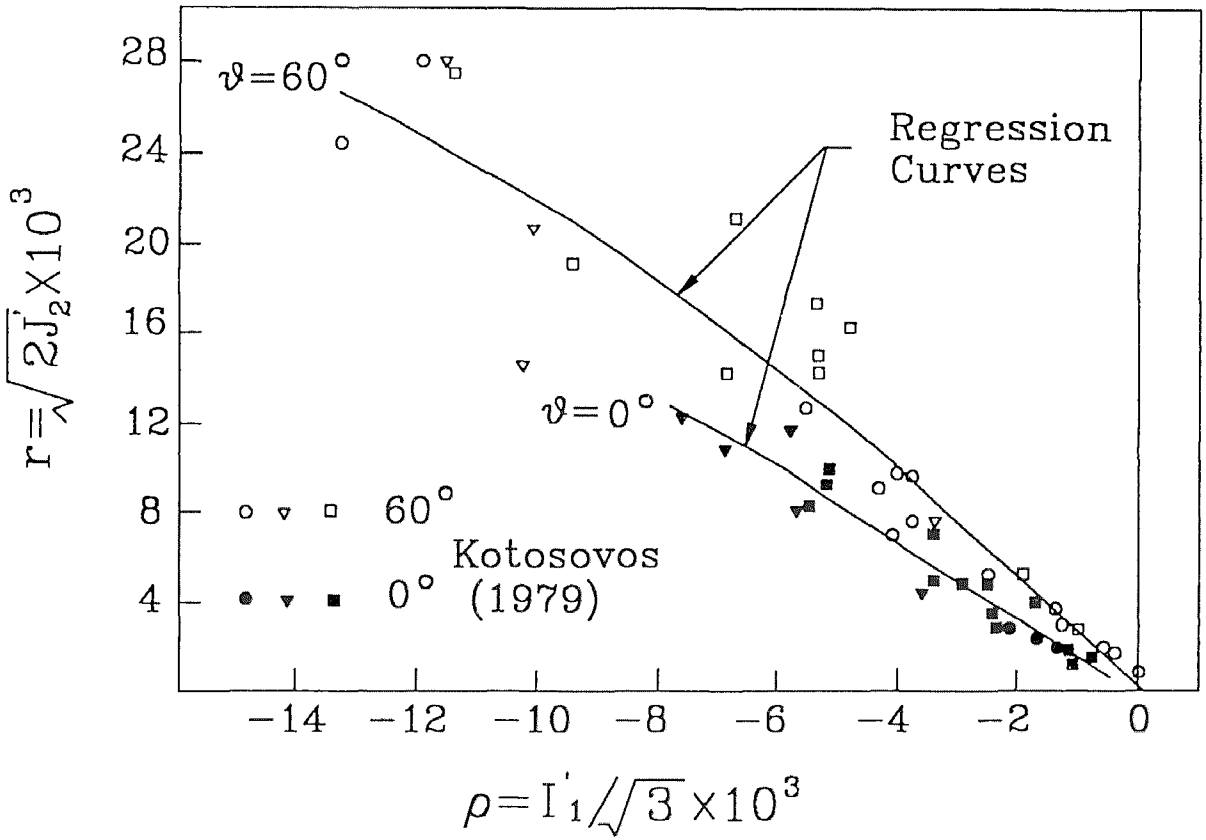


**Fig. 3.3** The $0^o$ and $60^o$ Meridians from Kotsovos and Newman (1979)

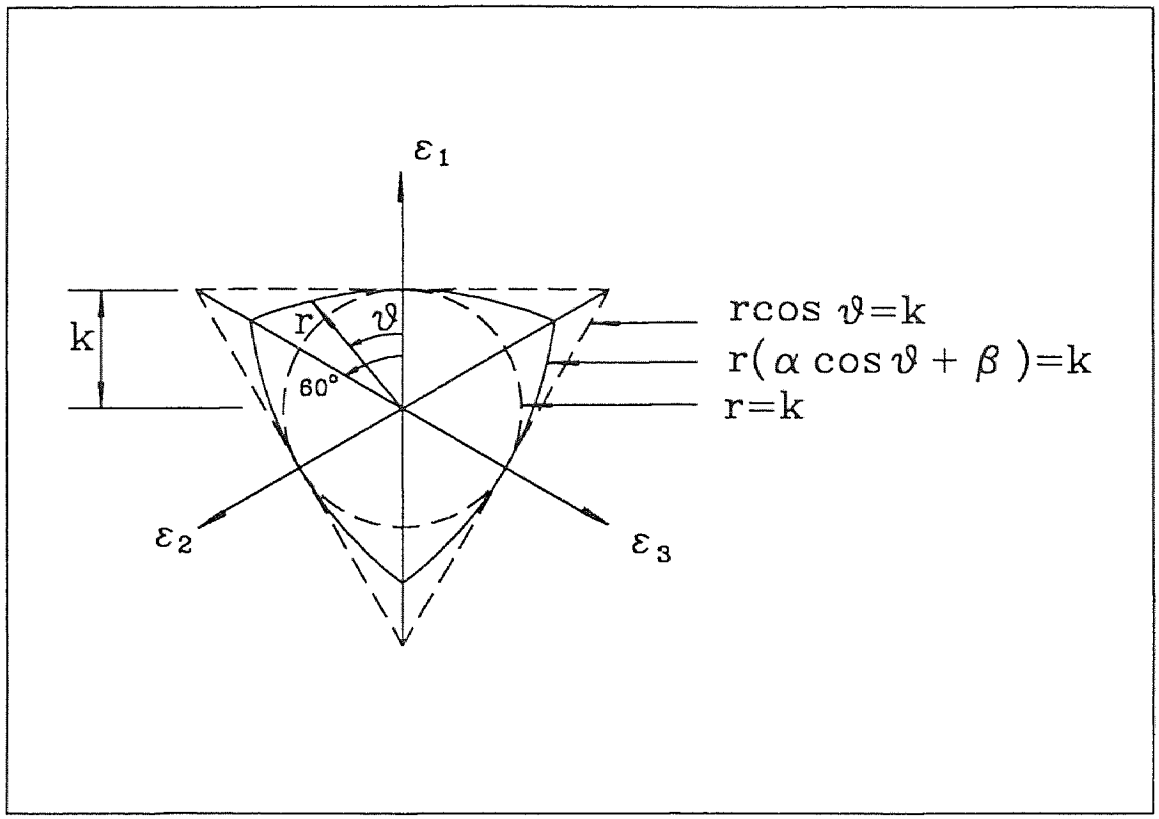


**Fig. 3.4** Geometry on the Deviatoric Plane

### 3.3 Determination of Material Constants

To determine the above mentioned four material constants in Eq. (3), four typical points on the critical surface are needed. They can be chosen corresponding to the four conditions of test: uniaxial compression ( $\varepsilon_1 = \varepsilon_2 > 0, \varepsilon_3 < 0$ ), uniaxial tension ( $\varepsilon_1 > 0, \varepsilon_2 = \varepsilon_3 < 0$ ), biaxial compressions ( $\varepsilon_1 > 0, \varepsilon_2 = \varepsilon_3 < 0$ ), and a triaxial compression ( $\varepsilon_1 \geq \varepsilon_2 \geq \varepsilon_3$ ).

With these test data, the critical surface of a concrete can be fully determined.

However, it is not an easy task to do all these four material tests at present stage, especially the tension and triaxial compression tests. In view of

lacking of basic test data, the following method is suggested to approximately calculate the results of tensile tests from the uniaxial compression result. This approximate method is based on assumptions: 1) When under tension, the strain states deviate little from those computed with Hooke's law (Kupfer et al (1969), Wastiels (1979)). 2) Tensile strength in one direction is not affected by the tensile actions on the other direction (Ahmad (1981), Tasuji et al (1978)). 3) Under tensile action, the critical strain state can be chosen to be about 95 percent of the strength. 4) The uniaxial tensile strength is approximately equal to $f_t = 0.295\,(f_c')^{\frac{2}{3}}$ , ( $f_t$ and $f_c'$ are in $N/mm^2$ ) (Wastiels (1979)).

Further, the poisson's ratio and the modulus of elasticity in tension are assumed to be the same values as those in tension, respectively. With above assumptions, the strain state at the critical stress in tension can be computed approximately by using the Hooke's law.

The confined uniaxial compressive test can give a point under triaxial compression. In the case of no triaxial compressive data, $\left( \frac{I_1'}{(\sqrt{3}\varepsilon_o)} , \frac{\sqrt{2J_2'}}{\varepsilon_o} \right) = (2, 6.3)$ on the 60-degree meridian can be used, which seems to give the best fit to the test results by Kupfer et al (1969). $\varepsilon_o$ here is the strain at critical stress on the uniaxial compressive stress-strain curve.

### 3.4 Verification and Discussion of Formulated Surface

From the limited available test data, the parabola-like meridians are obtained. According to the 0 and 60 degree meridians together with the reasonable deduction, the general shape of critical surface is given in Eq. (3.3). To verify that Eq. (3.3) is valid for the strain combination not on the 0 or 60 degree meridians, comparison is needed between the test data and prediction of the

formula proposed. The most efficient way is to check on the deviatoric plane. Test results of Kupfer et al (1969), Schickert and Winkler (1977),and Nelissen (1972) are adopted.

### 3.4.1 Comparison with Test Data of Kupfer et al (1969)

The material constants used are modulus of elasticity *E=31700 MPa;* Poisson's ratio $\mu = 0.22$ ; uniaxial compressive strength $f_c' = 32.2\ MPa$ and the strain at the critical stress for uniaxial compression $\varepsilon_o$= 0.00153 *m/m.*

Table 3.1 gives the four basic input points to determine the critical surface. The four constants are determined as shown in Table 3.2. Fig. 3.5 shows the comparison between the test points and the predicted results.

**Table 3.1** Basic Input for Kupfer et al 's Critical Surface

| | $r$ (0.001) | $\rho$ ( 0.001) | $\theta$ (degrees) |
|---|---|---|---|
| Uniaxial Compression | 1.5690 | -0.4307 | 60 |
| Biaxial Compression | 3.3117 | -1.1605 | 0 |
| Uniaxial Tension | 0.1050 | 0.043 | 0 |
| Triaxial Compression | 9.6390 | -3.060 | 60 |

**Table 3.2** Critical Surface Constants of Kupfer et al 's

| $a$ | $\alpha$ | $\beta$ | $c$ |
|---|---|---|---|
| 5015.0 | 2434.0 | 2442.0 | 11350.0 |

### 3.4.2 Comparison with Test Data of Schickert and Winkler (1977)

The material constants used include modulus of elasticity $E$ = 22000 *MPa;* Poisson's Ratio $\mu = 0.24$; uniaxial compression $f_c' = 30.6\ MPa$; and the uniaxial strain at the critical stress $\varepsilon_o = 1.06\ m/m$.

Table 3.3 gives the basic input points to determine the critical surface and Table 3.4 contains the surface constants. Fig. 3.6 shows the comparison between the test points and predictions.

**Table 3.3** Basic Input for Schickert et al' s Critical Surface

| | $r$ (0.001) | $\rho$ ( 0.001) | $\theta$ (degrees) |
|---|---|---|---|
| Uniaxial Compression | 1.2125 | -0.303 | 60 |
| Biaxial Compression | 1.727 | -0.650 | 0 |
| Uniaxial Tension | 0.104 | 0.042 | 0 |
| Triaxial Compression | 6.678 | -2.120 | 60 |

**Table 3.4** Critical Surface Constants of Schickert et al 's

| $a$ | $\alpha$ | $\beta$ | $c$ |
|---|---|---|---|
| 20000.0 | 2428.0 | 2491.0 | 11624.0 |

### 3.4.3 Comparison with Test Data of Nelissen (1972)

The material constant used are modulus of elasticity $E$ = 3570000 *Psi* ; Poisson's ratio $\mu = 0.2$, and compressive strength $f_c' = 2923\ Psi$ . The strain of uniaxial compression at the critical stress is $\varepsilon_o = 0.839\ m/m$.

Table 3.5 contains the basic input points for the critical surface, and Table 3.6 gives the constants of the surface. Fig. 3.7 shows the comparison between Nelissen's test points and the formula predictions.

**Table 3.5** Basic Input for Nelissen' s Critical Surface

| | $r$ (0.001) | $\rho$ ( 0.001) | $\theta$ (degrees) |
|---|---|---|---|
| Uniaxial Compression | 0.887 | -0.199 | 60 |
| Biaxial Compression | 3.055 | -0.968 | 0 |
| Uniaxial Tension | 0.1058 | 0.0374 | 0 |
| Triaxial Compression | 5.034 | -1.678 | 60 |

**Table 3.6** Critical Surface Constants of Nelissen 's

| $a$ | $\alpha$ | $\beta$ | $c$ |
|---|---|---|---|
| 35000.0 | 2641.0 | 2323.0 | 11471.0 |

### 3.4.4 Strain State of High Hydrostatic Compression

The experimental points and the prediction by Eq. (3.3) on the deviatoric plane are shown in Figs. 3.5~3.7. It can be seen that the prediction is satisfactory.

In stress-space analysis, the concrete undergoes no failure in a hydrostatic compressive state $\sigma_1 = \sigma_2 = \sigma_3$ . This feature also holds in the strain-space analysis. However, the stress surface can extend with no limit along the hydrostatic axis, but the strain-space critical surface should have an upper limit on the hydrostatic axis because the volume of concrete can not decrease without limit under the hydrostatic loading. Thus, the critical surface is within a range on the hydrostatic axis. The upper limit is on the top of the cone, and the lower limit

is corresponding to the minimum volumetric strain under hydrostatic action. (From triaxial hydrostatic compression test of Schickert and Danssmann (1984), under 150 *MPa*, the volumetric strain reached -0.0125 *m/m* ). The possible minimum value, the shape of limit surface and the open end of critical surface, are the problems to be studied all together with the related experimental data. In spite of these uncertainties, the critical surface is still found to be useful for non-high-hydrostatic compressive situation.

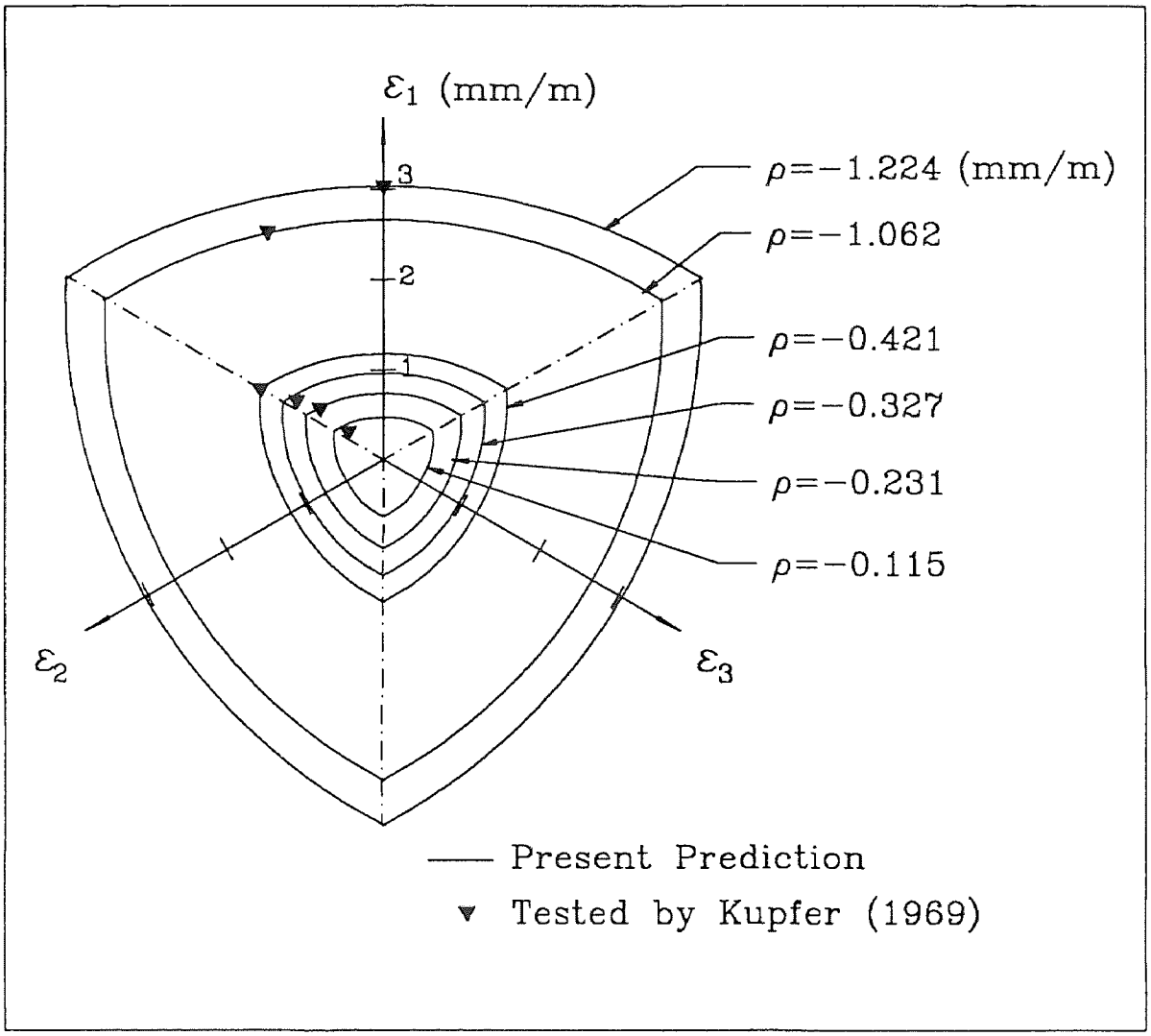


**Fig. 3.5** Test Points by Kupfer (1969) and Formula Prediction

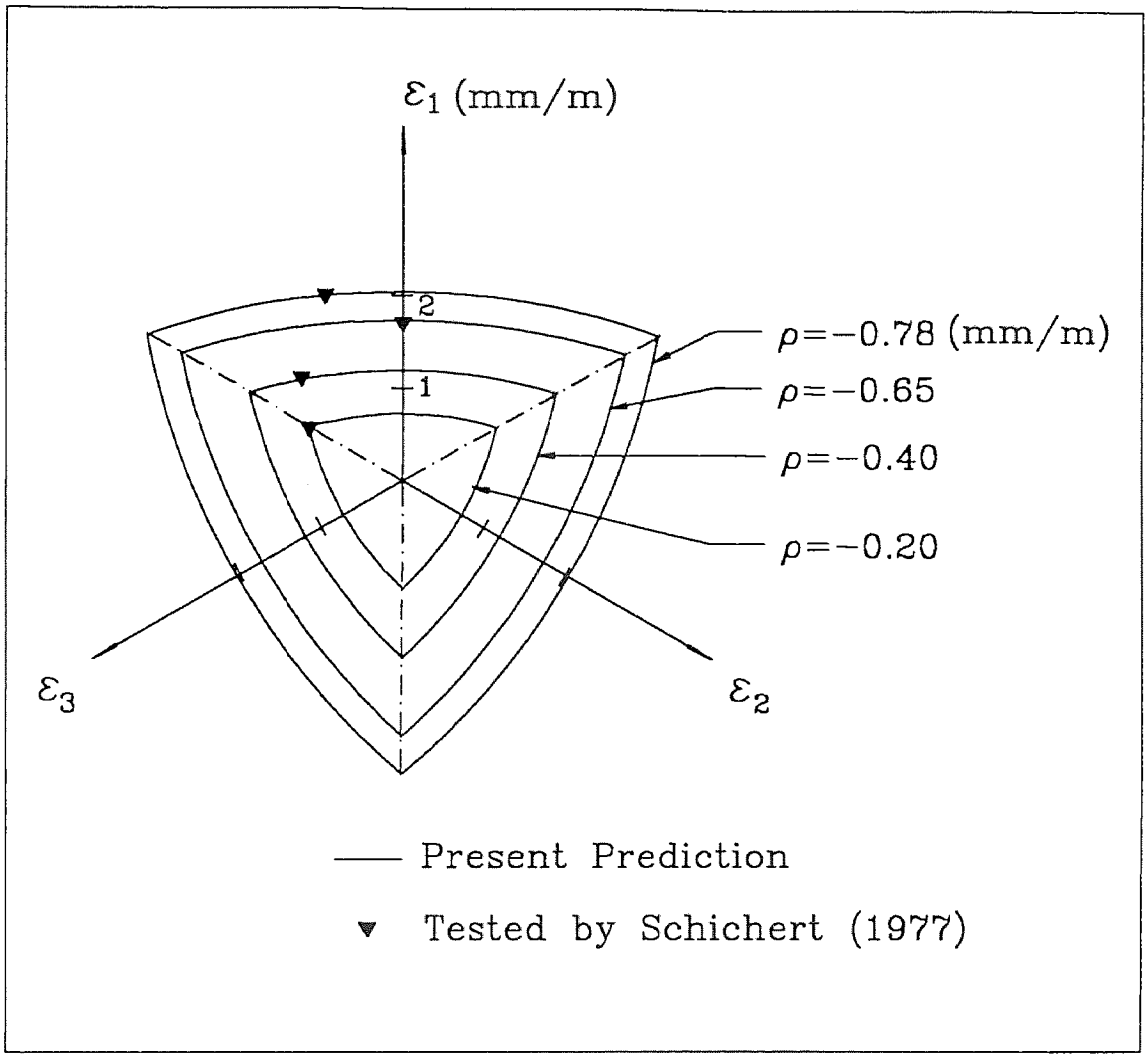


**Fig. 3.6** Test Points by Schickert (1977) and Formula Prediction

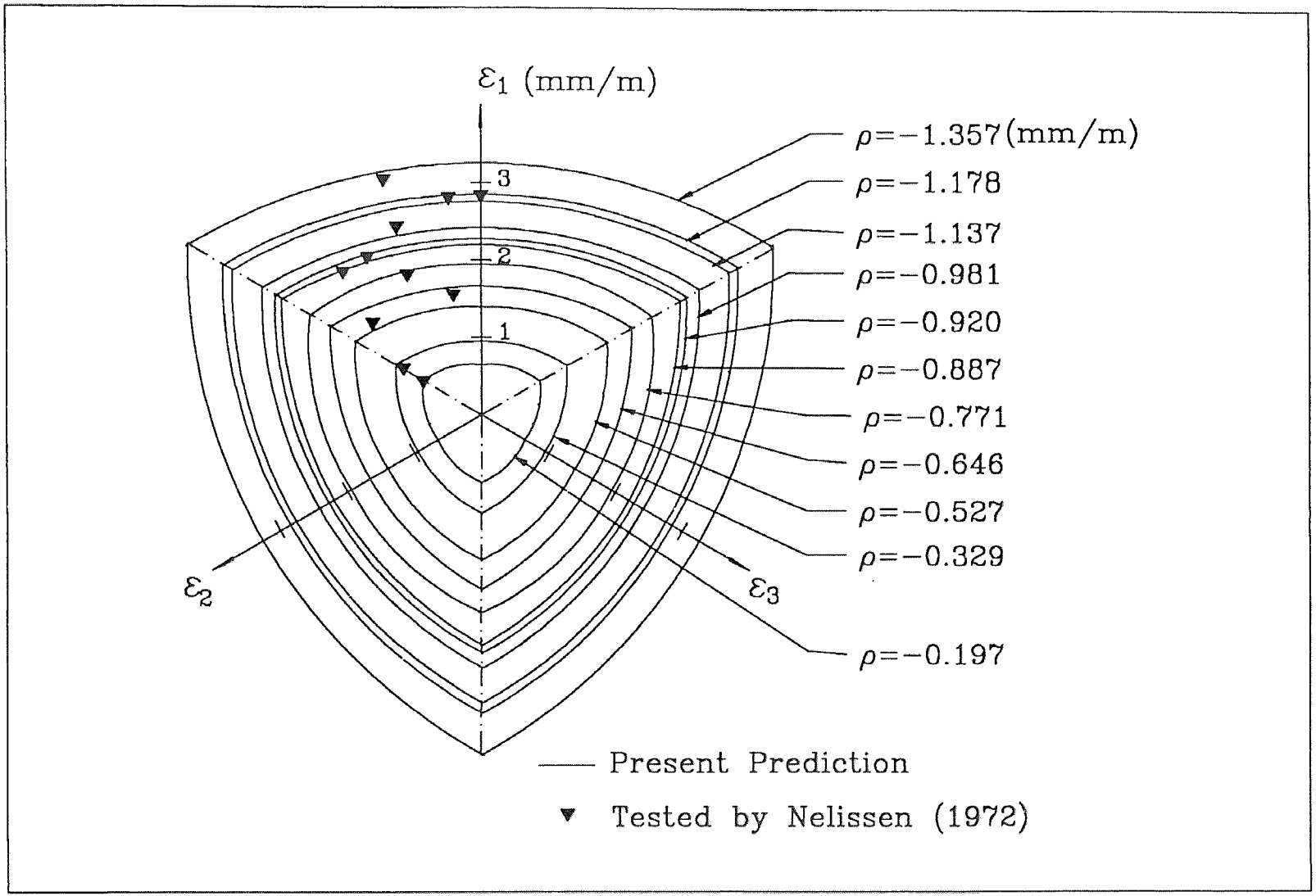


**Fig. 3.7** Test Points by Nelissen (1972) and Formula Prediction

# CHAPTER 4

# PROPOSED CONSTITUTIVE EQUATION

## 4.1 Introduction

Plasticity method is a phenomenological method. Its aim is to reproduce mathematically the macroscopic stress-strain relations for different loading conditions, neglecting the microscopic mechanism of the behavior. To set up a plasticity model, three components are essential. They are (1) an initial yield surface that defines the level in stress space or in strain space at which plastic responses start ; (2) a hardening rule that defines the change of the loading surface as well as the change of the hardening properties of the material during the course of plastic flow; and (3) a flow rule that is related to a plastic potential function and gives an incremental plastic stress-strain relation. The present strain-space plasticity model is also basically following the similar principles. Since the classical theory of plasticity is developed in the stress space, many assumptions and modifications are needed to apply in applying the plasticity theory to the strain-space version for concrete.

## 4.2 Yield Criterion

### 4.2.1 General Description

Yield criterion defines the elastic limit in a multiaxial stress state or its strain counterpart. For metals, the yield condition is used as a failure criterion, and is determined by the tests. The yield state for concrete is a fictitious quantity, and is used only in the mathematical constitutive law. In stress-space plasticity methods, the failure surface of concrete is considered as reference surface. For

simplicity, several plasticity models proposed that the yield surface has a similar shape to the failure surface but with a reduced size. However, it has been recognized that constitutive models based on this are only good in a quite narrow loading range. It may overestimate the plastic response in the tensile loadings and underestimate plastic component in the confined compressive loadings.

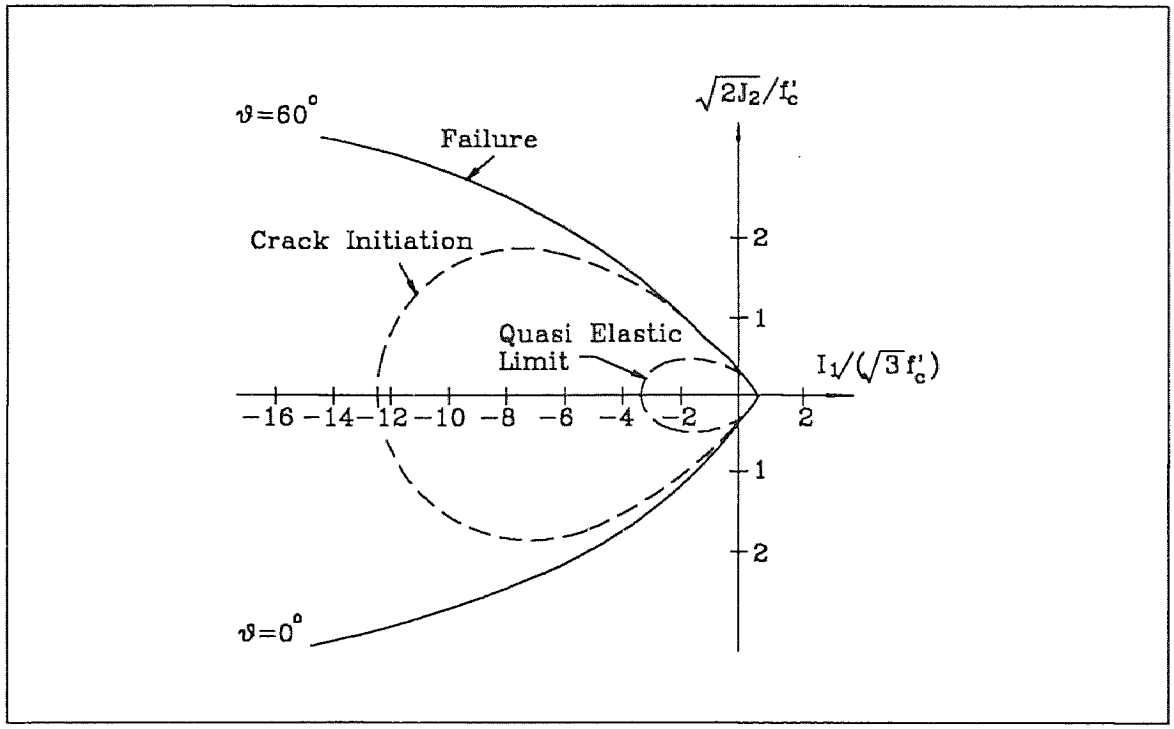


**Fig. 4.1** Results of Launay and Gachon's (1971) Study

There are very few experimental results reported on the shape of the yield surface in stress space. Launay and Gachon (1971) reported the elastic limit and crack initiation curves as shown in Fig. 4.1, which could be considered the quantitative description of the yield surface. In tensile and very low hydrostatic pressure region, the elastic limit or crack initiation curve almost coincides with

the failure curve, and the hardening-plastic zone has vanished. In a compressive region with hydrostatic confining pressure, the hardening zone can be quite large. It has been widely accepted that in stress space concrete has a closed initial yield surface.

In strain space, Kotsovos (1978) gave the similar closed-ended elastic limit shape, as the one in stress space (See Fig. 2.3).

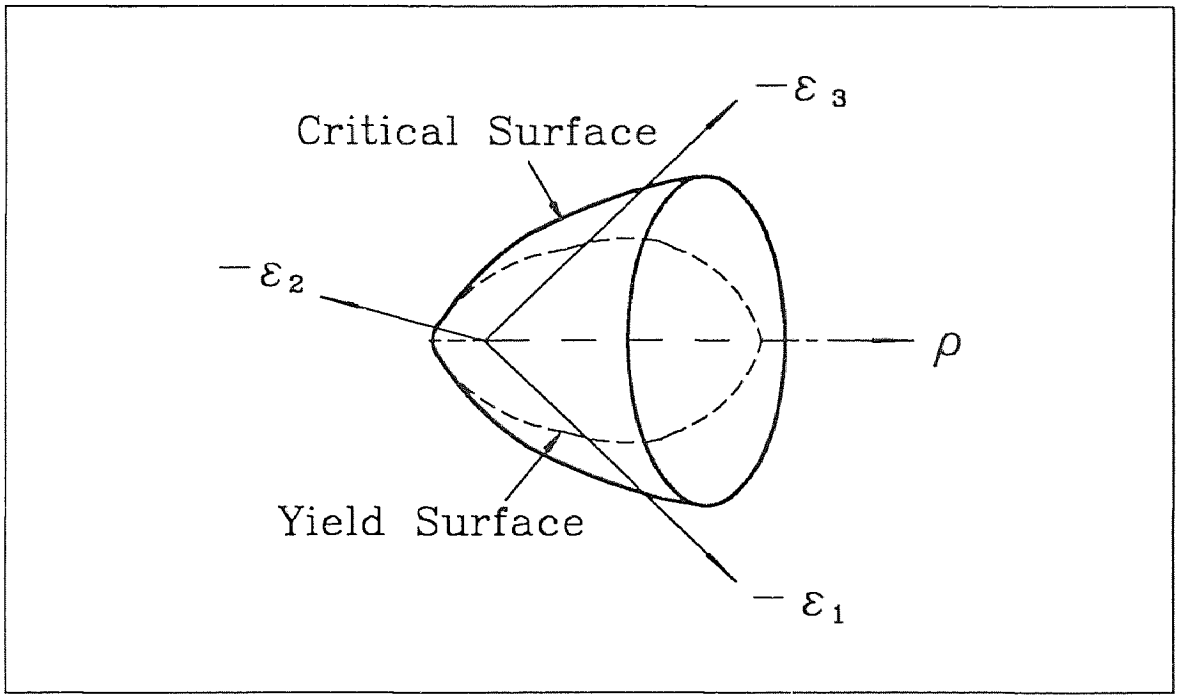


**Fig. 4.2** Strain-Space Yield and Critical Surfaces

Based on this observation and the stress-space counterpart, the proposed shape of the initial yield surface in strain-space is shown in Fig. 4.2. Here the critical surface is the reference. This initial yield surface coincides with the critical surface in the small compressive hydrostatic strain and tensile hydrostatic strain regions, and has a closed end along the compressive hydrostatic strain axis.

The subsequent yield surface, also called the loading surface defines the boundary of the current elastic region for an elastoplastically deformed material. If a state point (either in stress space or in strain space ) lies within the region, no additional plastic response takes places. On the other hand, if the state point is on the boundary of the elastic region and tends to move out of the current loading surface, additional plastic response occurs. In other words, the current loading surface will change its current configuration when plastic response takes place. Thus, the loading surface may be generally expressed as a function of the current state of stress (or strain) and some hidden variables. In strain space, one may have the loading surface

$$F(\varepsilon_{ij}, \varepsilon_{ij}^{p}, k_o) = 0 \tag{4.1}$$

where the hidden variables are the plastic strain $\varepsilon_{ij}^{p}$ and a hardening parameter $k_o$.

### 4.2.2 Formulation of Initial Yield Surface and Subsequent Yield Surfaces

The critical surface function given by Eq. (3.3) can be rewritten as

$$f(\rho, r, \theta) = r - r_c = 0 \quad , \ |\theta| \le 60^{o} \tag{4.2}$$

where

$$r_c = r_c(\rho, \theta) = [-(\alpha\cos\theta + \beta) + \sqrt{(\alpha\cos\theta + \beta)^2 - 4a(c\rho - 1)}]/(2a)$$

With the critical surface in Eq. (4.2) as the reference, the yield surface and subsequent yield surfaces are expressed in the form of

$$F(\rho, r, \theta, k_o) = r - k r_c = 0 \quad , \ |\theta| \le 60^{o} \tag{4.3}$$

where $k = k(\rho, k_o)$ is a shape factor which is a function of hydrostatic strain $\rho$, and a size parameter $k_o$. This shape factor modifies the critical surface so as to give a proper shape for the initial yield surface and subsequent yield surfaces.

The size parameter $k_o$ for a state is defined by the uniaxial compressive test result as the ratio of the current deviatoric strain to the deviatoric strain at critical stress (See Fig. 4.3 ), that is

$$k_o = \frac{r(\rho_1, 60^o)}{r_c(\rho_c, 60^o)} \tag{4.4}$$

where $\rho_1$ is the hydrostatic component of current strain state at uniaxial compressive loading path; and $\rho_c$ is that value at critical stress. Thus, $k_o$= 1 is the strain state at critical stress; and $k_o = k_y$ is corresponding to the initial yield surface when $k_y$ is from the strain state at about 40 percent of $f_c'$ on the uniaxial compressive path. $k_p$ is for the strain state at ultimate strength.

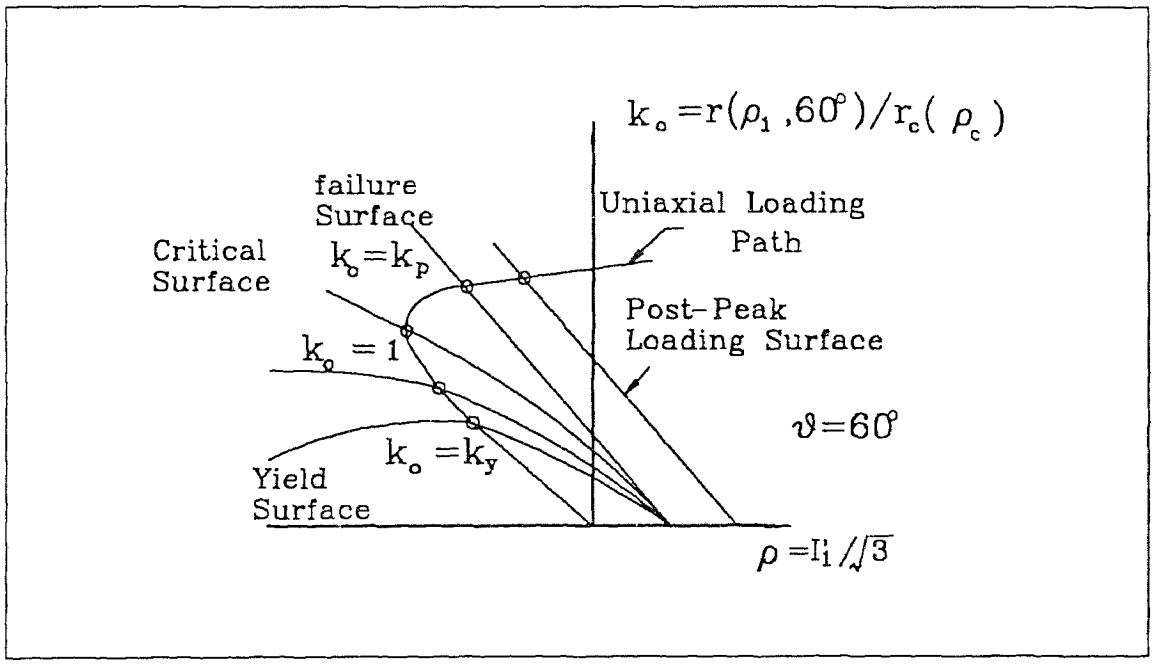


**Fig. 4.3** Definition of $k_o$

The shape factor $k = k(\rho, k_o)$ is assumed as a parabola before reaching the critical surface. From on the critical surface till the failure surface, $k = k(\rho, k_o) = k_1$, which is a horizontal line. The parabola requires three points to determine: $(\rho_t, 1)$, $(\bar{\rho}, 0)$ and $(\rho_1, k_1)$, where $\rho_t$ represents the dividing point for tensile and compressive regions; and is around 0; $\bar{\rho} = A/(1-k_o)$ gives a closed end of the loading surfaces. *A* is a constant, which can be calibrated according to the Launay and Gachon's result (1971). When $k_o$ approaches 1, $\bar{\rho}$ goes to infinity and the loading surface reaches the critical surface. $\rho_1 = \rho_1(k_o)$ is the relation between the hydrostatic strain of uniaxial case and $k_o$. For a strain state, this relation actually gives the hydrostatic component of the corresponding state point on the uniaxial compressive path, which can be obtained from the uniaxial compression test data. $k_1$ is the ratio between the deviatoric strain of uniaxial compression at $k_o$, to the deviatoric value of 60 degree meridian on the critical surface at $\rho_1$. Fig. 4.4 shows the relation between $k_o$, $k_1$, and $\rho_1$. From it, one can easy find

$$k_1 = \frac{AB}{AC} = \frac{k_o r_c(\rho_c, 60^o)}{r_c(\rho_1, 60^o)} \tag{4.5}$$

The shape factor for $k_y \le k_o \le 1$, where $k_y$ is corresponding to $k_o$, may be in the following form

$$k(\rho,k_o) = \begin{cases} 1 & (\rho \ge \rho_t) \\ k_\rho & (\rho_t > \rho > \bar{\rho}) \\ 0 & (\bar{\rho} \ge \rho) \end{cases} \tag{4.6}$$

where

$$k_\rho = \frac{[(\rho_1 - \bar{\rho}) - k_1(\rho_t - \bar{\rho})](\rho^2 - \bar{\rho}^2) + [(\rho_t^2 - \bar{\rho}^2)k_1 - (\rho_1^2 - \bar{\rho}^2)](\rho - \rho)}{(\rho_t^2 - \bar{\rho}^2)(\rho_1 - \bar{\rho}) - (\rho_1^2 - \bar{\rho}^2)(\rho_t - \bar{\rho})}$$

Fig. 4.5 is a graphic description of the shape factor.

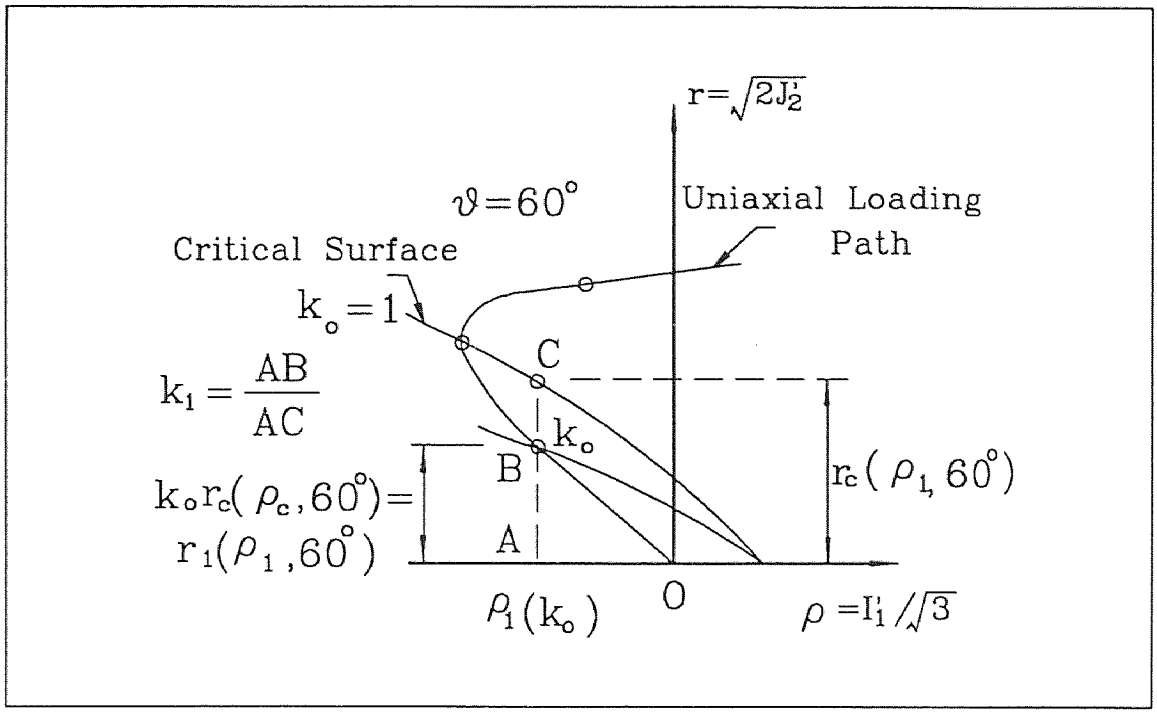


**Fig. 4.4** Relation Between $k_o$, $k_1$, and $\rho_1$

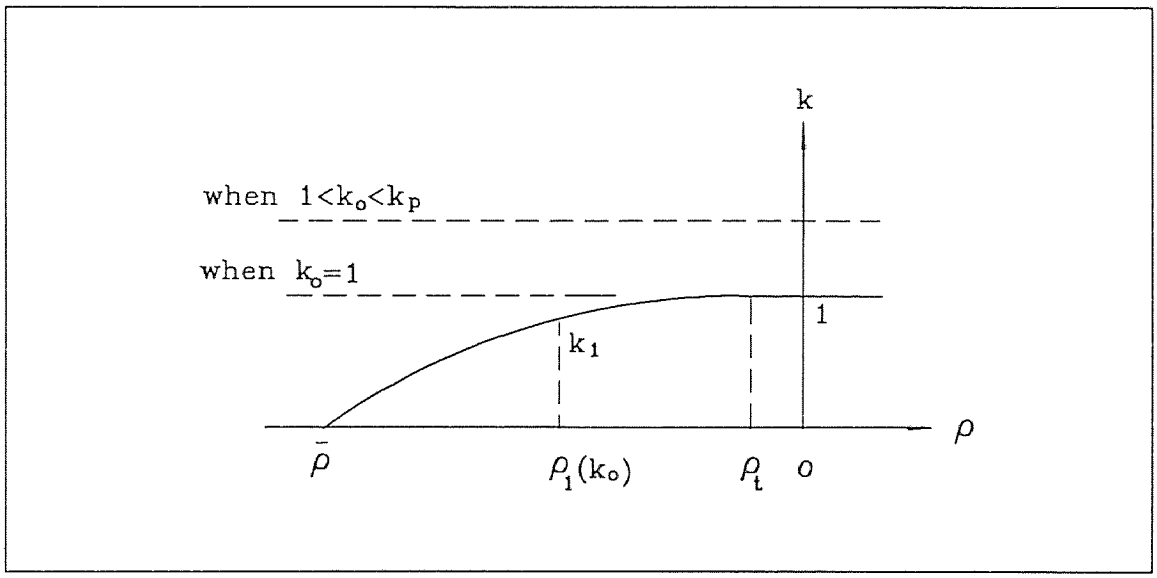


**Fig. 4.5** Shape Function $k = k(\rho, k_o)$

The General loading surface has so far been defined from Eqs. (4.3)~(4.6). However, the failure surface in strain space and the post-peak loading surface have not been determined yet. From Fig. 2.3, one can see that the failure surface is much open than the critical surface, and they have an almost same intersection with the hydrostatic strain axis. With the meridians become steep, the curvature reduces. Thus, the failure surface can be assumed to have straight meridians passing through the same point on the hydrostatic axis as the critical surface, and the 60 degree meridian passes through the failure point of the uniaxial compression. Therefore, the failure surface can be

$$F_f(\varepsilon_{ij}) = F_f(\rho, r, \theta) = (\alpha_1 \cos\theta + \beta_1) r + c\rho - 1 = 0 \quad , \quad |\theta| \le 60^\circ \tag{4.7}$$

where $\beta_1 = \left[1 - c\,\rho_1(k_p)\right] \Big/ \left[\left(\frac{\alpha}{\beta}\cos 60^\circ + 1\right) r_c(\rho_1(k_o), 60^\circ)\, k_p\right]$

$\alpha_1 = \beta_1 \left(\alpha/\beta\right)$.

and $k_p$ is the hardening parameter corresponding to the failure surface.

It can also be rewritten as

$$F_f(\rho, r, \theta) = r - r_f = 0 \quad , \quad |\theta| \le 60^\circ \tag{4.8}$$

where $r_f = -(c\rho - 1)/(\alpha_1 \cos\theta + \beta_1)$.

No information is available about the shape of the post-peak loading surface. According to the experimental observations, a prominent feature of post -peak behavior of concrete is a relatively rapid dilation of the overall volume. Based on this and the obtained failure surface, the volume dilation may be used to setup the post-peak loading surface. It may have the following form

$$F(\rho, r, \theta, k_o) = (\alpha_1 \cos\theta + \beta_1)\, r + c\,\rho - \gamma(k_o) = 0 \quad , \quad |\theta| \le 60^\circ \tag{4.9}$$

where $\gamma(k_o) = c\rho_o - 1$ for $k_o \geq k_p$, and $\rho_o$ is a function of $k_o$. From Fig. 4.6 , $\rho_o$ is determined when $\rho_1(k_o)$ is known.

The rewritten version is

$$F(\rho, r, \theta, k_o) = r - r_o = 0 \quad , \quad |\theta| \leq 60^\circ \tag{4.10}$$

where $r_o = [\gamma(k_o) - c\rho]/(\alpha_1 \cos\theta + \beta_1)$.

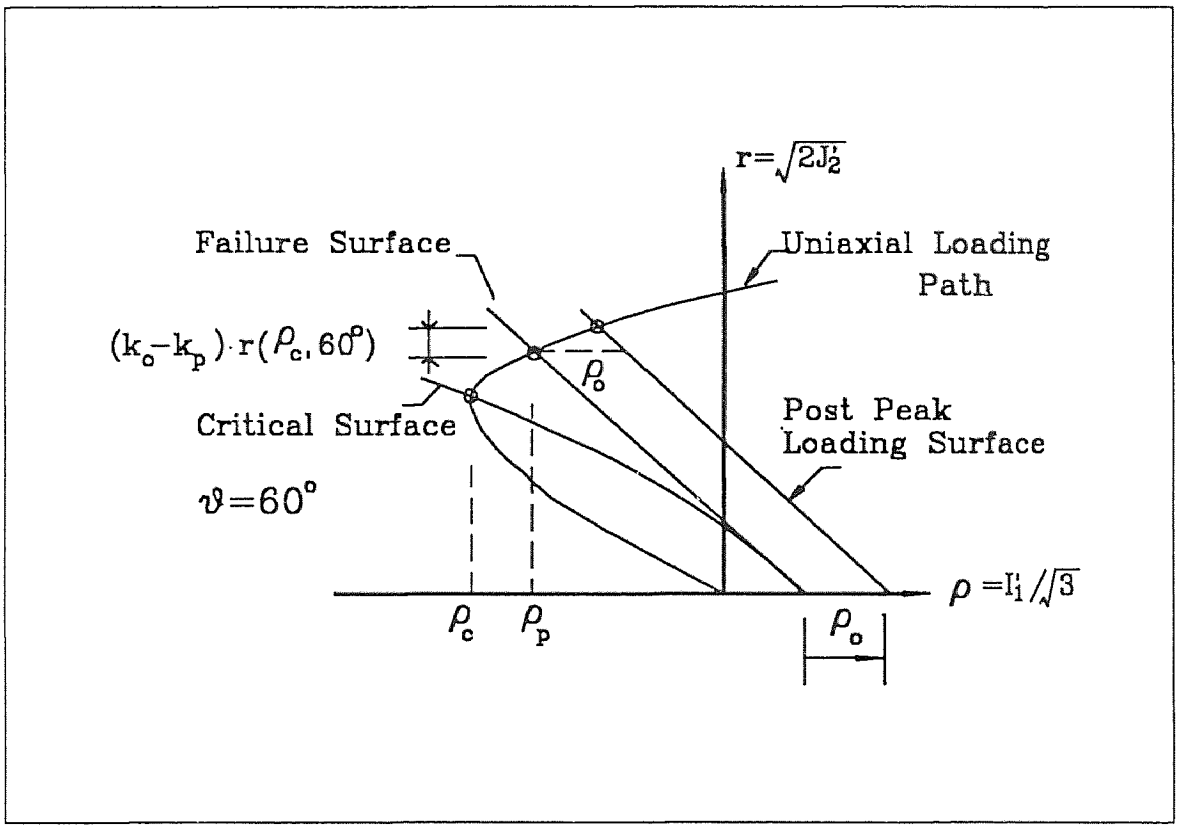


**Fig. 4.6** Relationship Between Failure Surface and Post-Peak Loading Surface

## 4.3 Hardening Rules

### 4.3.1 General

The post yield response, called the hardening rule, is described by specifying the rule for the evolution of the subsequent yield surfaces. Several hardening rules have been proposed in the past for use in plastic analysis. The most widely used rules are those of isotropic hardening, kinematic hardening, and a combination of both, which is called mixed hardening. In this study, a modified isotropic hardening rule and a kinematic hardening rule are used.

### 4.3.2 Modified Isotropic Hardening Rule

The isotropic hardening rule assumes that the initial yield surface expands uniformly without distortion and translation as the plastic flow occurs. In the modified isotropic hardening rule, the initial yield surface expands in the way as seen in Fig.2.11, rather than uniformly.

In the previous discussion, one can see that in the loading function Eq. (4.3) the size parameter $k_o$ plays an important role in defining the loading surface. With a given $k_o$, the corresponding loading surface can also be determined. This size parameter is called the hardening parameter in theory of plasticity. With $k_o$ changes from $k_y$ to 1 and further to $k_p$, the loading surface goes from the initial yield surface, through the critical surface and to the ultimate surface. In Fig. 2.11, with the strain hardening continues, the loading surface change from the initial close-ended shape to the open-ended surface. Since the shape factor is independent of the Lode angle $\theta$ , the loading surface on the deviatoric plane only changes its size, but not the shape.

One argument about this modified isotropic hardening procedure is what action mechanism causes this yield phenomenon if the loading path is along the

hydrostatic strain axis. The possible cause is the damage in the crushed pores or small holes. Although detailed and satisfied explanation is not available, the experimental research of Schickert and Danssmann (1984) did show that the progressive damage occurred under the increasing hydrostatic pressure action. In their test, they first applied the hydrostatic pressure with different values on the same batch of concrete cubic specimens. After taking off the pressure, they measured the change in ultrasonic pulse velocity and the uniaxial compressive strength. The results were quite consistent that the hydrostatic pressure cause the damage to the material structure.

### 4.3.3 Effective Strain and Plastic Effective Stress

To use the plasticity theory, one must relate the hardening parameter in the loading function to an experimental uniaxial compressive stress-strain curve. To this end, effective strain and effective stress must be defined, so that they can be plotted against each other and used to correlate the test results obtained by different loading programs. Further, the effective stress-strain curve could be calibrated against the uniaxial compressive stress-strain curve.

For a uniaxial compression, the loading function, Eq. (4.3) is expressed as

$$F = r_u - k(\rho_1, k_o)\, r_c(\rho_1, 60^\circ) = 0 \tag{4.11}$$

where

$r_u = \sqrt{\frac{2}{3}}\,(\rho_1/\sqrt{3} - \varepsilon_3)$, and $\rho_1 = \rho_1(k_o)$.

Let $\varepsilon_e = -\varepsilon_3$ and substitute it into Eq. (4.11). Then, the effective strain is defined as

$$\varepsilon_e = \sqrt{\tfrac{2}{3}}\, k(\rho_1, k_o)\, r_c(\rho_1, 60^o) - \rho_1/\sqrt{3} \tag{4.12}$$

Actually in this model, the effective strain is the uniaxial compressive strain for the given strain state.

The corresponding plastic effective stress $\sigma_p$ is hereby defined in terms of the plastic energy density

$$dw^p = \sigma\, d\varepsilon_e^p = \varepsilon_e^e\, d\sigma_p \tag{4.13}$$

where $\sigma$ is the effective stress, $\varepsilon_e^p$ and $\varepsilon_e^e$ are the plastic and elastic components of effective strain $\varepsilon_e$, respectively. The relationship between the elastic and plastic components and the plastic work increment is shown in Fig. 4.7 and Fig. 4.8, respectively

On the other hand,

$$dw^p = \varepsilon_{ij}^e\, d\sigma_{ij}^p = \varepsilon_{ij}^e\, d\lambda \frac{\partial G}{\partial \varepsilon_{ij}} \tag{4.14}$$

where, $\varepsilon_{ij}^e$ is the elastic component of strain tensor $\varepsilon_{ij}$, $\sigma_{ij}^p$ is the plastic component of stress tensor $\sigma_{ij}$., a non-associated flow rule is used here. *G* is the plastic potential function and $d\lambda$ is a positive scalar. Hence, according to the energy conservation law, by setting Eqs. (4.13) and (4.14) equal, the effective plastic stress may be expressed as

$$d\sigma_p = \phi\, d\lambda \tag{4.15}$$

where

$$\phi = \varepsilon_{ij}^e \frac{\partial G}{\partial \varepsilon_{ij}} \Big/ \varepsilon_e^e \ .$$

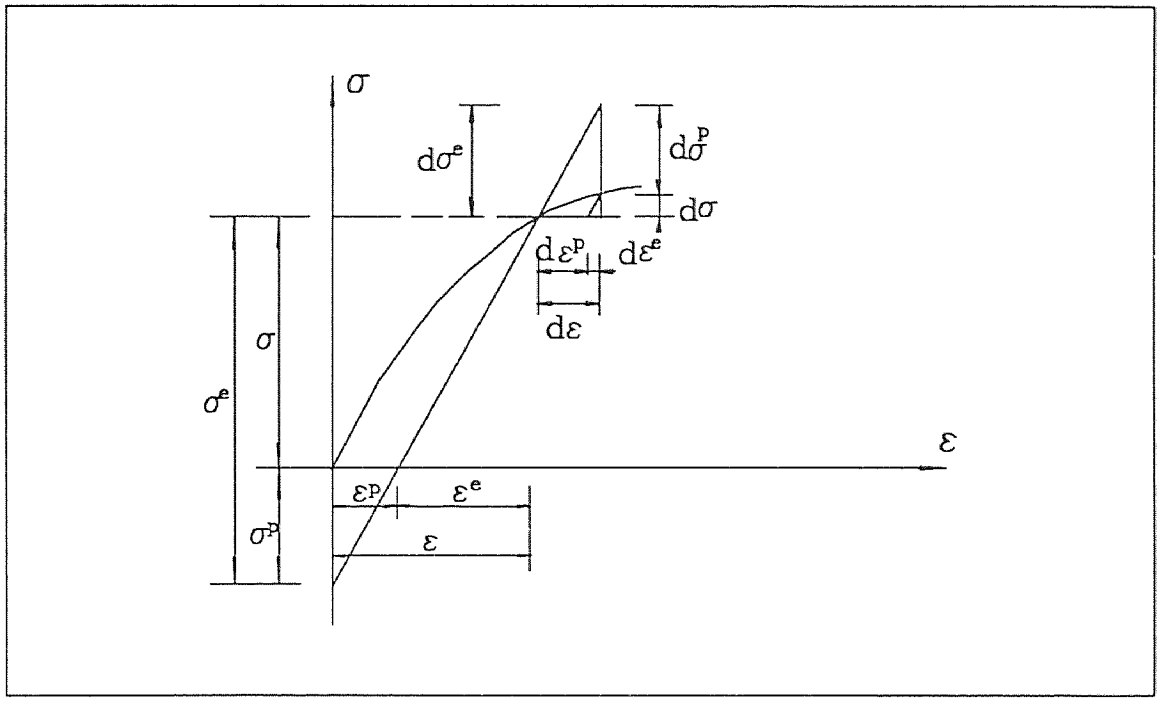


Fig. 4.7 Relationship Between Elastic and Plastic Components

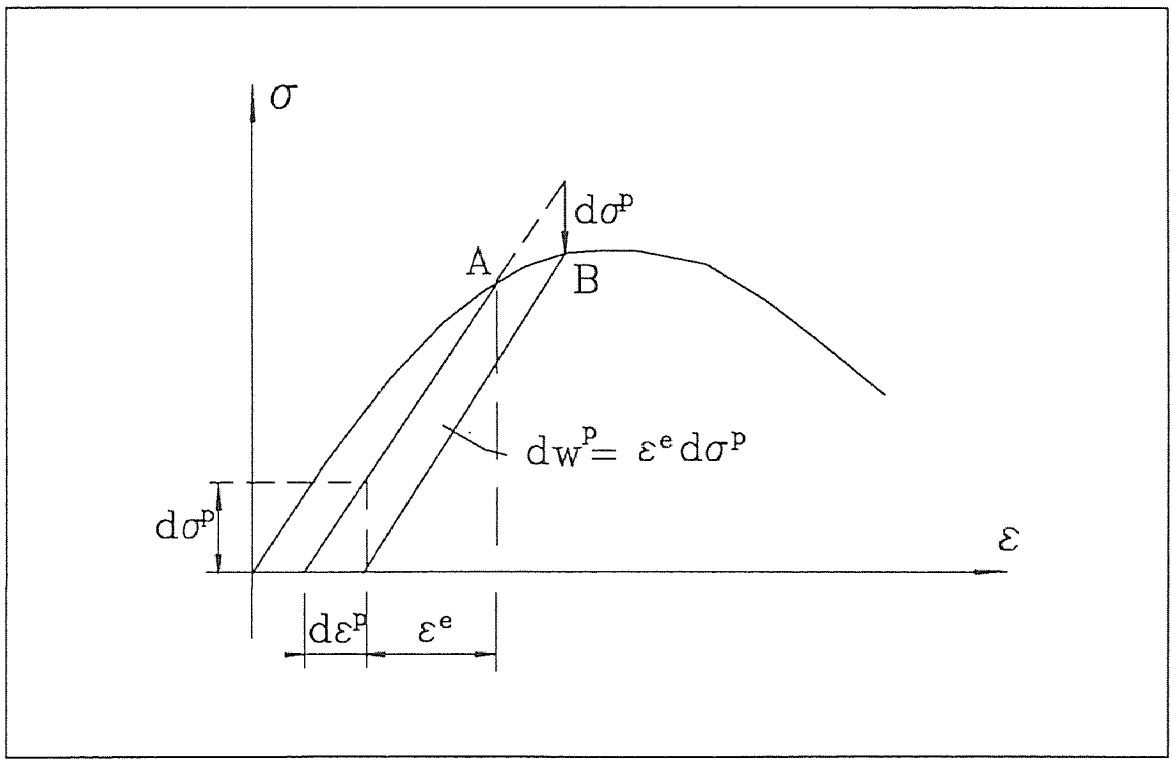


Fig. 4.8 Plastic Work Increment

### 4.3.4 Effective Strain and Plastic Effective Stress Relation

The effective strain-plastic effective stress relation, characterizing the hardening processes of material, is now calibrated on the uniaxial compression test, which has the form

$$\sigma_p = \sigma_p(\varepsilon_e) \tag{4.16}$$

The graphic expression and its relation with the general uniaxial stress-strain relationship were shown in Fig. 2.12.

Differentiation with Eq.(4.16) gives the following incremental relation

$$d\sigma_p = H_p^u(\varepsilon_e)\, d\varepsilon_e \tag{4.17}$$

where $H_p^u(\varepsilon_e)$ is a plastic modulus associated with rate of expansion of the yield or loading surfaces; and is the slope of the uniaxial plastic stress-strain curve at the current value of $\varepsilon_e$.

### 4.3.5 Relationship Between Hardening Parameter And Plastic Modulus

The hardening parameter $k_o$ is a function of plastic work and is related to plastic modulus $H_p^u$ which is derived from a uniaxial compressive curve. For a uniaxial compression, the loading function becomes

$$F_u(\rho_1, r_u, 60^\circ, k_o) = \sqrt{\tfrac{3}{2}}\,(\rho_1/\sqrt{3} + \varepsilon_e) - k(\rho_1, k_o)\, r_c(\rho_1, 60^\circ) = 0 \tag{4.18}$$

In this equation, the effective strain $\varepsilon_e$.and hardening parameter $k_o$ are variables. Differentiating the equation gives

$$dF_u = \frac{\partial F_u}{\partial k_o} dk_o + \frac{\partial F_u}{\partial \varepsilon_e} d\varepsilon_e = 0 \tag{4.19}$$

$$dk_o = \psi\, d\varepsilon_e \tag{4.20}$$

where

$$\psi = -\frac{\partial F_u}{\partial \varepsilon_e} \Big/ \frac{\partial F_u}{\partial k_o}$$

$$\frac{\partial F_u}{\partial \varepsilon_e} = \sqrt{\frac{3}{2}}$$

$$\frac{\partial F_u}{\partial k_o} = \frac{1}{\sqrt{2}} \frac{\partial \rho_1}{\partial k_o} - \left( \frac{\partial k}{\partial \rho_1} \frac{\partial \rho_1}{\partial k_o} + \frac{\partial k}{\partial k_o} \right) r_c - k \frac{\partial r_c}{\partial \rho_1} \frac{\partial \rho_1}{\partial k_o}$$

In such a manner, each loading surface or parameter $k_o$ is related to an effective strain $\varepsilon_e$, further to a plastic modulus $H_p^u$, also to the plastic work, implicitly.

### 4.3.6 Influence of Multiaxial Loading on Plastic Level

The plastic modulus $H_p^u$, taken from the experimental uniaxial compression test, is called the basic plastic modulus. It is fixed for a given loading surface, which represents a certain level of working-hardening. When it is zero, the material is in elastic stage. The larger it is, the stronger the plastic response is. Since it is taken from the uniaxial compression test, it may not be right to be used to describe the plastic degree for the multiaxial loading situation. Modification is necessary.

Multiaxial loadings may influence the plastic level of material mainly in two ways. The first is to change the confinement action. In the case of compression with confining pressures, concrete becomes more ductile. The other is to change the Lode angle. The former can be seen obviously in such normalized stress-strain curves as Fig. 4.9. The latter means with the same confinement action, the plastic procedure will be different if different loading direction on the deviatoric plane is followed since the loading surfaces are not circular.

In Fig. 4.9, the closer the curves to the perfect plastic lines OAB, the higher the plastic level the material undergoes. In other words, if the curve is closer to the 45 degree straight line, the less inelastic response will be. From this point of view, when the curve discussed is above the uniaxial curve, the plastic level is higher and the plastic modulus must be larger than the basic plastic modulus $H_p^u$. On the contrary, when the curve is below the uniaxial curve, a reduced value should be adopted.

To take into account of confinement, $\rho_s = I_1/\sqrt{3}$, the hydrostatic pressure in stress space is used. Thus, the influence of multiaxial loadings on the plastic level can be described by using a modification function of $\rho_s$ and $\theta$ to $H_p^u$. The modified plastic modulus is the equivalent plastic modulus for general case, which is then expressed as

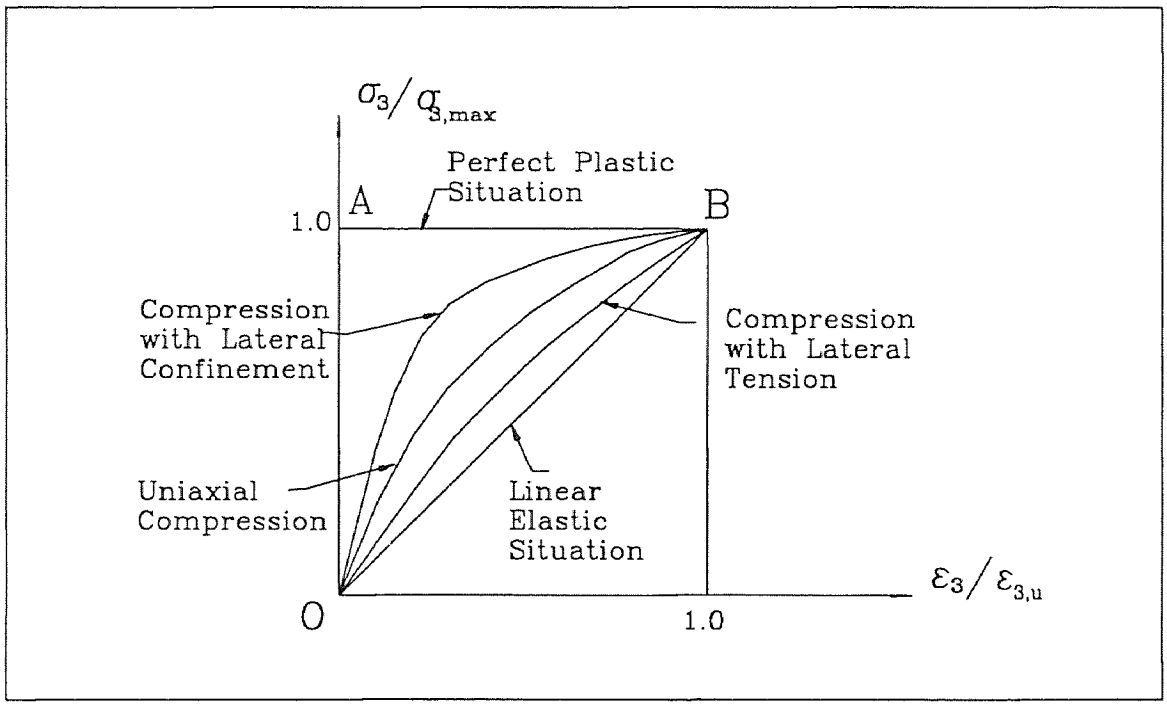


Fig. 4.9 Normalized Stress-Strain Curves

$$H_p = M(\rho_s, \theta)\, H_p^u \tag{4.21}$$

where the modification factor $M(\rho_s, \theta)$ is simply constructed in the form $M(\rho_s, \theta) = M_1(\rho_s)\, M_2(\theta)$.

By assuming that the influence of the multiaxial loadings to the plastic response is the same as other different states, it becomes much easier to determine this modification factor from the test data.

$M(\rho_s, \theta)$ is considered with two different situations. One with the confinement larger than that of the uniaxial compression, called case one; the other with confinement less than that of the uniaxial compression, called case two. Since $H_p^u$ is taken from the uniaxial compressive state, it is valid for the situation in which the hydrostatic stress $\rho_s$ is about $-\frac{1}{\sqrt{3}} f_c'$. Thus, when $\rho_s$ is smaller than $-\frac{1}{\sqrt{3}} f_c'$, which means larger confinement action than uniaxial compression, modification is needed. In a concrete cylinder compression test with confining pressure, as reported by Palanisway et al (1974) that there exists a transition confining pressure and it is around the value of $f_c'$ They concluded that when the confining pressure was less than $f_c'$, the increasing plastic response was observed with the increasing confining pressure (concrete exhibits more ductile behavior). However, if the confining pressure was greater than $f_c'$, the plastic response became smaller with the increasing pressure and less ductile failure behavior was found. Fig. 4.10 was the graph from their paper. Fig. 4.11 expresses the curves in the plastic stress-strain form. $M_1(\rho_s)$ is derived on the basis of this test result.

According to Han (1985), for the situation with the same hydrostatic pressure, the stress state at 60 degree meridian induces about two times as much as that is induced by stress state at the 0 degree meridian . For the strain state, in view of lacking the experimental information, the same effect as stress state is used.

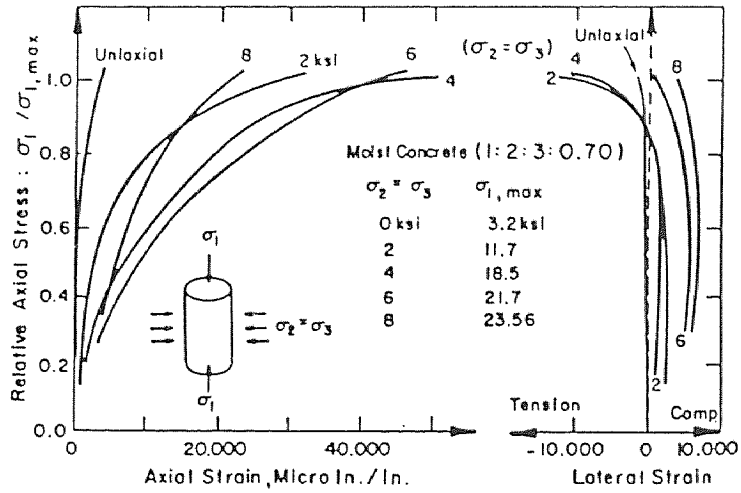


**Fig. 4.10** Confined Uniaxial Compression Test by Palanisway and Shah (1974)

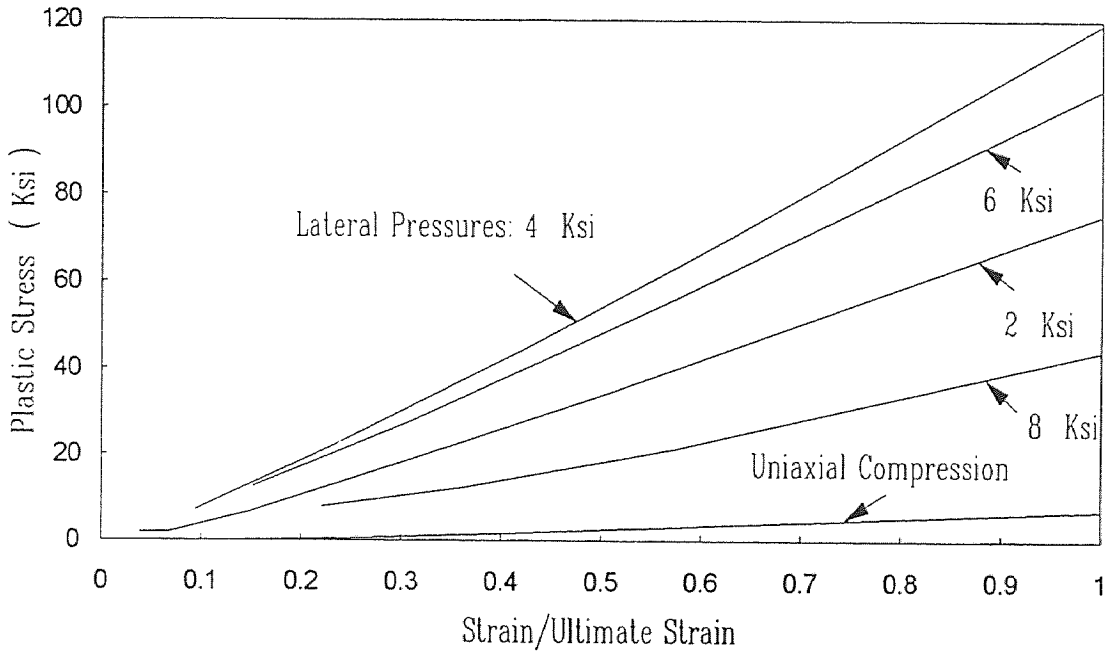


**Fig. 4.11** Plastic Stress-Strain Curves of Palanisway and Shah's Data

Based on the above analysis, the modification function for case one situation can be given

$$M(\rho_s, \theta) = [-1.04(4.5 - \left|\frac{I_1}{\sqrt{3}f_c'}\right|)^2 + 17.5](1.5 - \cos\theta) \qquad (4.22)$$

where $I_1 = \sigma_1 + \sigma_2 + \sigma_3$ is the first invariant of stress tensor $\sigma_{ij}$.

Case two may occur when combined tension and compression exist simultaneously. The contribution of Lode angle $\theta$ to the modification function can be ignored in this low hydrostatic pressure region. Thus, the case two is the region between OA and OC in Fig. 4.12, where OA is the uniaxial compressive loading path, OB is the uniaxial tensile loading path. For the stress state on OA, $M(\rho_s, \theta)$ =1, and on OC, $M(\rho_s, \theta)$=0. The transition of the plastic level from uniaxial compression to uniaxial tension is assumed here as a parabolic function. Therefore, the modification factor is

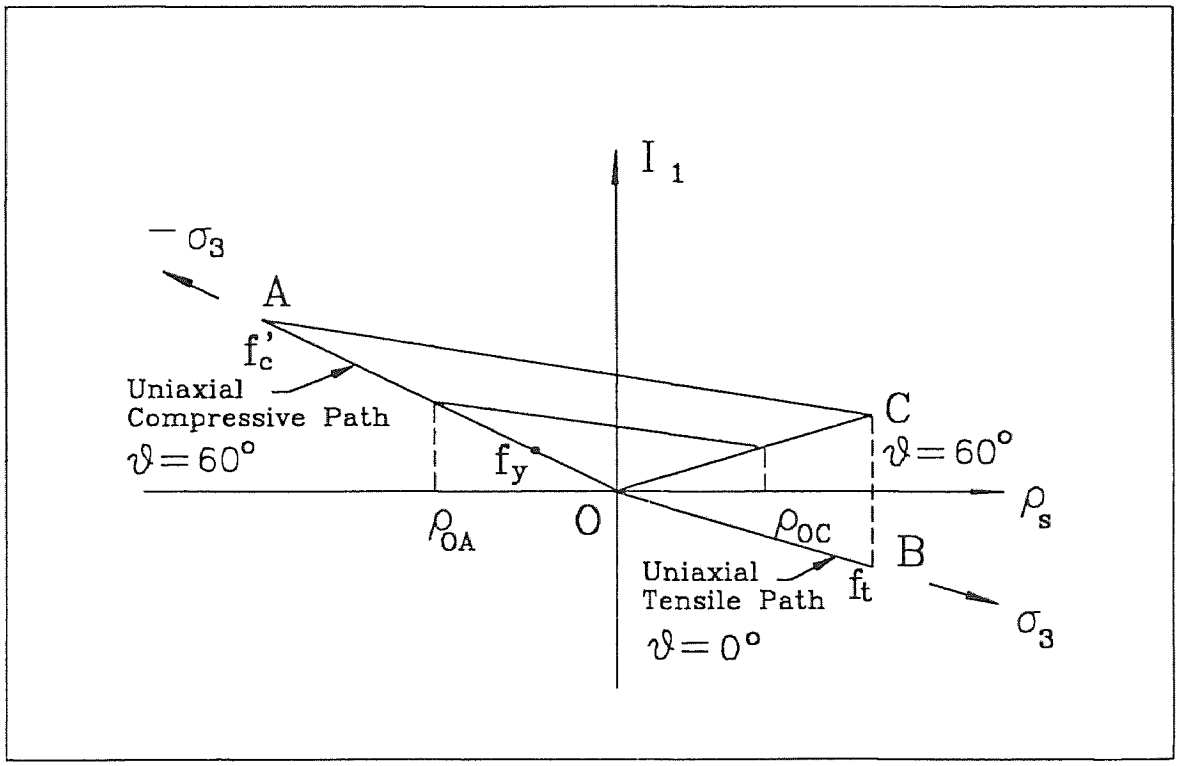


**Fig. 4.12** Tensile Influence on $M(\rho_s, \theta)$

$$M(\rho_s,\theta)=\left(\left|\frac{I_1}{\sqrt{3}f_c'}\right|-|\rho_{OA}|\right)^2\Big/(1.1\rho_{OA})^2 \tag{4.23}$$

where $\rho_{OA}=\sigma/\sqrt{3}$ the hydrostatic stress for the uniaxial compression, which is determined from the uniaxia stress-strain curve for a given $k_o$.

### 4.3.7 Kinematic Hardening Rule

In addition to the shape and size changes, the loading surface may also act like a rigid body translating in the strain space. This is called kinematic hardening (Fig. 4.13). This hardening rule provides a simple means of accounting for the Bauchinger effect, which is a type of directional anisotropy. The key to a subsequent yield surface based on a kinematic hardening rule is the determination of the coordinates of the center, $\alpha_{ij}$, which can be changed with the plastic response. Then, the loading surface becomes

$$F(\bar{\varepsilon}_{ij},\varepsilon_{ij}^p,k_o)=\bar{r}-k(\bar{\rho},k_o)\bar{r}_c=0 \tag{4.24}$$

in which $\bar{r}$ , $\bar{\rho}$ and $\bar{r}_c$ are calculated by the same equations but with $\bar{\varepsilon}_{ij}=\varepsilon_{ij}-\alpha_{ij}$ . In this model, the kinematic hardening is used between the critical surface and the failure surface. The translation of the loading surface in strain space is given according to Panos (1987) as

$$\alpha_{ij}=\varepsilon_{ij}^{\ p} \tag{4.25}$$

which implies the local unloading with the initial elastic stiffness for a uniaxial compression. When a state of strain is in the hardening stage, the total strain increment is always larger than the plastic strain increment; thus with this kinematic hardening rule, the loading surface will expand outward as well as move in the space.

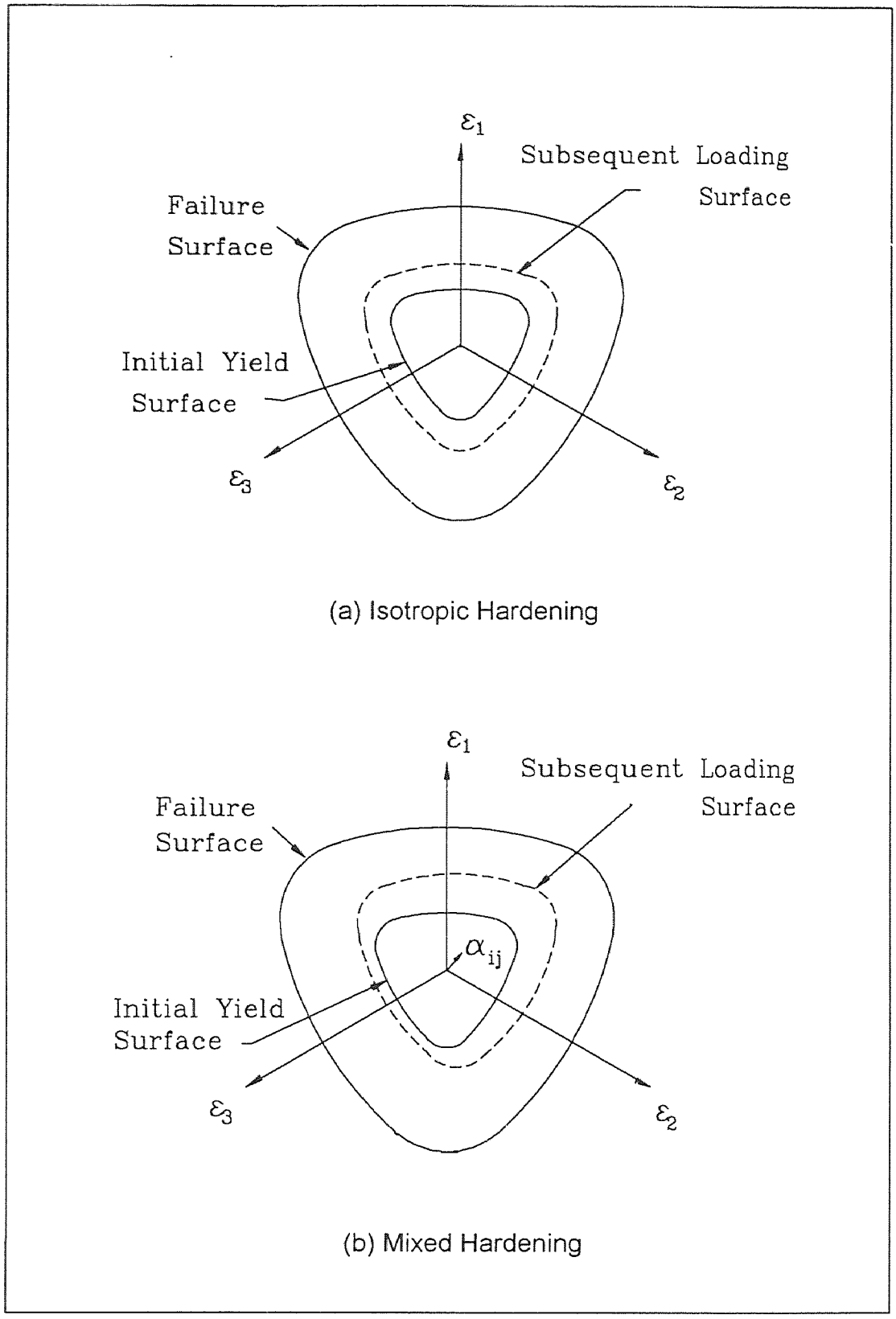


Fig. 4.13 Hardening Rules

## 4.4 Non-associated Flow Rule

When the current strain state reaches the yield surface, the material is in a state of plastic flow upon further loading. With the plastic potential surface $G(\varepsilon_{ij}, k^*)$, the direction of plastic stress vector is defined as the one which is normal to this surface (Chen (1982)), i.e.

$$d\sigma_{ij}^{p} = d\lambda \frac{\partial G}{\partial \varepsilon_{ij}} \tag{4.26}$$

where $d\lambda$ is a positive scalar factor of proportionality. If the plastic potential function coincides with the loading function, i.e. *G=F , thus*

$$d\sigma_{ij}^{p} = d\lambda \frac{\partial F}{\partial \varepsilon_{ij}} \tag{4.27}$$

that the plastic stress vector develops along the normal to the loading surface is called the associated flow rule (Chen (1982)).

The normals, $\frac{\partial G}{\partial \varepsilon_{ij}}$ can be generally expressed as

$$\frac{\partial G}{\partial \varepsilon_{ij}} = \frac{\partial G}{\partial I_1'}\delta_{ij} + \frac{\partial G}{\partial J_2'}s_{ij} + \frac{\partial G}{\partial J_3'}t_{ij} \tag{4.28}$$

where $\delta_{ij}$ is the Kronecker's delta, $s_{ij}$ the deviatoric strain tensor, and $t_{ij} = s_{ik}s_{kj} - \frac{2}{3}J_2'\delta_{ij}$. By substituting Eq. (4.28) into Eq. (4.26), noting that $s_{ii} = t_{ii} = 0$ , one obtains

$$d\sigma_{ii}^{p} = 3d\lambda \frac{\partial G}{\partial I_1'} \tag{4.29}$$

By using the Hooke's law in the form of bulk modulus, the plastic volumetric strain can be expressed as

$$d\varepsilon_{ii}^{p} = \frac{1}{3K} d\sigma_{ii}^{p} = \frac{1}{K} d\lambda \frac{\partial G}{\partial I_1'} \tag{4.30}$$

where $K = \frac{E}{3(1-2\mu)}$ is the bulk modulus, $E$ is the modulus of elasticity and $\mu$ is the poisson's ratio. The factor, $\frac{\partial G}{\partial I_1'}$ may be regarded as a plastic dilatancy factor, for it represents a measure of the fraction of plastic volume change. Experimental results (Fig. 2.4) indicate that for loading path with $I_1' < 0$, inelastic densification is occurred from the beginning till the critical stress state. After the critical stress, plastic dilatancy is observed. The critical stress point is a deflection point. Therefore, the plastic dilatancy factor $\frac{\partial G}{\partial I_1'}$ should change its value from negative to positive during the work hardening. After the ultimate strength, the larger volumetric expansion is expected. Thus, the plastic dilatancy factor should increase.

However, if the associated flow rule is used, the derivative $\frac{\partial F}{\partial I_1'}$ always has a nonnegative value for much loading region. This implies that no plastic volume contraction occurs all the way in the plastic flow. This is why the nonassociated flow rule must be used to define the ratio of the plastic stress components.

A Drucker-Prager type of plastic potential function is utilized here, which is widely used by many plasticity models (Han (1987)), (Bazant (1979)),

$$G = \varpi I_1' + \sqrt{J_2'} - k^* \tag{4.31}$$

where $\varpi$ and $k^*$ are constant. As can be seen that $k^*$ will not appear in the flow rule, while $\varpi = \frac{\partial G}{\partial I_1'}$ , which value should be properly chosen. Han et al (1987),

based on the experimental observation, expressed $\varpi$ as a linear function of hardening parameter, which at the beginning of yielding was -0.6 and 0.1~0.28 at ultimate strength. In this study, a second order function of hardening parameter $k_o$ is chosen. At yielding, $\varpi$ is -0.5~-0.6; at the critical stress, it is around 0; and $\varpi$ is 0.15~0.25 at ultimate strength.

## 4.5 Strain-Space Plasticity Formulation

The loading surfaces can be simply expressed as

$$F[(\varepsilon_{ij} - \alpha_{ij}), k_o] = 0 \tag{4.32}$$

in which $\alpha_{ij}$ is the coordinates of the loading surface, and $k_o$ is the isotropic hardening parameter. The strain increment can be resolved into elastic and plastic components as

$$d\varepsilon_{ij} = d\varepsilon_{ij}^e + d\varepsilon_{ij}^p \tag{4.33}$$

The stress increment is

$$d\sigma_{ij} = d\sigma_{ij}^e - d\sigma_{ij}^p \tag{4.34}$$

There exist the following relations

$$d\sigma_{ij}^p = C_{ijkl}\, d\varepsilon_{kl}^p \tag{4.35}$$

$$d\sigma_{ij}^e = C_{ijkl}\, d\varepsilon_{kl} \tag{4.36}$$

$$d\varepsilon_{kl}^e = D_{ijkl} d\sigma_{kl} \tag{4.37}$$

where $C_{ijkl}$ is the isotropic tensor of elastic moduli and $D_{ijkl}$ is the inverse of $C_{ijkl}$. The following formulas can represent $C_{ijkl}$ and $D_{ijkl}$, respectively (Chen (1982))

$$C_{ijkl} = \frac{\mu E}{(1+\mu)(1-2\mu)}\delta_{ij}\,\delta_{kl} + \frac{E}{2(1+\mu)}(\delta_{ik}\,\delta_{jl} + \delta_{il}\,\delta_{jk}) \tag{4.38}$$

$$D_{ijkl} = -\frac{\mu}{E}\delta_{ij}\,\delta_{kl} + \frac{(1+\mu)}{2E}(\delta_{ik}\,\delta_{jl} + \delta_{il}\,\delta_{jk}) \tag{4.39}$$

The relations of these quantities can be written as

$$d\sigma_{ij} = C_{ijkl}\,d\varepsilon_{kl} - d\sigma^{p}_{ij} \tag{4.40}$$

Il'iushin's postulate (1961) states that the work done by the external forces in a closed-cycle of deformation of an elasto-plastic material is non-negative. According to Il'iushin's postulate, a non-associated flow rule with plastic potential *G* can be used as

$$d\sigma^{p}_{ij} = d\lambda\frac{\partial G}{\partial \varepsilon_{ij}} \tag{4.41}$$

in which, $d\lambda$ is a scalar determined by the consistency condition of loading surface as

$$dF = \frac{\partial F}{\partial \varepsilon_{ij}}d\varepsilon_{ij} - \frac{\partial F}{\partial \varepsilon_{ij}}d\alpha_{ij} + \frac{\partial F}{\partial \varepsilon_{ij}}dk_{o} = 0 \tag{4.42}$$

The plastic stress increment can be split into two collinear parts

$$d\sigma^{p}_{ij} = d\sigma^{j}_{ij} + d\sigma^{k}_{ij} \tag{4.43}$$

where $d\sigma^{j}_{ij}$ is associated with the expansion of loading surface and $d\sigma^{k}_{ij}$ is associated with the translation of the loading surface.

$$\begin{aligned} d\sigma^{j}_{ij} &= M d\sigma^{p}_{ij} \\ d\sigma^{k}_{ij} &= (1-M) d\sigma^{p}_{ij} \end{aligned} \tag{4.44}$$

where $0 \le M \le 1$, is the mixed hardening parameter.

Kinematic hardening rule of incremental form is used, then

$$d\alpha_{ij} = d\varepsilon_{ij}^{\ p} = D_{ijkl}\, d\sigma_{ij}^{k} = D_{ijkl}\, d\lambda \frac{\partial G}{\partial \varepsilon_{ij}} (1-M)\, d\sigma_{ij}^{p} \tag{4.45}$$

Substitute Eqs. (4.15), (4.17), (4.20),(4.21) and (4.44) into Eq. (4.42) and solve for

$$d\lambda = \frac{\frac{\partial F}{\partial \varepsilon_{ij}}\, d\varepsilon_{ij}}{D_{ijkl} \frac{\partial F}{\partial \varepsilon_{ij}} \frac{\partial G}{\partial \varepsilon_{ij}} (1-M) - \frac{\partial F}{\partial k_o} \psi \frac{1}{H_p} \phi M} \tag{4.46}$$

By using Eq. (4.40) and substituting Eq. (4.46) into it , the constitutive equation is obtained as

$$d\sigma_{ij} = [C_{ijkl} - \frac{\frac{\partial G}{\partial \varepsilon_{ij}} \frac{\partial F}{\partial \varepsilon_{ij}}}{D_{ijkl} \frac{\partial F}{\partial \varepsilon_{ij}} \frac{\partial G}{\partial \varepsilon_{ij}} (1-M) - \frac{\partial F}{\partial k_o} \psi \frac{1}{H_p} \phi M}] d\varepsilon_{ij} \tag{4.47}$$

This constitutive equation is valid in the whole loading range, including work-hardening and softening.

## 4.6 Special Treatment on Post-Peak Behavior

### 4.6.1 Failure Modes

To perform complete failure analysis of a structure, the failure modes of concrete needs to be discussed. They are classified as cracking, mixed type and crushing. According to Hsieh et al (1982) and Han (1987), for the cracking failure mode, positive(tension) stress and strain must exist in a certain direction, and the states of stress in other directions have no effect on this failure modes, i.e. for biaxial condition, failure is caused by tension-tension or tension-compression. The mixed type of failure is caused by uniaxial, biaxial, or triaxial

compressive loading, but positive (tension) strain still exist in a certain direction in the element. For the crushing failure mode, the three principal strain components are all compressive, i.e., no tensile strain appears in any direction.

In this study, concrete is considered to be brittle when tensile loading is present. Once the tensile strength is reached, the stress is assumed to fall to zero. In the mixed type of failure, the concrete element is assumed to experience a multiaxial softening process until it loses its resistance in the direction of maximum compression. Volumetric dilation accompanies failure, and final rupture of concrete is attributed to bond failure between the paste and aggregate. In the crushing mode, the high confining pressure reduces the possibility of band cracking and the failure occurs by crushing of cement paste. For simplicity, the residual stiffness and strength of a crushed concrete element are neglected. Thus, the post-failure behavior becomes perfectly deformable (Han (1987)). Since the crushing mode of failure requires a nearly uniform hydrostatic condition, it is unlikely to be encountered in most design application, and the stress concentration in compression zone is not as serious as in tension zone. So this assumption is an acceptable approximation.

From the above discussion, the strain softening occurs only for the mixed failure mode in the proposed mode. However, when fracture mechanics is used, the tension softening can also be extended to this phenomenon(Han (1987)).

### 4.6.2 Stiffness Degradation in Strain Softening

From Fig. 2.5, one can see that the concrete exhibits both irrecoverable deformation and a stiffness degradation, which are believed to be caused by fracturing as well as slip in the aggregate-cement interface. The classical theory of plasticity assumes that the nonlinearity is due solely to the irreversible deformation induced by slip and that the elastic properties remain unchanged. In

contrast, the progressively fracturing theory of Dougiil (1976) assumes that the material nonlinearity, either hardening or softening is due to the degradation of the fractured material stiffness. To model the behavior of concrete, the plastic-fracturing theory, combining the classical theory of plasticity with the fracturing theory, was proposed by Bazant and Kim (1979). Han and Chen (1986) further developed this theory.

In this model, the stiffness degradation is considered in strain softening, for this feature becomes prominent only in the post-peak stage. The basic concept was from Han and Chen (1986). And the kinematic hardening is not considered in the strain softening.

When fracturing is considered, the stress increment $d\sigma_{ij}$ is assumed to comprise three components ( Fig. 4.14 ) as

$$d\sigma_{ij} = d\sigma_{ij}^{e} - d\sigma_{ij}^{p} - d\sigma_{ij}^{f} \tag{4.48}$$

where $d\sigma_{ij}^{e}$ is the elastic response to the total strain increment, i.e.

$$d\sigma_{ij}^{e} = C_{ijkl}\, d\varepsilon_{kl} \tag{4.49}$$

in which $d\sigma_{ij}^{p}$ is the stress increment related to the plastic strain increment as

$$d\sigma_{ij}^{p} = C_{ijkl}\, d\varepsilon_{kl}^{p} \tag{4.49}$$

while $d\sigma_{ij}^{f}$ is the stress increment due to stiffness degradation. It is defined as

$$d\sigma_{ij}^{f} = -dC_{ijkl}\ \ \varepsilon_{kl}^{e} \tag{4.50}$$

and it is related to the fracturing strain as

$$d\sigma_{ij}^{f} = C_{ijkl}\ \ d\varepsilon_{kl}^{f} \tag{4.51}$$

In Eqs. (4.49)~(4.51), $C_{ijkl}$ is the tensor of current elastic moduli and $dC_{ijkl}$ is its increment at the moment. The elastic strain increment $d\varepsilon_{kl}^{e}$ is defined as the elastic response to the total stress increment,

$$d\varepsilon_{ij}^{e} = D_{ijkl}\, d\sigma_{kl} \tag{4.52}$$

where $D_{ijkl}$ is the tensor of current compliance, the inverse of tensor $C_{ijkl}$.

From Eqs. (4.48)~(4.52), a relation for the strain increments can be obtained as

$$d\varepsilon_{ij} = d\varepsilon_{ij}^{e} + d\varepsilon_{ij}^{p} + d\varepsilon_{ij}^{f} \tag{4.53}$$

Fig. 4.14 illustrates the relation of all these quantities of strains and stresses in one-dimensional case.

Denote $d\sigma_{ij}^{pf}$ as the sum of plastic stress increment, $d\sigma_{ij}^{p}$ and fracturing stress increment, $d\sigma_{ij}^{f}$, that is

$$d\sigma_{ij}^{pf} = d\sigma_{ij}^{p} + d\sigma_{ij}^{f} \tag{4.54}$$

Using non-associated flow rule gives

$$d\sigma_{ij}^{pf} = d\lambda \frac{\partial G}{\partial \varepsilon_{ij}} \tag{4.55}$$

After failure, the plastic energy increment $dw^{p}$ is replaced by the plastic fracturing energy $dw^{pf}$ (see Fig. 4.15). And the effective strain-plastic effective stress relation is replaced by effective strain-plastic fracturing effective stress relation. Followed the same method as in the strain hardening stage, the effective strain is

$$\varepsilon_{e} = \sqrt{\tfrac{2}{3}}\; r_{o}(\rho_{1}, 60^{\circ}) - \rho_{1}/\sqrt{3} \tag{4.56}$$

The $\psi$ in Eq. (4.20), $dk_{o} = \psi\, d\varepsilon_{e}$, becomes $\psi = -\sqrt{\frac{3}{2}} \Big/ \left( \frac{1}{\sqrt{2}} \frac{\partial \rho_{1}}{\partial k_{o}} - \frac{\partial r_{o}}{\partial \rho_{1}} \frac{\partial \rho_{1}}{\partial k_{o}} \right)$.

The incremental plastic-fracturing effective stress is

$$d\sigma_{pf} = \phi\; d\lambda \tag{4.57}$$

where $\phi = \varepsilon_{ij}^{e} \dfrac{\partial G}{\partial \varepsilon_{ij}} \Big/ (\varepsilon_{e}^{e} + Q)$ and

$$Q = \tfrac{1}{2}\varepsilon_{e}^{e} E' \varepsilon_{e}^{e} \tfrac{1}{H_p} - \tfrac{1}{2}\varepsilon_{ij}^{e} C'_{ijkl} \varepsilon_{kl}^{e} \tfrac{1}{H_p}$$

in which $E'$ is the derivative of current modulus of elasticity, which can be obtained from a uniaxial cyclic compression test or simply use the empirical formula to calculate; and $C'_{ijkl}$ is the derivative of the stiffness tensor..

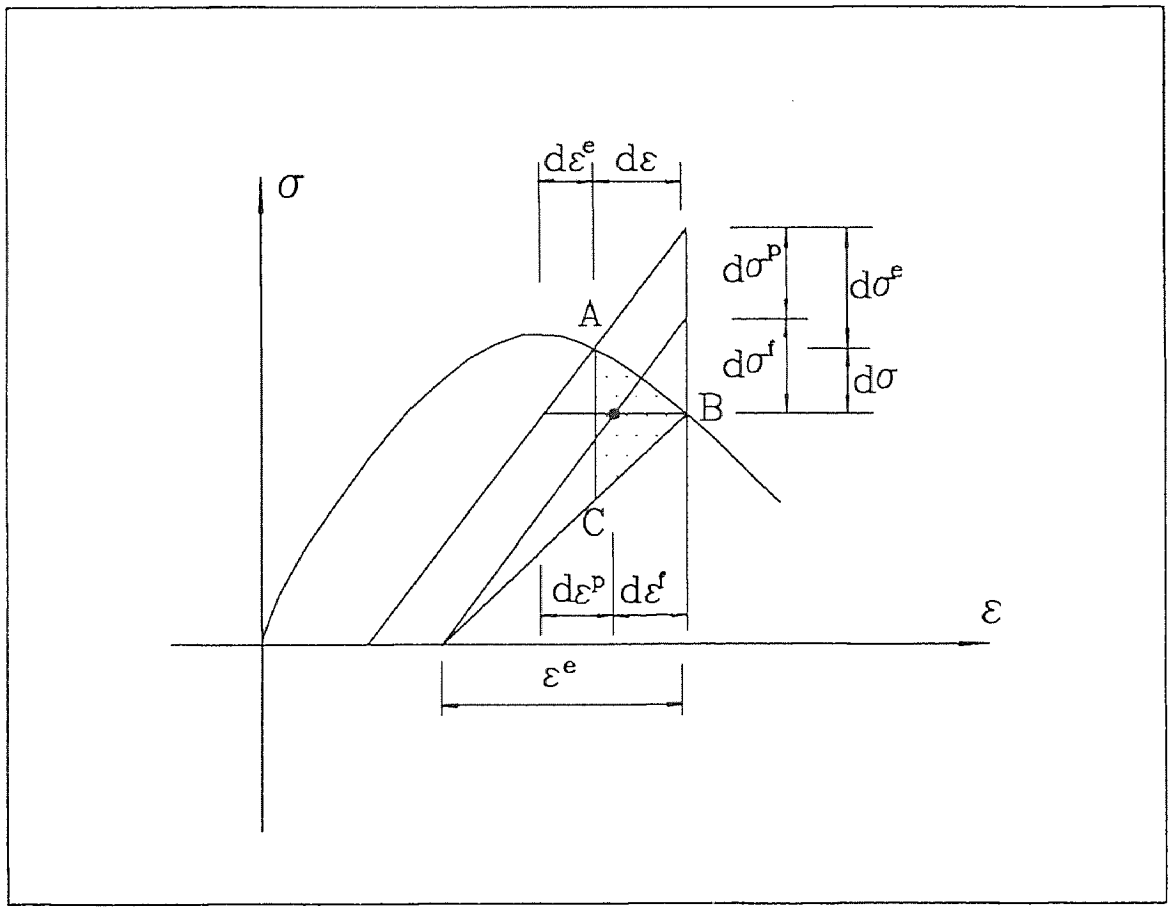


Fig. 4.14 Stress And Strain Increments( Han 1986))

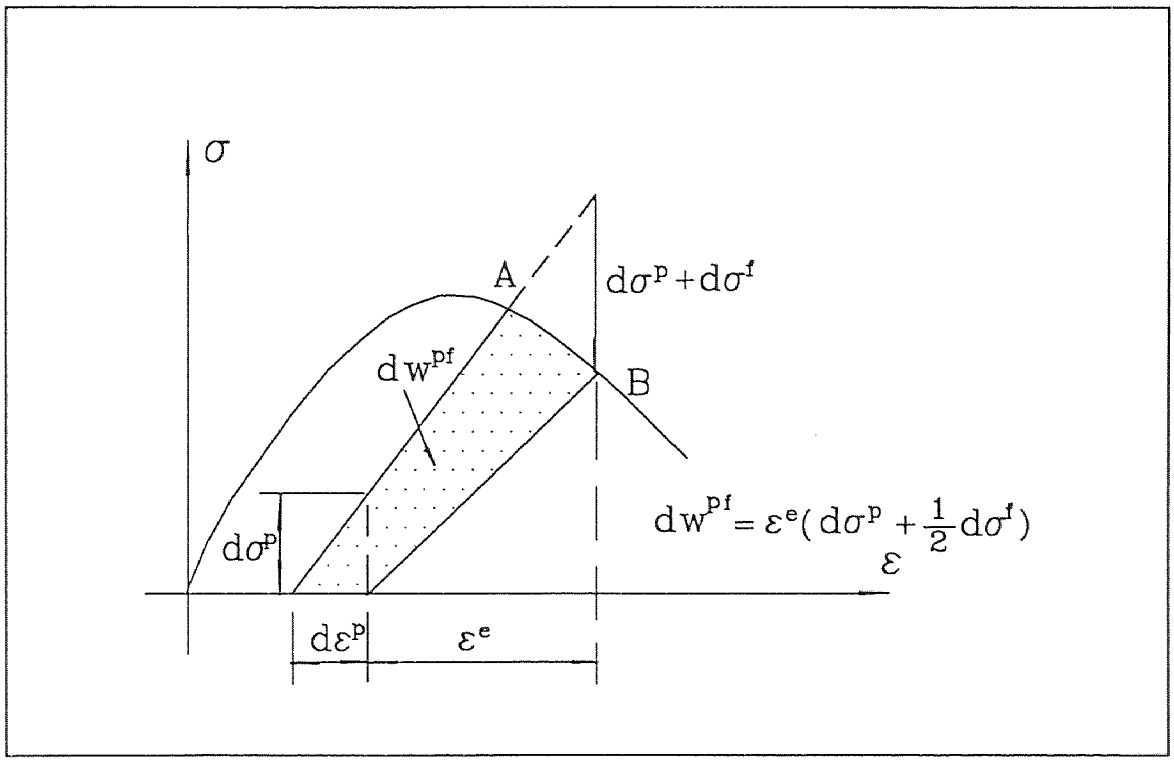


**Fig. 4.15** Incremental Plastic-Fracturing Energy( Han (1986))

# CHAPTER 5

# MODEL PREDICTIONS

## 5.1 Introduction

The performance of the proposed model must be examined before it can be used in a finite element analysis program for a structural analysis. When a structure is subject to external loading, various stress states or strain states could occur in the structure. A good constitutive model is therefore required to be usable for all the possible states.

The present model is built up on the strain space. Thus, the basic input is the strain tensor. Because of the restriction of testing machines and human habit, most multiaxial experimental data available are from the stress-controlled tests. Thus, when using the model for predictions, the strain tensor or simply the three principal strains are needed to be extracted from the experimental data for each increment. And the comparison will be performed on the stresses. The input file requires the following information:

(1) Input the most basic material properties, such as the modulus of elasticity $E$, the poisson's ratio $\mu$, and the uniaxial compressive strength $f_c'$.

(2) Determine the four-parameter critical surface by the approach given in Chapter 3.

(3) Determine the relationship between the hydrostatic strain of the uniaxial case and the hardening parameter , that is, $\rho_1 = \rho_1(k_o)$.

(4) Determine the constants $A$, $\rho_t$, $\rho_c$ ,$k_y$ and $k_p$ for the loading functions.

(5) Choose $M$ for the ratio of Kinematic and Non-isotropic hardenings. It is advised to use 1 before the critical surface, and 0 after the failure surface.

(6) Obtain the theoretical expression of the uniaxial stress-strain relationship. The expression is used to derive the plastic stress-strain relation, which is further used for the calibration of the plastic effective stress-effective strain curve.

(7) The non-associated flow rule of Drucker-Prager type is adopted in the program. The factor $\varpi$ changes from initial value, -0.5~-0.6 at yield to 0~0.02 at the critical surface, and to 0.15~0.25 at the ultimate strength. They are dependent upon the strength of concrete and type of loading. A concrete with lower strength seems to exhibit relatively larger compaction/dilatation behavior, and the dilatation seems to be larger in biaxial compression loadings than in triaxial compression cases. A simple choice can be made based on this.

## 5.2 Stiffness Matrix $C_{ijkl}$ in Strain Softening

### 5.2.1 Degradation of Stiffness in Uniaxial Case

In Fig. 2.5, the stiffness degradation can be seen from the slope decrease of the dashed lines with increasing strain. The change rate could be obtained by a strain controlled uniaxial cyclic compression test. In general, however, such a test data is not available. In this situation, the following empirical relationship by Karsan and Jirsa (1969) can be used to compute the slope-strain relationship $E'(\varepsilon)$.

$$\frac{\varepsilon_p}{\varepsilon_c} = 0.145\left(\frac{\varepsilon}{\varepsilon_c}\right)^2 + 0.13\left(\frac{\varepsilon}{\varepsilon_c}\right) \tag{5.1}$$

where $\varepsilon$ is the current strain at unloading point; $\varepsilon_c$ is the strain at $f_c'$ ; and $\varepsilon_p$ is the residual strain or plastic strain at zero stress.

### 5.2.2 Stiffness Degradation Rate of Tensor $C'_{ijkl}$

To accurately determine the stiffness degradation rate with 21 components is difficult or even impossible at the present time, due to lack of good and comprehensive experimental data. However, under the isotropic assumption, which is an acceptable approximation in the mixed type failure mode, the elastic tensor has only two independent constants, the modulus of elasticity $E$ and poisson's ratio $\mu$. With the current $E(\varepsilon)$, $\mu(\varepsilon)$ and their rates are known, $C'_{ijkl}$ may be expressed in the following equation

$$\left[C'_{ijkl}\right]=\begin{bmatrix} C_1 & C_2 & C_2 & & & \\ C_2 & C_1 & C_2 & & 0 & \\ C_2 & C_2 & C_1 & & & \\ & & & C_3 & & \\ & 0 & & & C_3 & \\ & & & & & C_3 \end{bmatrix} \tag{5.2}$$

where

$$C_1=\frac{E'(1-\mu)}{(1+\mu)(1-2\mu)}+E\mu'\frac{2\mu(2-\mu)}{(1+\mu)^2(1-2\mu)^2}$$

$$C_2=\frac{E'\mu}{(1+\mu)(1-2\mu)}+E\mu'\frac{1+2\mu^2}{(1+\mu)^2(1-2\mu)^2}$$

$$C_3=\frac{E'}{2(1+\mu)}-\frac{E\mu'}{(1+\mu)^2}$$

Since the poisson's ratio $\mu(\varepsilon)$ is not easy to be determined and its range is also a problem to be studied, for simplicity, it may be chosen as a constant.

## 5.3 Comparison Between Model Prediction and Experimental Results

In this study, comparison of the model predictions have been performed with three sets of test results.

The most well-known Kupfer's test (Kupfer et al (1969)), is considered first, which provides stress-strain behavior of concrete under biaxial loadings. The second set of test data is taken from Liu et al's data (Liu et al (1972)). And the third is given by Schickert and Winkler (1977). The last set of data include the proportional loadings as well as non-proportional ones.

### 5.3.1 Comparison with Kupfer's Test

The four critical surface constants are given in Table 3.1. The other material constants are in Table 5.1, in which $k_y$ corresponds to a uniaxial compressive yield stress $0.4f_c'$. The uniaxial compressive stress-strain curves have been given by the test itself, which is used as a material input, and also is used to compute the relationship $\rho_1 = \rho_1(k_o)$.

**Table 5.1** Basic Material Constants of Kupfer et al's Test

| E (MPa) | $\mu$ | $f_c'$ (MPa) | A | $\rho_t$ (m/m) | $\rho_c$ (m/m) | $k_y$ | $k_p$ |
|---|---|---|---|---|---|---|---|
| 31700 | 0.22 | 32.8 | $-4.827\times10^{-4}$ | 0 | $-4.327\times10^{-4}$ | 0.262 | 1.55 |

Fig. 5.1~Fig.5.3 show the comparison for uniaxial and biaxial compressive loadings. The predicted curves are in good agreement with the test data in both softening as well as hardening ranges. Figs. 5.4 and 5.5 discuss the

cases of compression-tension loadings. One can see that the difference between the theory and the test data is very small.

### 5.3.2 Comparison with Liu et al' s Tests

The Liu et al's tests have been considered as the reliable data for case of biaxial loadings. Many previous researchers used them to calibrate model parameters or to compare their model predictions. Table 5.2 contains the basic material constants as the input of present prediction. Fig. 5.6~Fig. 5.13 are the comparisons of model predictions with the test results. From these figures, a good correlation between the model predictions and test results is observed.

**Table 5.2** Basic Material Constants of Liu et al's Test

| E (Ksi) | $\mu$ | $f_c'$ (Psi) | A | $\rho_t$ (m/m) | $\rho_c$ (m/m) |
|---|---|---|---|---|---|
| 2635.94 | 0.21 | 4918 | $-8.333\times10^{-5}$ | 0 | $-5.66\times10^{-4}$ |
| $k_y$ | $k_p$ | $a$ | $\alpha$ | $\beta$ | $c$ |
| 0.333 | 1.331 | 197000 | 2604 | 496 | 6884 |

### 5.3.3 Comparison with Schickert and Winkler's Test

The third set of data selected for comparison are the triaxial compressive experimental results of Schickert and Winkler (1977). Three cases with different loading paths are compared. The three loading paths in their test are defined as:

(1) Path 1: Apply hydrostatic loading to 25.5 Mpa. Then keep this value constant, and load along the compressive meridian, i.e., load on the deviatoric plane and along $\theta = 60^{o}$.

(2) Path 2: Apply hydrostatic loading to 51 Mpa. Then keep this value constant and load along the shear meridian, i.e., load on the deviatoric plane and along $\theta = 30^{o}$ .

(3) Path 3: Apply hydrostatic loading to 42.5 Mpa. Then keep this value constant, and load along the tensile meridian, i.e., load on the deviatoric plane and along $\theta = 0^{o}$.

The four critical surface constants are given in Table 3.6. The other material constants are given in Table 5.3. Fig.5.14 shows the uniaxial compressive curves. They are in good agreement. Fig .5.15~Fig. 5.17 are for the triaxial compressive curves. From these figures, one can find that with high hydrostatic pressures sustained, the predictions are not as good as Fig. 5.14. But the trend of the predictions is right. Thus, these predictions are acceptable.

**Table 5.3** Basic Material Constants of Schickert et al's Test

| E (MPa) | $\mu$ | $f_c'$ (MPa) | A | $\rho_t$ (m/m) | $\rho_c$ (m/m) | $k_y$ | $k_p$ |
|---|---|---|---|---|---|---|---|
| 21000 | 0.23 | 30.6 | $-8.45\times10^{-4}$ | 0 | $-3.0\times10^{-4}$ | 0.44 | 1.40 |

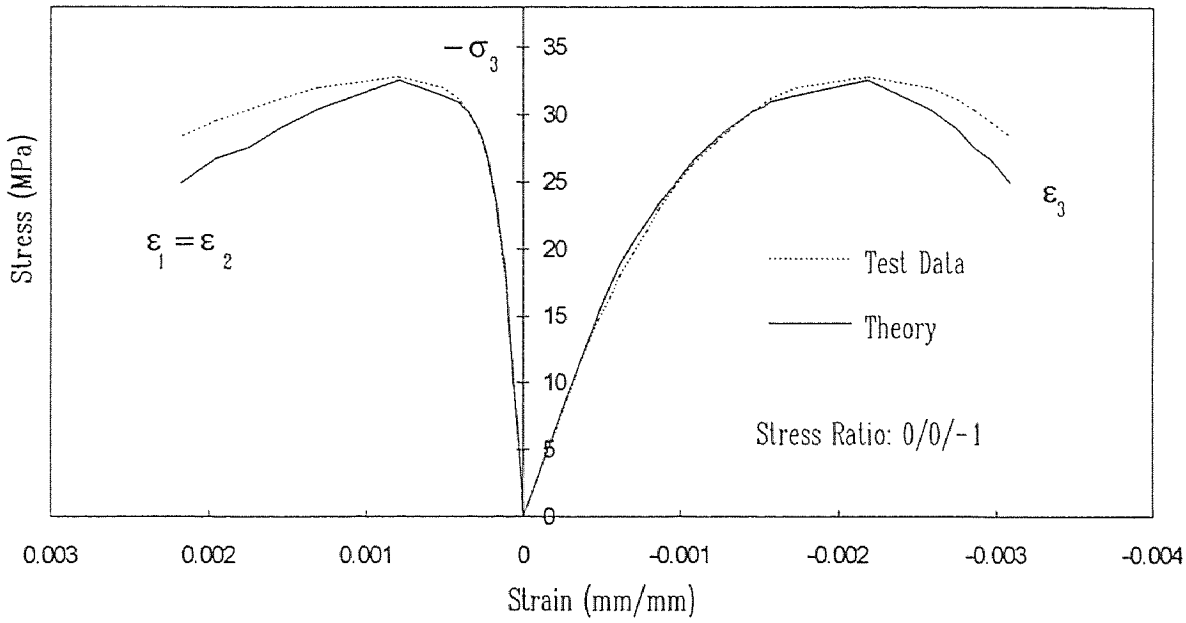


**Fig. 5.1** Comparison of Unaxial Compressive Loading by Kupfer's Data

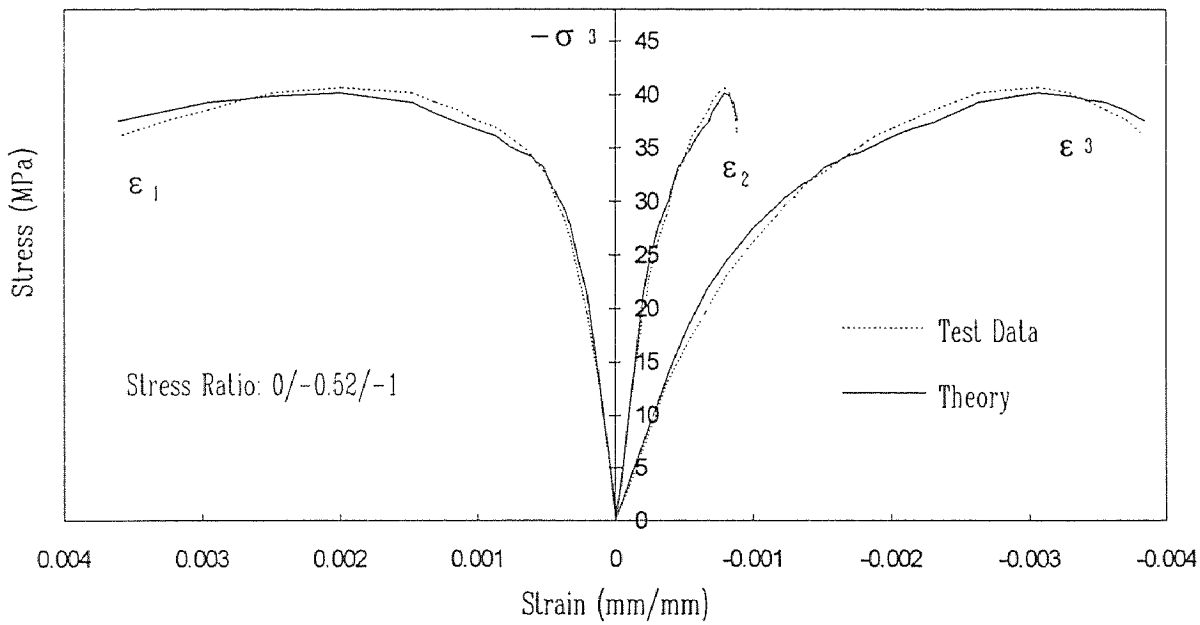


**Fig. 5.2** Comparison of Biaxial Compressive Loading by Kupfer's Data

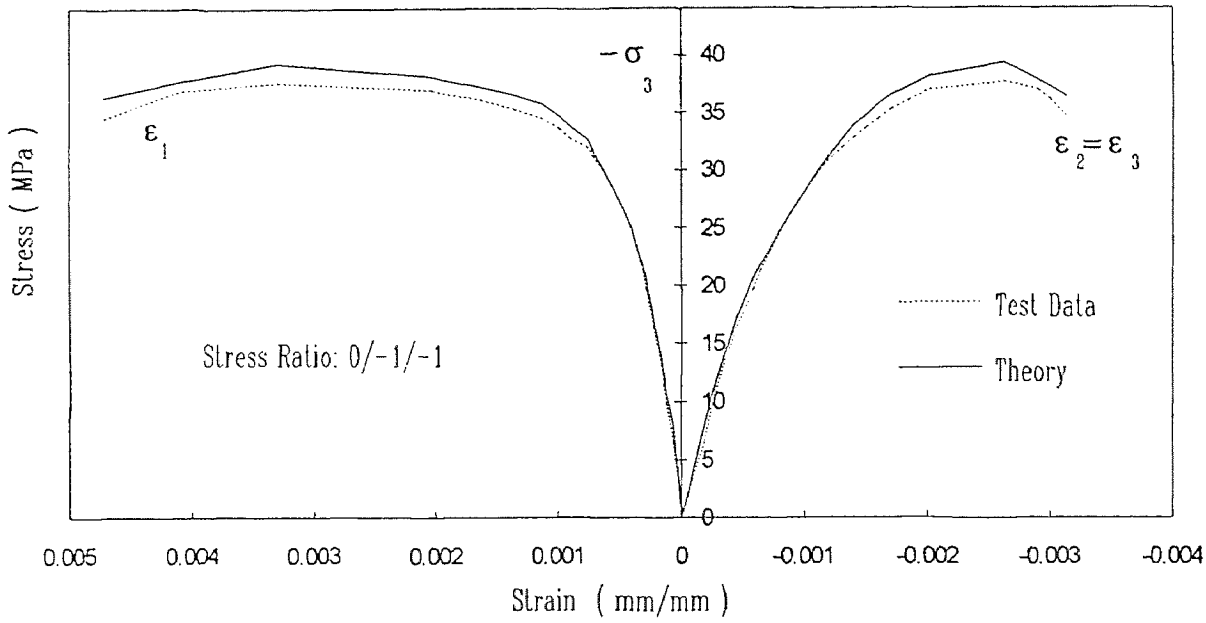


Fig. 5.3 Comparison of Biaxial Compressive Loading by Kupfer's Data

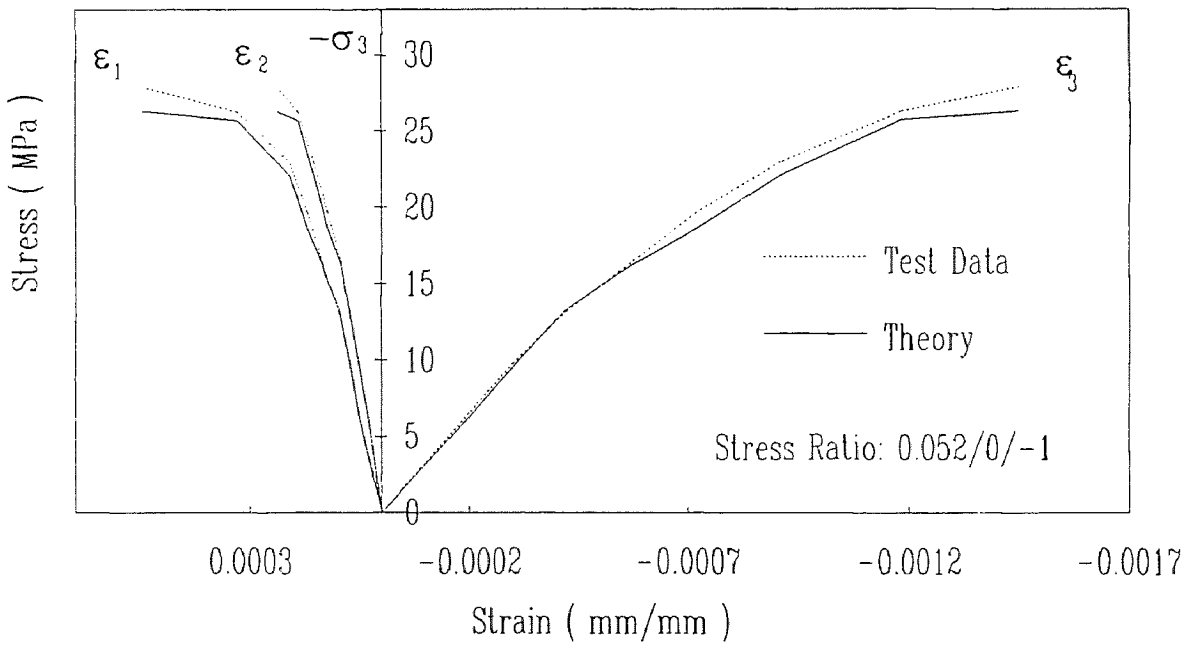


Fig. 5.4 Comparison of Compression-Tension Loading by Kupfer's Data

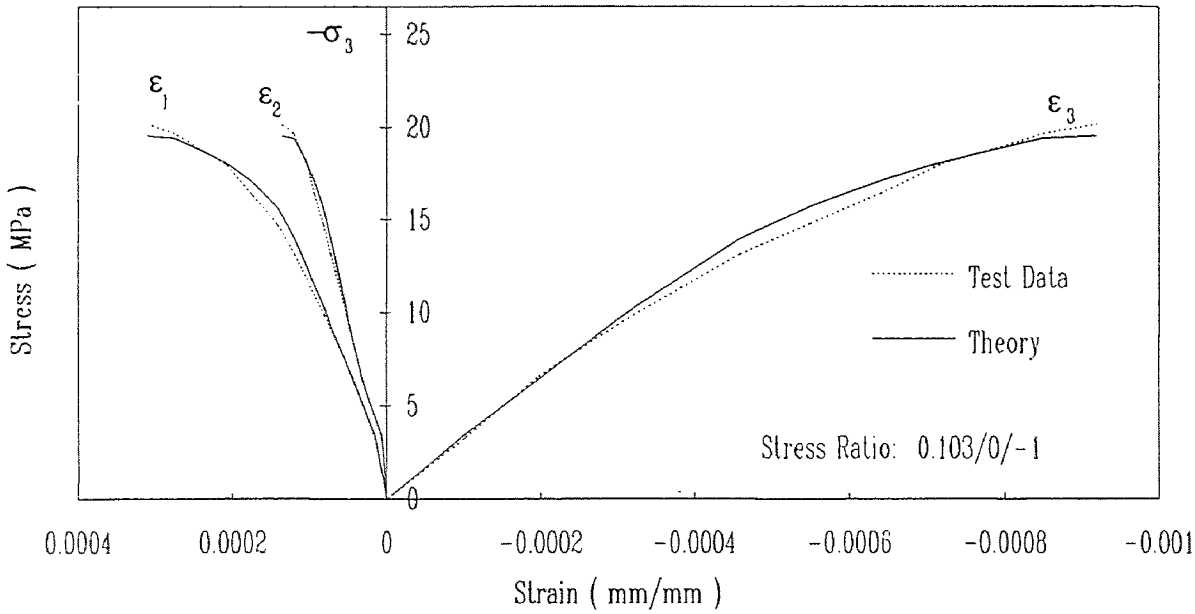


Fig. 5.5 Comparison of Compression-Tension Loading by Kupfer's Data

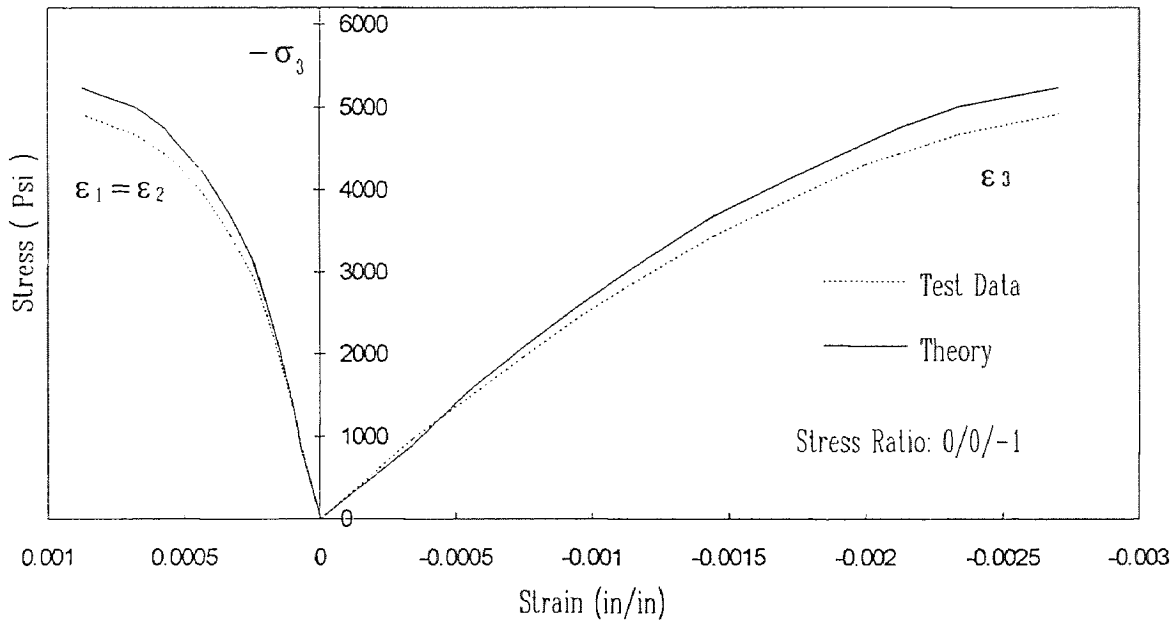


Fig. 5.6 Comparison of Uniaxial Compressive Loading by Liu et al's Data

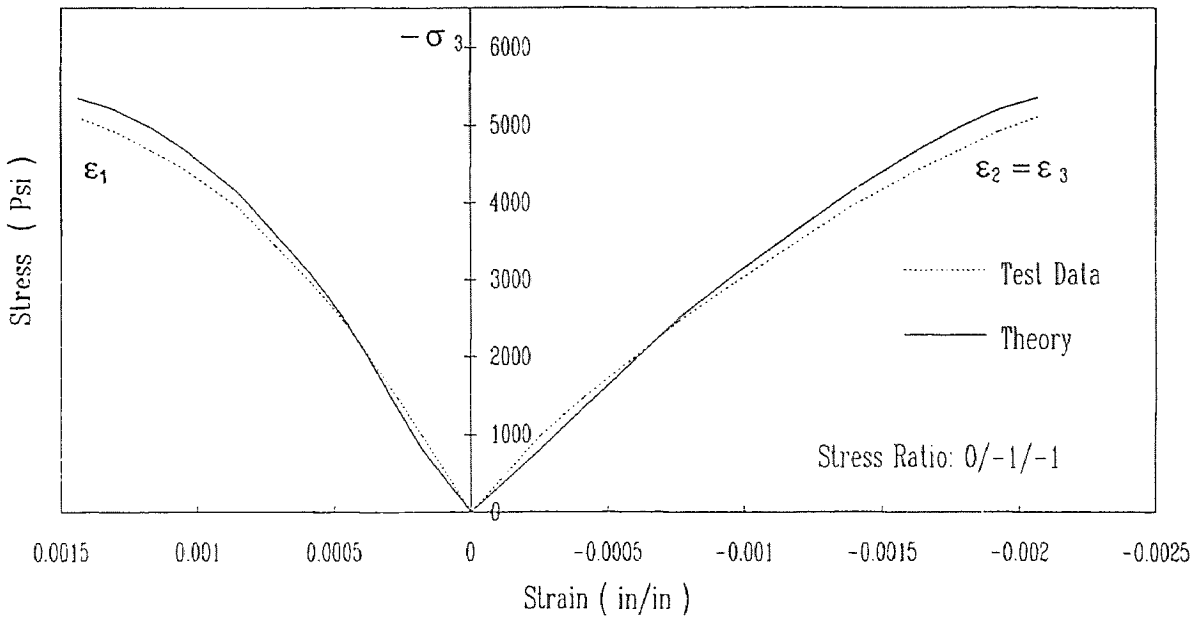


**Fig. 5.7** Comparison of Biaxial Compressive Loading by Liu et al's Data

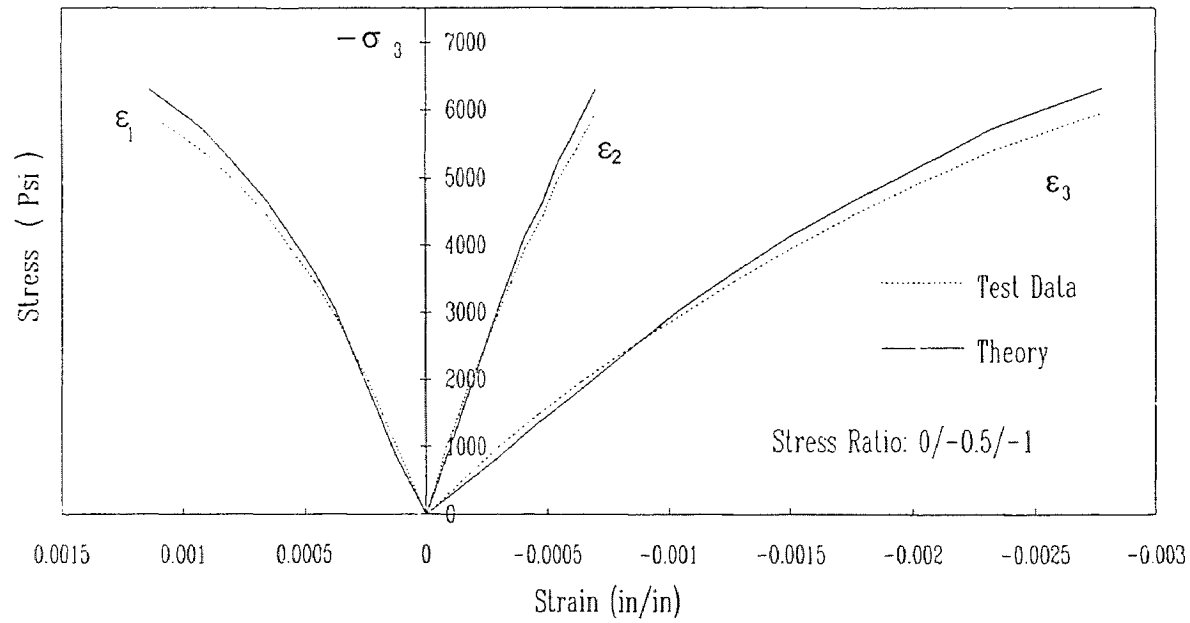


**Fig. 5.8** Comparison of Biaxial Compressive Loading by Liu et al's Data

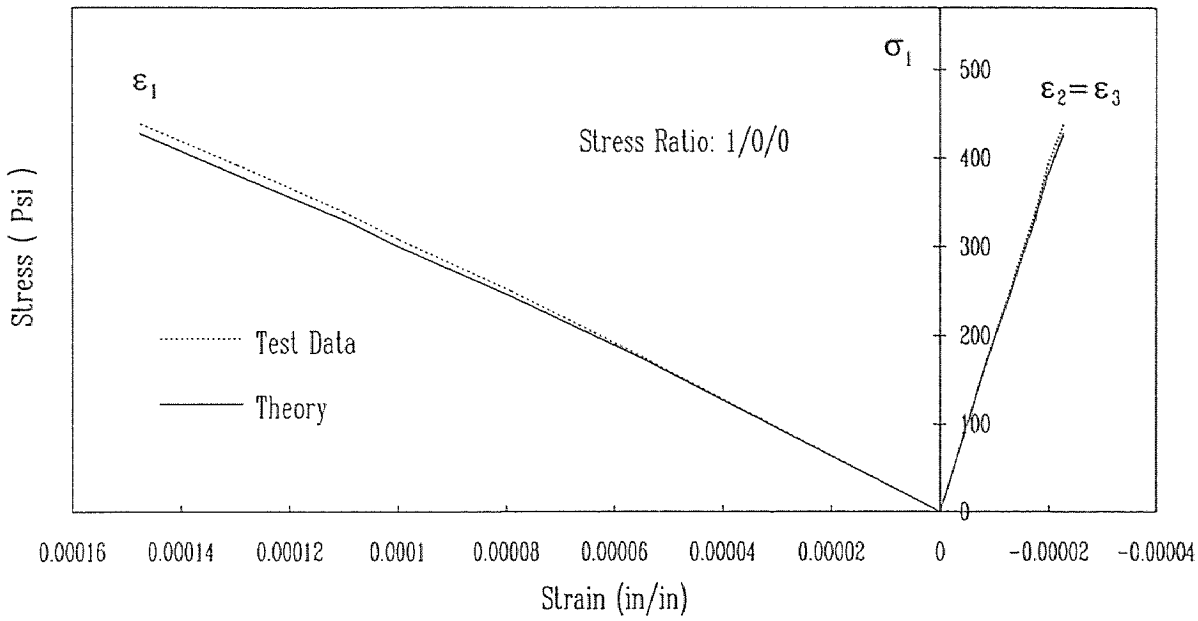


**Fig. 5.9** Comparison of Uniaxial Tensile Loading by Liu et al's Data

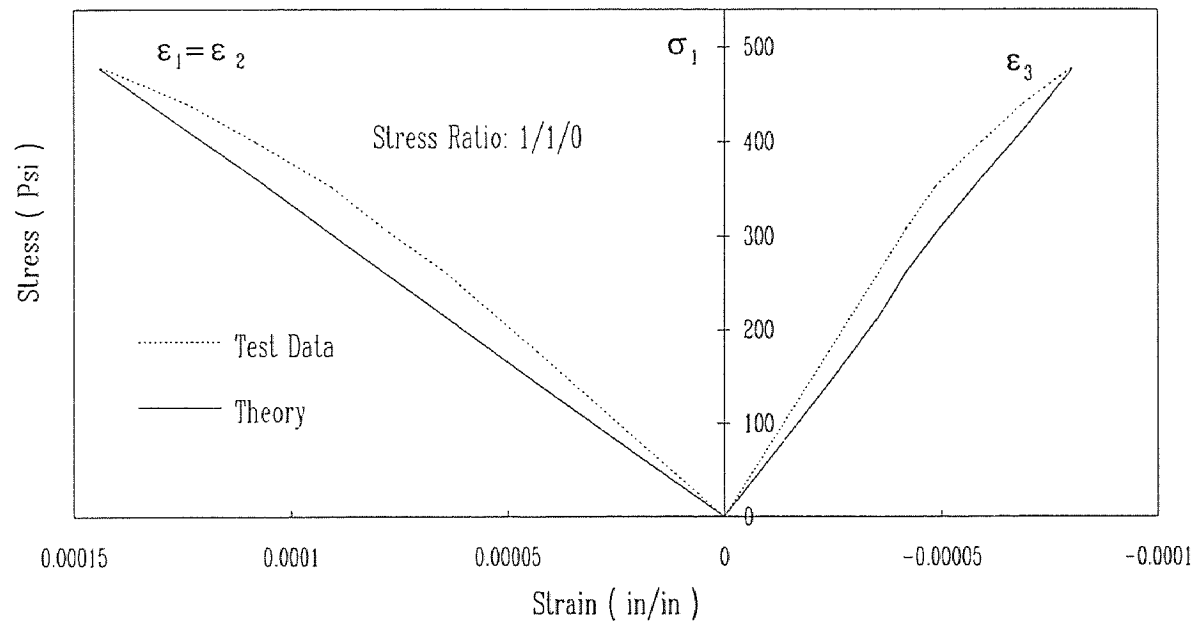


**Fig. 5.10** Comparison of Biaxial Tensile Loading by Liu et al's Data

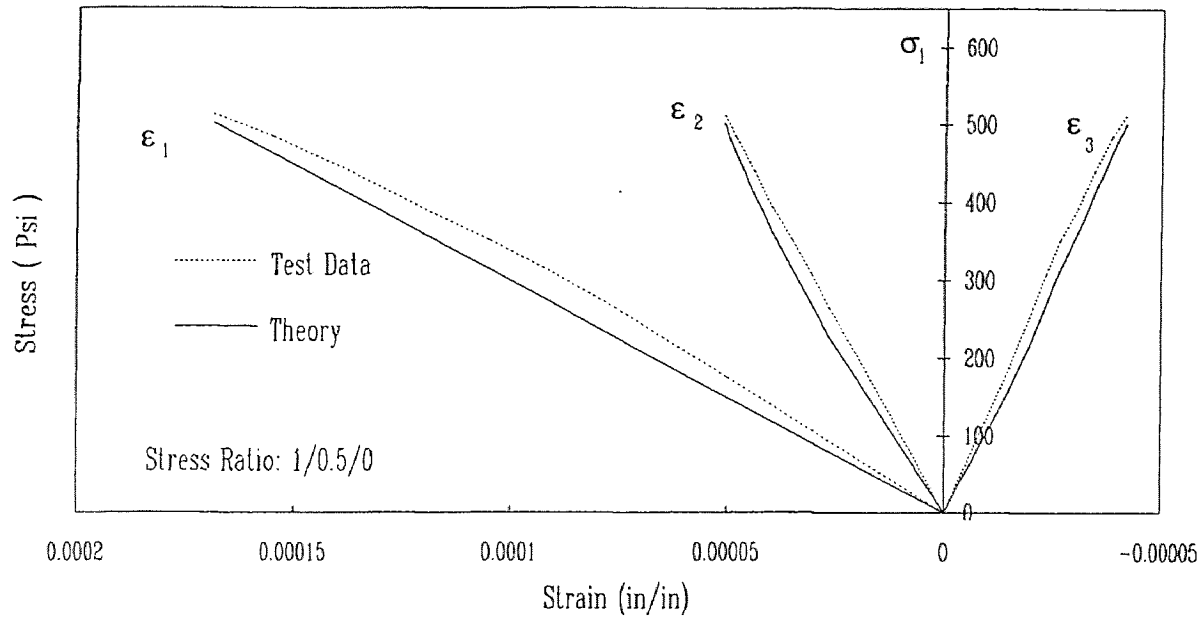


**Fig. 5.11** Comparison of Biaxial Tensile Loading by Liu et al's Data

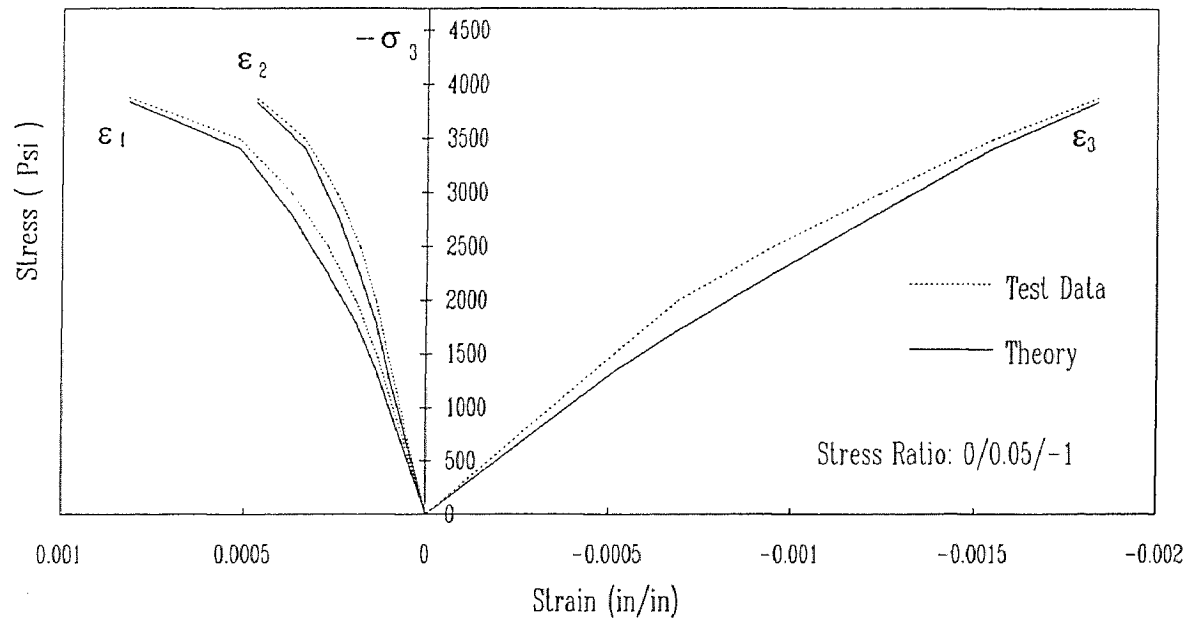


**Fig. 5.12** Comparison of Compression-Tension Loading by Liu et al's Data

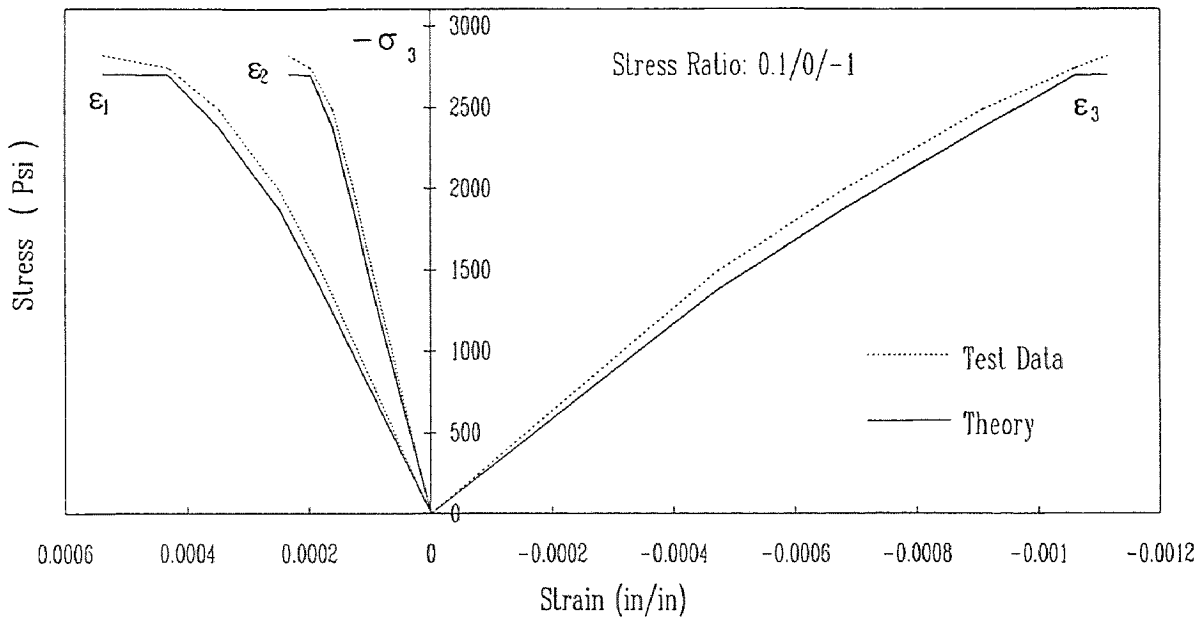


**Fig. 5.13** Comparison of Compression-Tension Loading by Liu et al's Data

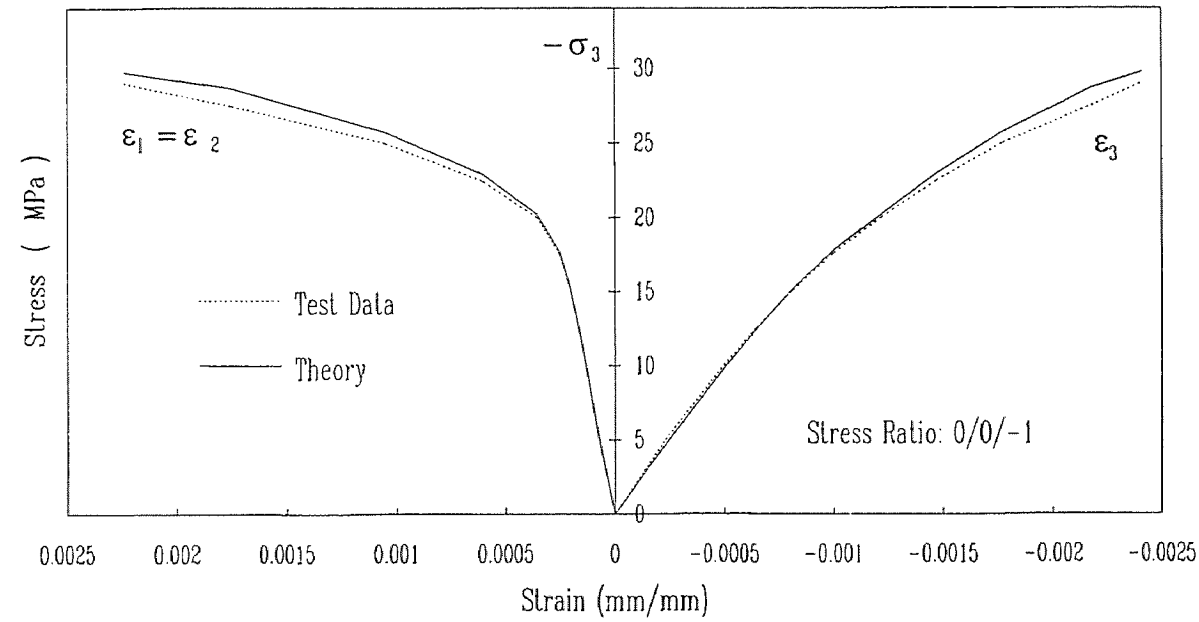


**Fig. 5.14** Comparison of UniaxialCompressive Loading by Schickert's Data

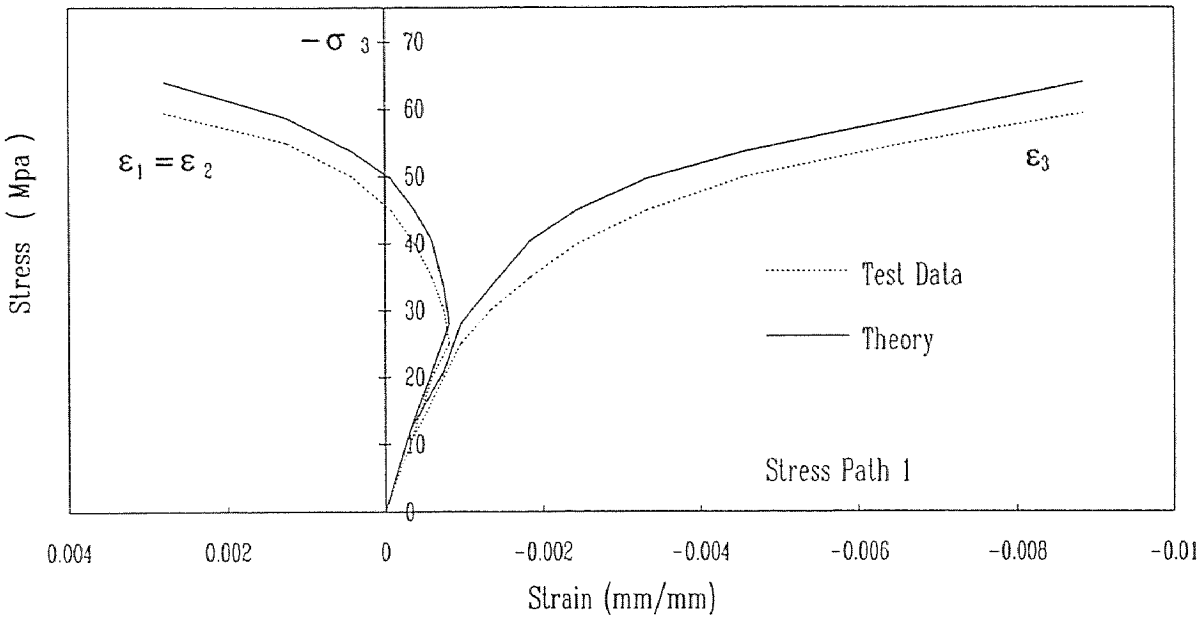


**Fig. 5.15** Comparison of Nonproportional Loading by Schickert's Data (Path 1)

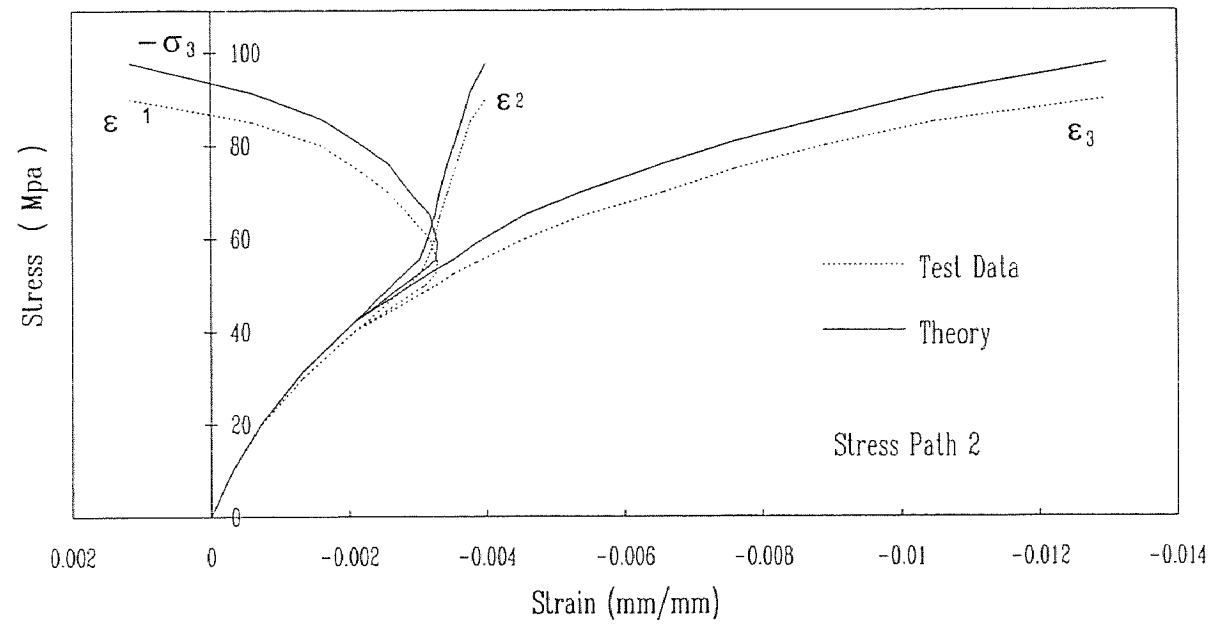


**Fig. 5.16** Comparison of Nonproportional Loading by Schickert's Data (Path 2)

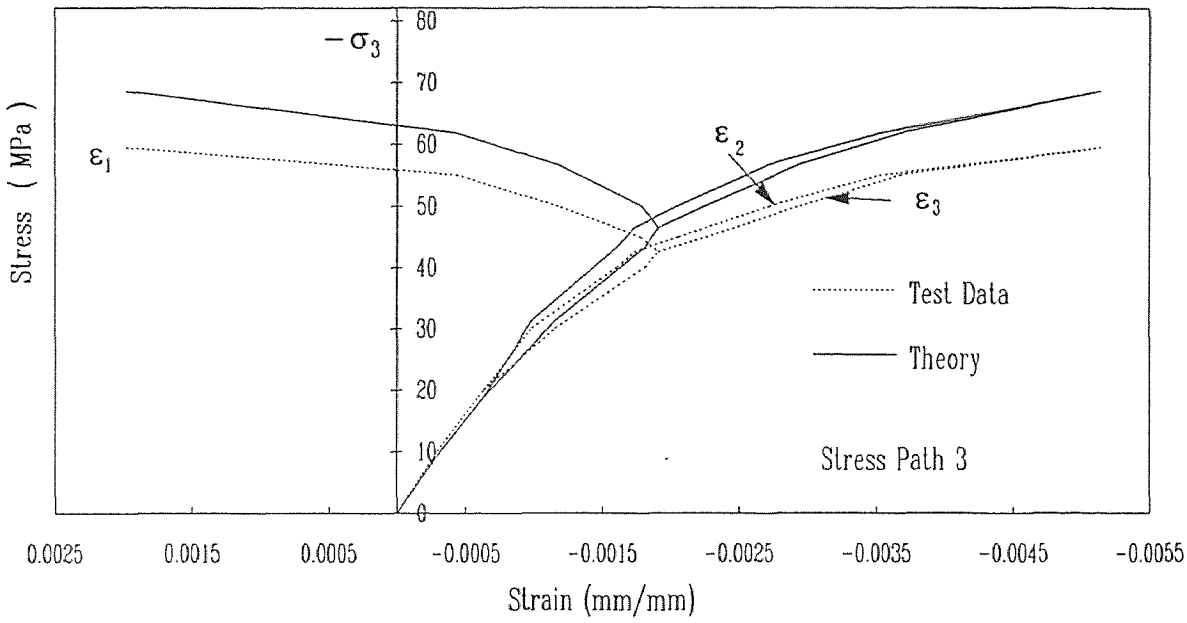


**Fig. 5.17** Comparison of Nonproportional Loading by Schickert's Data (Path 3)

# CHAPTER 6

# SUMMARY AND CONCLUSIONS

Concrete is a widely used material. Its constitutive relationship has been studied through many approaches. It is well-known that the plasticity method is an excellent tool to describe the behavior of concrete. In this study, a relatively complete constitutive model is developed for concrete in strain space within the framework of plasticity theory. A critical surface in strain space is set up at the point of the critical stress. With the critical surface as a reference surface, the initial and subsequent yield surfaces, including the failure surface, are defined according to the test results and appropriate assumptions. A modified isotropic hardening rule and a simple kinematics hardening rule are adopted. A non-associated flow rule in Drucker and Prager's form is used to account for an inelastic dilatant behavior of concrete. The working-hardening level is described by the modified plastic modulus, which is obtained on the basis of the plastic modulus of a uniaxial compressive plastic stress-strain relationship and a modification factor of the hydrostatic pressure sensitivity and the dependence of lode angle. The stiffness degradation in the post-peak range is accounted for. The predicted stress-strain curves are found to compare well with the experimental data. Based on the results and observations, the following conclusions can be made.

(1) The strain-space plasticity theory can be used to model concrete behavior in both strain-hardening and strain softening. The strain-space formulation overcomes the difficulties encountered in the application of stress-space formulation to strain-softening modeling.

(2) It is reasonable to use a continuum theory to discuss the strain softening of concrete under the mixed failure, in which the microcracks or fractures are generally not strongly oriented but may distribute randomly.

(3) The behavior of plastic deformation coupled with an elastic degradation is observed for concrete materials in the post-peak range. It is logical and practical to combine the concept of fracturing theory into the plasticity theory.

(4) Since very limited experimental data is available about strain state of concrete, little and incomplete information of the strain state behavior is known. It is impossible to set up a model depending completely on the test result. In other words, appropriate assumptions on the basis of qualitative results need to be made in determining the yield surface, hardening rule, and flow rule. In this situation, a simple and clear model is practical and preferable. In this model, the loading surfaces at different stages are defined on the limited test data together with reasonable assumptions. Results show that this is a good and effective approach.

(5) The most important inelastic behaviors of concrete have been represented by this model, including brittle failure in tension, ductile behavior in compression, hydrostatic sensitivities, and volumetric dilation under compressive loadings.

(6) The model provides rooms and flexibilities to fit wide range experimental data. The parameters used are shape factor $k$, the plastic modulus modification factor, $M(\rho_s, \theta)$, and the dilation factor $\varpi$ can further be adjusted and calibrated on the basis of experimental data. As the broad data become available and the detailed behavior of concrete becomes known, this model can be further improved.

# APPENDIX A

# DERIVATIVE OF LOADING FUNCTION AND PLASTIC POTENTIAL

## A.1 Derivative of Loading Function

### A.1.1 General Expressions

The derivatives of a general loading function

$$F(\varepsilon_{ij}, \varepsilon_{ij}^{p}, k_o) = 0 \tag{A.1}$$

for an isotropic material, it can be expressed by the chain rule as

$$\frac{\partial F}{\partial \varepsilon_{ij}} = \frac{\partial F}{\partial I_1'}\delta_{ij} + \frac{\partial F}{\partial J_2'}s_{ij} + \frac{\partial F}{\partial J_3'}t_{ij} \tag{A.2}$$

in which

$$\delta_{ij} = \frac{\partial I_1'}{\partial \varepsilon_{ij}} \tag{A.3}$$

is the Kronecker delta,

$$s_{ij} = \frac{\partial J_2'}{\partial \varepsilon_{ij}} \tag{A.4}$$

is the stress deviator tensor, and

$$t_{ij} = \frac{\partial J_3'}{\partial \varepsilon_{ij}} = s_{ik}s_{kj} - \tfrac{2}{3}J_2'\delta_{ij} \tag{A.5}$$

is the deviation of the square of the stress deviation.

Denoting

$$B_o = \frac{\partial F}{\partial I_1'} \quad , \qquad B_1 = \frac{\partial F}{\partial J_2'} \quad , \qquad B_2 = \frac{\partial F}{\partial J_3'} \tag{A.6}$$

the derivatives are further expressed as

$$\frac{\partial F}{\partial \varepsilon_{ij}} = B_o \delta_{ij} + B_1 s_{ij} + B_2 t_{ij} \tag{A.7}$$

### A.1.2 In Ascending Part

The loading surface in the ascending range is defined by Eq. (4.3) as

$$F(\rho, r, \theta, k_o) = r - k r_c = 0 \quad , \quad |\theta| \le 60^\circ \tag{A.8}$$

where $k = k(\rho, k_o)$ and

$$r_c = r_c(\rho, \theta) = [-(\alpha\cos\theta+\beta) + \sqrt{(\alpha\cos\theta+\beta)^2 - 4a(c\rho-1)}]/(2a)$$

Form Eq. (A.8) the derivatives $B_o$, $B_1$ and $B_2$ can written as

$$\begin{aligned} B_o &= \frac{\partial F}{\partial I_1'} = \frac{\partial k}{\partial I_1'} r_c - k A_o \\ B_1 &= \frac{\partial F}{\partial J_2'} = \frac{1}{r} - k A_1 \\ B_2 &= \frac{\partial F}{\partial J_3'} = -k A_2 \end{aligned} \tag{A.9}$$

and

$$\begin{aligned} A_o &= \frac{\partial r_c}{\partial I_1'} = -\frac{\sqrt{3}c}{3h_2} \\ A_1 &= \frac{\partial r_c}{\partial J_2'} = \frac{\alpha\sin\theta}{2a}\left[1 - \frac{(\alpha\cos\theta+\beta)}{h_2}\right]\frac{\partial\theta}{\partial J_2'} \\ A_2 &= \frac{\partial r_c}{\partial J_3'} = \frac{\alpha\sin\theta}{2a}\left[1 - \frac{(\alpha\cos\theta+\beta)}{h_2}\right]\frac{\partial\theta}{\partial J_3'} \end{aligned} \tag{A.10}$$

in which $h_2 = \sqrt{(\alpha\cos\theta+\beta)^2 - 4a(c\rho-1)}$ and

$$\frac{\partial\theta}{\partial J_2'} = \frac{3\sqrt{3}}{4\sin 3\theta}\frac{J_3'}{J_2'^{5/2}}$$
$$\frac{\partial\theta}{\partial J_3'} = -\frac{\sqrt{3}}{2\sin 3\theta}\frac{1}{J_2'^{3/2}} \qquad \text{(A.11)}$$

### A.1.3 In Descending Part

The loading function is defined by Eq. (4.10) as

$$F(\rho, r, \theta, k_o) = r - r_o = 0 \quad , \quad |\theta| \le 60^o \qquad \text{(A.12)}$$

where $r_o = [\gamma(k_o) - c\rho]/(\alpha_1 \cos\theta + \beta_1)$.

From Eq. (A.12), one has

$$B_o = \frac{\partial F}{\partial I_1'} = -A_o$$
$$B_1 = \frac{\partial F}{\partial J_2'} = \frac{1}{r} - A_1 \qquad \text{(A.13)}$$
$$B_2 = \frac{\partial F}{\partial J_3'} = -A_2$$

where

$$A_o = \frac{\partial r_o}{\partial I_1'} = -\frac{\sqrt{3}c}{3(\alpha_1\cos\theta + \beta_1)}$$
$$A_1 = \frac{\partial r_o}{\partial J_2'} = \frac{[\gamma(k_o) - c\rho]\,\alpha_1 \sin\theta}{(\alpha_1\cos\theta + \beta_1)^2}\frac{\partial\theta}{\partial J_2'} \qquad \text{(A.14)}$$
$$A_2 = \frac{\partial r_o}{\partial J_3'} = \frac{[\gamma(k_o) - c\rho]\,\alpha_1 \sin\theta}{(\alpha_1\cos\theta + \beta_1)^2}\frac{\partial\theta}{\partial J_3'}$$

in which $\frac{\partial\theta}{\partial J_2'}$ and $\frac{\partial\theta}{\partial J_3'}$ are represented by Eq. (A.11).

### A.1.4 Derivative at $\theta = 60^0$

It should be noted that the term $\sin 3\theta$ in Eq. (A.11) would go to zero if $\theta$ approaches to $60^o$ , and the derivatives at $60^o$ would be infinite. This is because there are three corners in the deviatoric sections where there do not exist derivatives. To treat such singularity, one can simply assume that

$$\frac{\partial F}{\partial(\cos\theta)} = 0 \quad , \quad \theta = 60^0 \tag{A.15}$$

and hence in Eqs. (A.9) and (A.13)

$$\begin{matrix} A_1 = 0 \\ A_2 = 0 \end{matrix} \quad , \quad \theta = 60^0 \tag{A.16}$$

This implies that the normal vector of the failure curve at $\theta = 60^0$ coincides with the radial direction, which is independent of $\theta$.

## A.2 Derivative of Plastic Potential Function

The derivative of the plastic potential function $G$ can be expressed in the form of tensor invariants as

$$\frac{\partial G}{\partial \varepsilon_{ij}} = \frac{\partial G}{\partial I_1'}\delta_{ij} + \frac{\partial G}{\partial J_2'}s_{ij} + \frac{\partial G}{\partial J_3'}t_{ij} \tag{A.17}$$

In this research, The Drucker-Prager type of plastic potential function is used (Eq.(4.31)), thus the derivative can be simplied as

$$\frac{\partial G}{\partial \varepsilon_{ij}} = \varpi\delta_{ij} + \frac{1}{\sqrt{2}r}s_{ij} \tag{A.18}$$

# APPENDIX B
# FLOW CHART OF MATERIAL SUBROUTINE

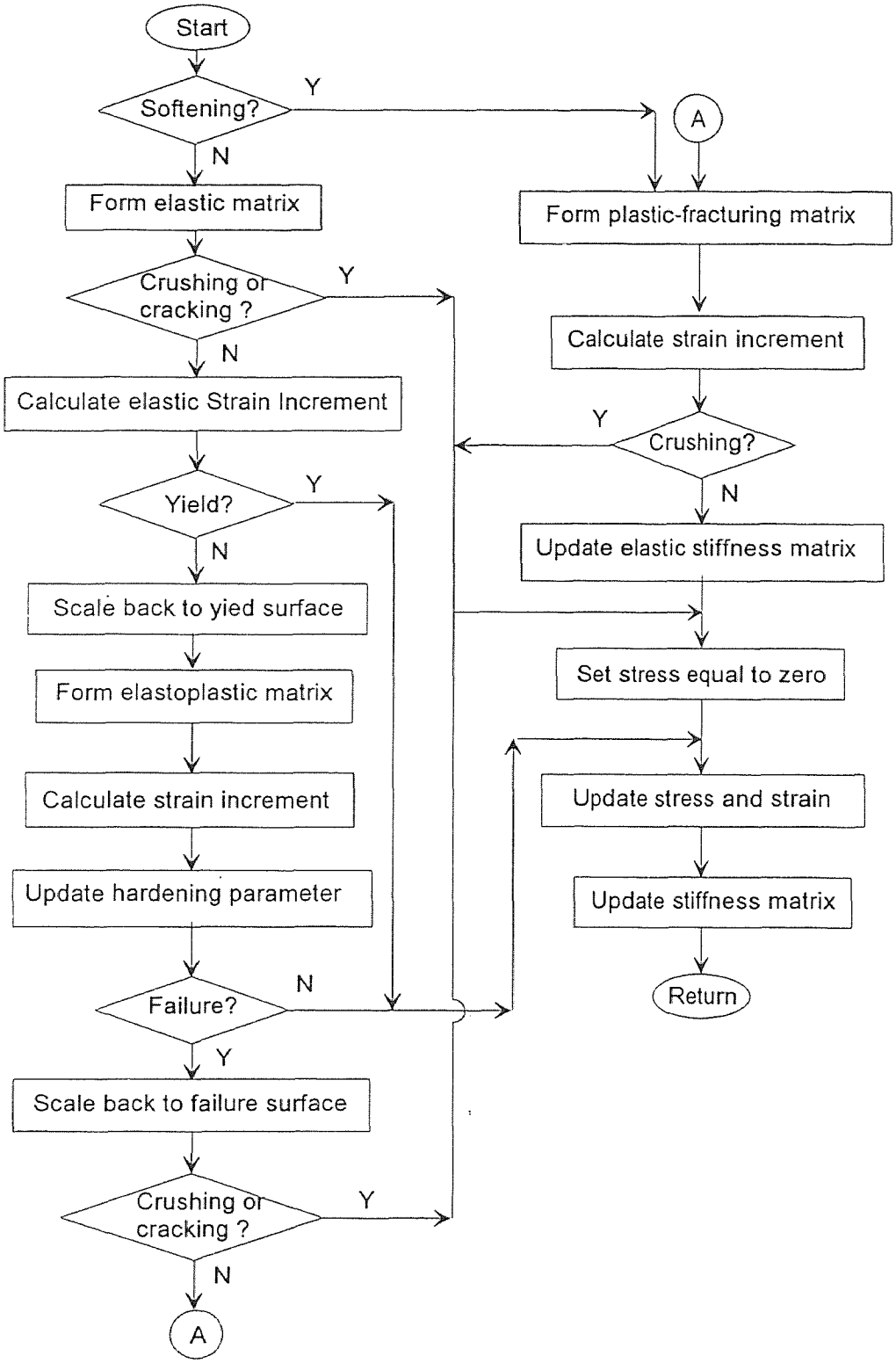

# REFERENCES


Ahmad, S. H. (1981). "Complete Triaxial Stress-Strain Curves for Concrete." *Ph. D Dissertation in University of Illinois at Chicago.*

Argyris, J. H., Faust, G., Szimmat, J., Warnke, E. P., and Willam, K. J. (1974)."Recent Development in the Finite Element Analysis of Prestressed Concrete Reactor Vessels." *Nuclear Engineering and Design*, 28(1), 42-75.

Argyris, J. H., Faust, G., and Willam, K. J. (1976)." Limit Load Anasis of Thick-Walled Concrete Structures-A Finite Element Approach to Fracture." *Computer Method in Applied Mechanics and Engineering*, Vol. 8, North-Holland Co. 215-243.

Bazant, Z. P. (1971). Discussion of "Triaxial State of Stress of Concrete Structures," by L. Janda. *International Conference on Structural Mechanics in Rector Technology, Berlin*, 22.

Bazant, Z. P. and Bhat, P. D. (1976). "Endochronic Theory of Inelasticity and Failure of Concrete." *Engrg Mech., ASCE,* 102(5), 701-722.

Bazant, Z. P. and Kim, S. S. (1979). "Plastic-Fracturing Theory for Concrete." *Engrg Mech., ASCE*, 105(3), 407-428.

Bazant, Z. P. and Shieh, C. L. (1980). "Hysteric Fracturing Endochronic Theory for Concrete." *Engrg. Mech., ASCE*, 106(6), 929-950.

Buyukozturk, O. (1977). "Nonlinear Analysis of Reinforced Concrete Structures." *Computers and Structures*, Vol. 7, 149-156.

Buyukozturk, O. (1979). "A Constitutive Model for Concrete in Compression." *Proceedings of the Third ASCE Engrg. Mech. Div. Specialty Conference, Austin, Texas*

Carino, N. J. (1976). "Limitation Tensile Strain Criterion for Failure of Concrete." *ACI Journal*, 73(3), 160-165.

Casey, J. and Naghdi, P. M. (1981). "On the Characterization of Strain-Hardening in Plasticity." *J. of Applied Mechanics, Transactions of the ASME*, 48(2), 285-295.

Casey, J. and Naghdi, P. M. (1983a). "A Remark on the Definition of Hardening, Softening and Perfectly Plastic Behavior." *Acta Mechanica,* Vol. 48, 91-94

Casey, J. and Naghdi, P. M. (1983b). "On the Nonequivalence of the Stress Space and Strain Space Formulations of Plasticity Theory." *J. of Applied Mechanics, Transaction of ASME.* 50(2), 3540-35.

Cedolin, L., Crutzen, Y. R. J. and Dei Poli, S. (1977). "Triaxial Stress-Strain Relationship for Concrete." *Engrg. Mech., ASCE*, 103(3), 423-439.

Chen, A. C. T. and Chen, W. F. (1975). "Constitutive Relations for Concrete." *Engrg Mech., ASCE*, 101(4), 465-481.

Chen, E. Y. T. and Schnobrich, W. C. (1981). "Material Modeling of Plain Concrete." *Advanced Mechanics of Reinforced Concrete*, IABSE Colloquium, Delft, the Netherlands, 33-51.

Chen, W. F. (1982). Plasticity in Reinforced Concrete. McGraw-Hill Inc.

Dafalias, Y. F. (1977a). "Elasto-Plastic Coupling within Thermodynamic Strain Space Formulation of Plasticity." *International Journal of Nonlinear Mechanics,* Vol. 12, 327-337.

Dafalias, Y. F. (1977b). "Il'iushin's Postulate and Resulting Thermodynamic Conditions on Elasto-Plastic Coupling." *International Journal of Solids and Structures*, 13(3), 239-251.

Darwin, D. and Pecknold, D. A. (1974). "Inelastic Model for Cyclic Biaxial Loading of Reinforced Concrete." *Civil Engineering Studies SRS*, No. 409, University of Illinois at Urbana-Champaign.

Dougill, J. W. (1976). "On Stable Progressively Fracturing Solids." *Journal of Applied Mathematics and Physics(ZAMP)*, Vol. 27, 423-437.

Dragon, A. and Mroz, Z. (1979). "A Continuum Theory for Plastic-Brittle Behavior of Rock and Concrete." *International Journal of Engineering Science*, Vol. 17, No. 2, 121-137

Drucker, D. C. (1950). "Some Implications of Work Hardening and Ideal Plasticity." *Quarterly of Applied Mathematics*, 7(4), 411-418.

Ferrara, G., Rossi, R., Rossi, P. P. and Ruggeri, L. (1976). "Dispositive Di Prova Per L'analisi Sperimentale Del Comportamento Di Conglomerati Cementizi Sottoposti a Stati Triassiali Di Sollecitazione." *Presented at the 4th Association Italiana Annalisi Sollecitazione Congress, Held at Rome, Italy.*

Frantziskonis, G. and Desai, C. S. (1987). "Constitutive Model with Strain Softening." *International Journal of Solids and Structures*, Vol. 23, No. 6, 733-750.

Gerstle, K. H. (1980). "Behavior of Concrete under Multiaxial Stress States." *Engrg. Mech., ASCE*, 106(6), 1383-1403.

Gerstle, K. H. (1981). "Simple Formulation of Biaxial Concrete Behavior." *ACI Journal,* 78(1), 62-68.

Green, S. J. and Swanson, S. R. (1973). "Static Constitutive Relations for Concrete." *Technical Report No. AFW-TR-72-244 (AD761820)*, Air Force Weapons Lab, New Mexico.

Han, D. J. and Chen, W. F. (1985). "A Nonuniform Hardening Plasticity Model for Concrete Materials." *Journal of Mechanics of Materials*, Vol. 4, 283-302.

Han, D. J. and Chen, W. F. (1986). "Strain-Space Plasticity Formulation for Hardening-Softening Materials with Elasto-Plastic Coupling." *International Journal of Solid and Structures*, 22(8), 935-950.

Han, D. J. and Chen, W. F. (1987). "Constitutive Modeling in Analysis of Concrete Structures." *Engrg. Mech., ASCE,* 113(4), 577-593.

Hobbs, D. W. (1974). "Strength and Deformation Properties of Plain Concrete Subjected to Combined Stress." *Part 3, Technical Report 42, Cement and Concrete Association, London, England.*

Hsieh, S. S., Ting, E. C., and Chen, W. F. (1982). "A Plasticity Fracture Model for Concrete." *International Journal of Solids and Structures*, 18(3), 181-197.

Hsu, C.T.T.(1972). Discussion of "Stress-Strain Response and Fracture of Concrete in Uniaxial and Biaxial Compression," by Liu, T.C.Y. et al. *ACI Journal*, 69(11), 711-712.

Il'iushin, A. A. (1961). "on the Postulate of Plasticity." PMM, 25(3), 503-507 (746-752 in English Translation Edition).

Jiang, L., Huang, D. and Xie, N. (1991). "Behavior of Concrete Under Triaxial Compressive-Compressive-Tensile Stresses." *ACI Materials Journal,* 88(2), 181-185.

Kachanov, L. M. (1958). "Time of Rupture Process under Creep Conditions." *Izvestia Aksdemii Nauk*, USSR, 8 (in Russian), 26-31.

Karsan, P. and Jirsan, J. O. (1969). " Behavior of Concrete Under Compressive Loading." *Struct. Div., ASCE*, 95(12), 2543-2563.

Kotsovos, M. D. and Newman, J. B. (1977). "Behavior of Concrete Under Multiaxial Stress." *ACI Journal*, 74(6), 443-446.

Kotsovos, M. D. and Newman, J. B. (1978). "Generalized Stress-Strain Relations for Concrete." *Energ. Mech., ASCE*, 104(4), 845-856.

Kotsovos, M. D. (1979). "Effect of Stress Path on the Behavior of Concrete under Triaxial Stress States." *ACI Journal*, 76(2), 213-223.

Krajcinovic, D. and Fonseka (1981). "The Continuous Damage Theory of Brittle Materials." *Journal of Applied Mechanics*, Vol. 48, No. 4, 809-815.

Krajcinovic, D. (1985). "Constitutive Theories for Solids with Defective Microstructure." *Damage Mechanics and Continuum Modeling, N. Stubbs and D. Krajcinovic eds. ASCE*, 39-56.

Kupfer, H. and Hilsodorf, H. K. (1969). "Behavior of Concrete Under Biaxial Stresses." *ACI Journal,* 66(8), 656-666.

Kupfer, H. and Gerstle, K. H. (1973). "Behavior of Concrete under Biaxial Stresses." *Engrg. Mech., ASCE*, 99(4), 853-866.

Launay, P. and Gachon, H (1971). "Strain and Ultimate Strength of Concrete Under Triaxial Stresses." *Special Publication, SP-34, ACI*, 269-282.

Liu, T. C. Y., Nilson, A. H., and Slate, F. O. (1972). "Stress-Strain Response and Fracture of Concrete in Uniaxial and Biaxial Compression." *ACI Journal*, 69(5), 1025-1034.

Loland. K. E. (1980). "Continuous Damage Model for Load Response Estimation of Concrete." *Cement and Concrete Research*, 10(3), 495-402.

Lubliner, J., Oliver, J.,Oller, S. and Onate, E. (1989). "A Plastic-Damage Model for Concrete." *International Journal of Solids and Structures*, 25(3), 299-326.

Mazars, I. (1981). "Mechanical Damage and Fracture of Concrete Structure." *Advances in Fracture Research, 5th International Conference on Fracture, D. Francois, ed.*

Mizuno, E. and Shigemitsu, H. (1992). "Compressive Softening Model for Concrete." *Energ. Mech., ASCE*, 118(8), 1546-1563.

Naghdi, P. M. and Trapp, J. A. (1975). "the Significance of Formulating Plasticity Theory with Reference to Loading Surfaces in Strain Space." *International Journal of Engineering Science,* Vol. 13, 785-797.

Nelissen, L. J. M. (1972). "Biaxial Testing of Normal Concrete." Heron(Delft), 18(1), 1-90.

Newman, S. B. and Newman, K. (1972). "The Cracking and Failure of Concrete Under Combined Stresses and its implications for Structural Design." *RILEM-Symposium on the Deformation and Rupture of Solids Subjected to Multiaxial Stresses, Part I, Concrete, Cannes*, 1972, Paper I/10, 149-168.

Ngo, D., and Scordelis, A. C. (1976). "Finite Element Analysis of Reinforced Concrete Beam." *ACI Journal*, 64(3), 152-163.

Ortiz, M. (1985). "A Constitutive Theory for the Inelastic Behavior of Concrete." *Mechanics of Materials*, 4(1).

Ottosen, N. S. (1977). "A Failure Criterion for Concrete." *Engrg. Mech., ASCE,* 103(4), 527-536.

Ottosen, N. S. (1979). "Constitutive Model for Short-Time Loading of Concrete." *Engrg. Mech. ASCE*, 105(1), 127-141.

Palaniswamy, R. and Shah, S. P. (1974). "Fracture and Stress-Strain Relationship of Concrete under Triaxial Compression." *Struct. Engrg., ASCE*, 100(5), 901-916.

Pekau, O. A., Zhang, Z. X. and Liu, G. T. (1992). "Constitutive Model for Concrete in Strain Space." *Engrg. Mech., ASCE*, 118(9), 1907-1927.

Peterson, P. E. (1981). "Crack Growth and Development of Fracture Zone in Plain Concrete and Similar Materials," *Division of Building Materials*, Lund Institute of Technology, Lund, Sweden.

Pietruszczak, S., Jiang, J. and Mirza, F. A. (1988). "An Elastoplastic Constitutive Model for Concrete." *International Journal of Solids and Structures*, 24(7), 705-722.

Resende, L. (1987). "A Damage Mechanics Constitutive Theory for Inelastic Behavior of Concrete." *Conput. Methods Appl., Mech. Engrg.*, 60(1), 57-93.

Richart, F. E., Brandtzaeg, A. and Brown, R. L. (1929). "The Failure of Plain and Spirally Reinforced Concrete in Compression." *University of Illinois Bulletin*, Vol. XXVI, No. 31.

Schickert, G. and Winkler, W. (1977). "Results of Test Concerning Strength and Strain of Concrete Subjected to Multiaxial Compressive Stress." *Vertriek Durch Verlag Wilhelm Ernst and Sohngk Berlin-Munchen-Dusselvorf.*

Schickert, G. and Danssmann, J. (1984). "Behavior of Concrete Stressed by High Hydrostatic Compression." *RILEM-CEB-CNRS, Int. Conf. on Concrete under Multi-Conditions*, Toulouse, 69-84.

Shah, S. P. and Chandra, S. (1968). "Critical Stress, Volume Change and Microcracking of Concrete." *ACI Journal*, 65(5), 770-781.

Simo, J. C. and Ju, J. W. (1987). " Strain and Stress Based Continuum Damage Models." *Part 1: Formulation, International Journal of Solids and Structures*, 23(7), 821-840.

Sinha, B. P., Gerstal, K. H. and Tulin, L. G. (1964). "Stress-Strain Relation for Concrete Under Cyclic Loading." *ACI Journal*, 61(2), 195-211.

Suidan, M. and Schnobrich, W. C. (1973). "Finite Element Analysis of Reinforced Concrete." *Struct. Engrg., ASCE,* 99(10), 2109-2122.

Tasuji, M. E., Slate, F. O., and Nilson, A. H. (1978). "Stress-Strain Response and Fracture of Concrete in Biaxial Loading." *ACI Journal*, 75(7), 306-312.

Torrent, R. J., Dvorkin, E. N., and Alvaredo, A. M. (1987). "A Model for Work-hardening Plasticity and Failure of Concrete under Multiaxial Stress." *Cement and Concrete Research*, Vol. 17, 939-950.

Valanis, K. C. (1971). "A Theory of Viscoelasticity without a Yield Surface." *Archiwum Mechaniki Stossowarej (Archives of Mechanics, Warsaw)*, Vol. 23, 517-551.

Wastiels, J. (1979). "Behavior of Concrete under Multiaxial Stresses--- A review." *Cement Concrete Research*, 9(1), 35-44.

Willam, K. J. and Warnke, E. P. (1974). "Constitutive Model for the Triaxial Behavior of Concrete." Presented at *the 1974 International Association for Bridge and Structural Engineering Seminar on Concrete Structures Subjected to Triaxial Stresses, Held at Bergamo, Italy.*

Yazdani, S. and Schreyer, H. L. (1990). "Combined Plasticity and Damage Mechanics Model for Plain Concrete." *Engrg. Mech., ASCE*, 116(7), 1435-1451.

Yoder, P. J. and Iwan, W. D. (1981). "On the Formulation of Strain-space Plasticity With Multiple Loading Surfaces." *J. of Applied Mechanics, ASME*, 48(4), 773-778.